INFRARED LASER-INDUCED REACTIONS

OF

HALOGENATED ETHANES

by

Tsae Shyan Lee

B. S., National Taiwan University,1979

A MASTER'S THESIS

submitted in partial fulfillment of the

requirements for the degree

Master of Science

Department of Chemistry

KANSAS STATE UNIVERSITY
Manhattan, Kansas

1983

Approved by

Major Professor

LIST OF FIGURES

This work is dedicated to my parents and my dear Alpha.

ACKNOWLEDGEMENT

INTRODUCTION

Since the development of the high power CO_2 laser, multi-photon laser induced chemical reactions has been an active field of study[1,2]. Somewhat surprisingly many molecules can "climb up the vibrational ladder" and absorb large amounts of energy from the intense, monochromatic radiation field provided by infrared lasers. With commercially available pulsed CO_2 lasers, it is easy to introduce 50-100 kcal/mole or more with each pulse when the laser is tuned to a strong absorption band (a mole of IR photons at 1000 cm^{-1} is equivalent to only 2.86 kcal/mole).

Pulsed megawatt irradiation is a convenient way to study vibrationally excited molecules with temperatures $>1000^oK$. Reactions can be obtained in what is essentially a room-temperature apparatus. The effective temperature is readily changed over wide ranges by changing the laser fluence. This permits detailed study of reactions heretofore inaccessible because of their high activation energies. Reactions induced by laser absorption frequently have fewer side reactions than the thermally induced reaction for several reasons: the reactant is exposed to high temperature condition for only a short length of time. The initial "heating rate" is in the range of $10^6 - 10^{11}$ $^oK/s$, the subsequent "cooling rate" is in the range of $10^3 - 10^{6} {}^oK/s$ (pressure dependent). Also the sample is activated first with vibrational energy and in some cases the translational(bulk) temperature never reaches high values. This is a new approach to excitation of chemical reactions and differs from the traditional thermal excitation, in which energy

is supplied in Boltzmann form by collisions among the energetic molecules.

Small molecules at low energies have discrete vibrational and rotational states and it usually requires fairly intense laser radiation to excite a subfraction of the molecule over these discrete states via a coherent, resonant absorption process[2,3]. Excitation through this discrete regime appears to depend upon the laser power rather than the laser energy. The density of states increases very rapidly with an increase in energy and once the requisite number of photons(typically thought to be ~3-4) are absorbed, the molecule reaches a second region termed the vibrational quasi-continuum. In this regime there is such a high density of states that the anharmonicity problem vanishes, since there is always a rotational/vibrational level in resonance with the monochromatic laser light. Once in the quasi-continuum, the laser energy rather than the laser power appears to be responsible for further exciting the molecules up to or even beyond the reaction threshold level. Once excited to the threshold, reaction can occur in competition with further excitation beyond the threshold. Since such excitation is time dependent, the laser power rather than energy again becomes important in determining the ultimate level of excitation achieved before the reaction rate becomes so rapid that additional up-pumping is impossible. Since most current lasers have a pulse length of $~10^{-7}$ s, once a molecule acquires sufficient energy to react with a rate constant of $~10^{-7} - 10^{-8}$ s^{-1}, reaction will, indeed, compete with any further up-pumping.

The CO_2 laser induced multiphoton absorption(MPA) and multiphoton dissociation(MPD) of many small polyatomic molecules have been studied[4-7]. Some of the more thoroughly studied cases are SF_6 and halogenated methanes and ethanes. The elimination of HX (X=Cl,Br or F) from alkyl halides is one of the best studied elementary unimolecular processes[5]. Two elimination processes are possible: (1) a four-centered process[5] (the hydrogen and halogen were originally from adjacent carbons) and (2) a three-centered process (the hydrogen and halogen were originally on the same carbon). Normally the four-centered process has the lower thermal energy of activation. Both CF_3CH_3 and CFH_2CH_3 have been studied by chemical[7(c)] and MPA excitation[5,8]. The multiphoton absorption of CF_3CH_3 does not follow Beer's law, rather the absorption increases with CF_3CH_3 pressure[5]. The reaction probability ($P(\emptyset) \sim 0.15$) saturates above 3 J/cm^2. Both the absorption data and the reaction yield data for absorption of photons can be explained by a bottleneck in the lower level. Experiments suggest that CF_3CH_3 acts more like a small molecule, such as the halogenated methanes. The C_2H_5F molecule shows the same behavior as CF_3CH_3 in absorption measurement experiment and reaction probability[5]. One additional point of interest for small molecules is that small quantities of inert gas may enhance reaction probability via aiding the absorption process. This is a consequence of rotational hole filling by collisions, or collisional release of other bottlenecks.

In contrast to the small molecule behavior, i.e., bottlenecks which limit absorption and the extent of laser

driven reaction, large molecules have no or few bottlenecks. More specifically, a large molecule is considered as possessing a density of vibrational and rotational states exceeding $\sim 10^3$ - $10^4/cm^{-1}$ at room temperature[2]. The Kansas State University laboratory has characterized the MPD and MPA of large molecules, especially organic esters[5,6]. A list of some of the characteristic features of the multiphoton excitation/reaction of large molecules follows[2].

(1) The high density of vibrational/rotational states essentially places the molecule in or very near the quasi-continuum at room temperature.

(2) As a consequence of (1), large molecules will frequently exhibit low laser threshold fluence and high reaction probabilities. There are examples with essentially 100% reaction per laser pulse at relatively moderate fluences.

(3) Because of the relatively large number of degrees of freedom and concomitant high density of state, the RRKM rate constants of molecules excited to just beyond the threshold energy can be quite low.

(4) As a consequence of (3), collisional quenching of vibrationally excited large molecules by unexcited reactant molecules or added bath gases can frequently compete efficiently with reaction, particularly at low or moderate laser fluences.

(5) Also as a result of (3), reaction of the excited molecules in the irradiated volume produced initially by the laser pulse

is nearly always in competition with relaxation via a complex interplay of cooling process in both the irradiated and surrounding volumes. Only with low pressures and sufficiently intense laser radiation to ensure essentially complete reaction during the laser pulse will such cooling not be significant.

(6) The heat capacity of a large molecule is comprised largely of the vibrational component. Thus, intramolecular collisional relaxation of vibrational excitation into translational and rotational energy(for the molecule in the irradiated volume) results in only a relatively small decrease of the effective vibrational temperature of the molecule.

(7) The vibrational energy population resulting from absorption of the laser irradiation is relatively broad and can be approximated by a Boltzmann distribution. It must be stressed that the true distribution is not known with certainty.

Experiments with CF_3CH_2Br[9] showed that this molecule behaved like a "large" molecule in contrast to CF_3CH_3. For example the laser absorption cross-section, $\sigma_L(\emptyset)$, is independent of CF_3CH_2Br pressure, the $\sigma_L(\emptyset)$ value approached the broad-band absorption cross-section at low $\emptyset$, and showed a weak dependence on $\emptyset$. Also the reaction probabilities are quite high, reaching 0.4 at 3 J/cm^2. In this thesis the reaction probability and laser absorbed energy for CF_3CH_2Cl was systematically studied. The reason we chose CF_3CH_2Cl for study is because this molecule should connect the behavior of CF_3CH_3 and CF_3CH_2Br. Also there are three reaction channels which

makes this an interesting case for study of parallel unimolecular reactions. It can react via a four-centered elimination (-HF), a three-centered elimination (-HCl) and C-Cl homolytic bond rupture. We will compare the laser photolysis behavior of CF_3CH_3, CF_3CH_2Cl and CF_3CH_2Br. It was of significance to determine if they act as small molecules or large molecules in MPA and MPD.

Ther thermal decomposition of CF_3CH_2Cl[10] has been investigated by the single-pulse shock tube technique between 1120° and $1300^\circ K$ at pressures from ~2610 to 3350 torr. Under these conditions, the major reaction was reported as the three-centered (HCl) elimination,

$$CF_3CH_2Cl \longrightarrow CF_3CH: + HCl$$
$$CF_3CH: \longrightarrow CF2=CHF$$

with $\log(k, sec^{-1}) = 13.3 \pm 0.4 - (65.5 \pm 2.2 \text{ kcal})/2.303 \text{ RT}$. The study also reported the slower four-centered HF elimination,

$$CF_3CH_2Cl \longrightarrow CF_2=CHCl + HF$$

with $\log(k, sec^{-1}) = 12.7 \pm 0.5 - (67.6 \pm 2.7 \text{ kcal})/2.303 \text{ RT}$. At temperatures above $1270^\circ K$, homolytic C-Cl rupture was reported as a third reaction channel. As will be discussed in this thesis, there is reason to suspect that secondary or side reactions affected these data and that the Arrhenius parameters are not reliable.

Highly vibrationally excited CF_3CH_2Cl have been generated by combination of CF_3 with CF_2Cl radicals by Bert Holmes[11]. He observed only H-F elimination and calculated the rate constant to be 2.8×10^6 sec^{-1}; the threshold energy $E_o(HF)=76$ kcal/mole,

was assigned from RRKM calculation. This value looks reasonable and will be mentioned in the discussion section.

The four-centered elimination reaction of CF_3CH_2Cl are a classic system for unimolecular reaction studies. The infrared multiphoton decomposition of C_2H_5Cl initiated by absorbed in the C-C stretching mode, of the molecule was studied by Steinfield[12(a)]. Tunable 3.3 m laser pulses used to excite the C-H stretching mode of ethyl chloride was studied by Moore[12(b)]. All methods found that C_2H_4 from four-centered elimination was the only product and that the system followed RRKM behavior.

The IR photochemistry of Freon 123 (CF_3CHCl_2) was studied by Marling[12(c)]. The primary observed photoproducts for 1065 cm^{-1} photolysis were $CF_2=CHF$, $CF_2=CFCl$ and CF_3CCl_3. The C-Cl rupture channel was assigned as the main primary step, with HCl three-centered elimination occuring to a much lesser extent. The $CF_2=CHF$ product was formed via radical reactions. The HF four-centered elimination giving $CF_2=CCl_2$ was not observed, perhaps because the activation energy is higher than for CF_3CH_3 or CF_3CH_2Cl.

The dependence of the laser induced-reaction probability of CF_3CH_2Cl on laser fluence, pressure of reactant and addition of bath gas was studied in this work. Also reported are the product distributions of MPD from CF_3CH_2Cl. Laser sensitization using SiF_4 was done to help understanding the product distributions. Laser absorption measurements were made in order to define the efficiency of the MPD process. These data are compared to similar studies of CF_3CH_2Br and CF_3CH_3.

EXPERIMENTAL PROCEDURE

I. Operation of Laser

A Lumonics Model 103 TEA CO_2 laser was used in this work. The TEA laser operates by transverse electrical excitation of a three-gas mixture. All studies were conducted using a CO_2-He-N_2 mixture (8.0:2.0:0.8 SCFH) using regular tank gases, which pro- duced an initial $\sim$130-ns fwhm pulse followed by a long tail extending to $\sim$1-2 μs. Approximately half the energy was con- tained within the initial spike and half within the tail. Three low-lying vibrational-rotational systems of the CO_2 molecules are responsible for the laser transitions. The $00^{\circ}1$ to $10^{\circ}0(9.6\mu m)$ and $00^{\circ}1$ to $02^{\circ}0$ (10.6μm) transitions are utilized, the 10.6 μm lines are weaker than 9.6 μm lines. The laser was tuned with an intercavity grating to a single rotational line for these studies. The pulse energy varies with rotational quantum number. The energy fluence from R(30) line of the $00^{\circ}1-02^{\circ}0$ band, which was mainly used in this work, was 1.34 J/cm^2 without focusing.

Selection of a particular rotational line is achieved by rotating the micrometer located at the back of the laser unit, which turns the intracavity grating until the desired line is obtained. The wave length of the rotational line was identified with a pre-calibrated Model 16-A laser spectrum analyzer made by Optical Engineering Inc. After the desired line was observed in the spectrum analyzer, the micrometer was varied slightly until a maximum energy output was obtained.

The micrometers attached in front of the laser unit, which

move the output coupler vertically and horizontally, were varied until the highest energy and spatially uniform beam were obtained. An iris with a 3/4" or 1 cm diameter was used to reduce the beam size and was positioned to get the most uniform energy beam. The laser beam profile for the 3/4" size beam was measured using a 1/8" diameter iris placed at different positions across the 3/4" beam. The beam profile is shown in Figure 1. The variation in fluence, ~5% across the beam, was very small. This was determined by Clara Jang[5].

The energy of the laser pulse was measured by a pre-calibrated Scientech energy meter, Model 38-0102. This energy meter was carefully calibrated again after long term experiments. No big deviation was observed. A fluence of $0.5-1.3$ J/cm^2 for R(30) could be obtained without focusing. The energy fluence was reduced by placing successive layers of Handi Wrap (Dow Chemical) plastic film between the sample and laser. For higher energy fluence, up to 3.8 J/cm^2, a Galilean telescope was used. It consisted of two BaF_2 lenses, one converging (f=75 cm) and the other diverging (f=37.5 cm). The diverging lens was place 37.5 cm away from the converging lens. The maximum energy fluence that could be obtained by the telescope was ~4 J/cm^2, without damage to the second diverging lens. The telescope gives a uniform energy fluence and a uniform irradiated volume throughout the reaction cell.

For fluences higher than 3.8 J/cm^2, only one long focal length (f = 75 cm) lens was used, i.e., no second lens was inserted to make the laser beam parallel. The sample, which was
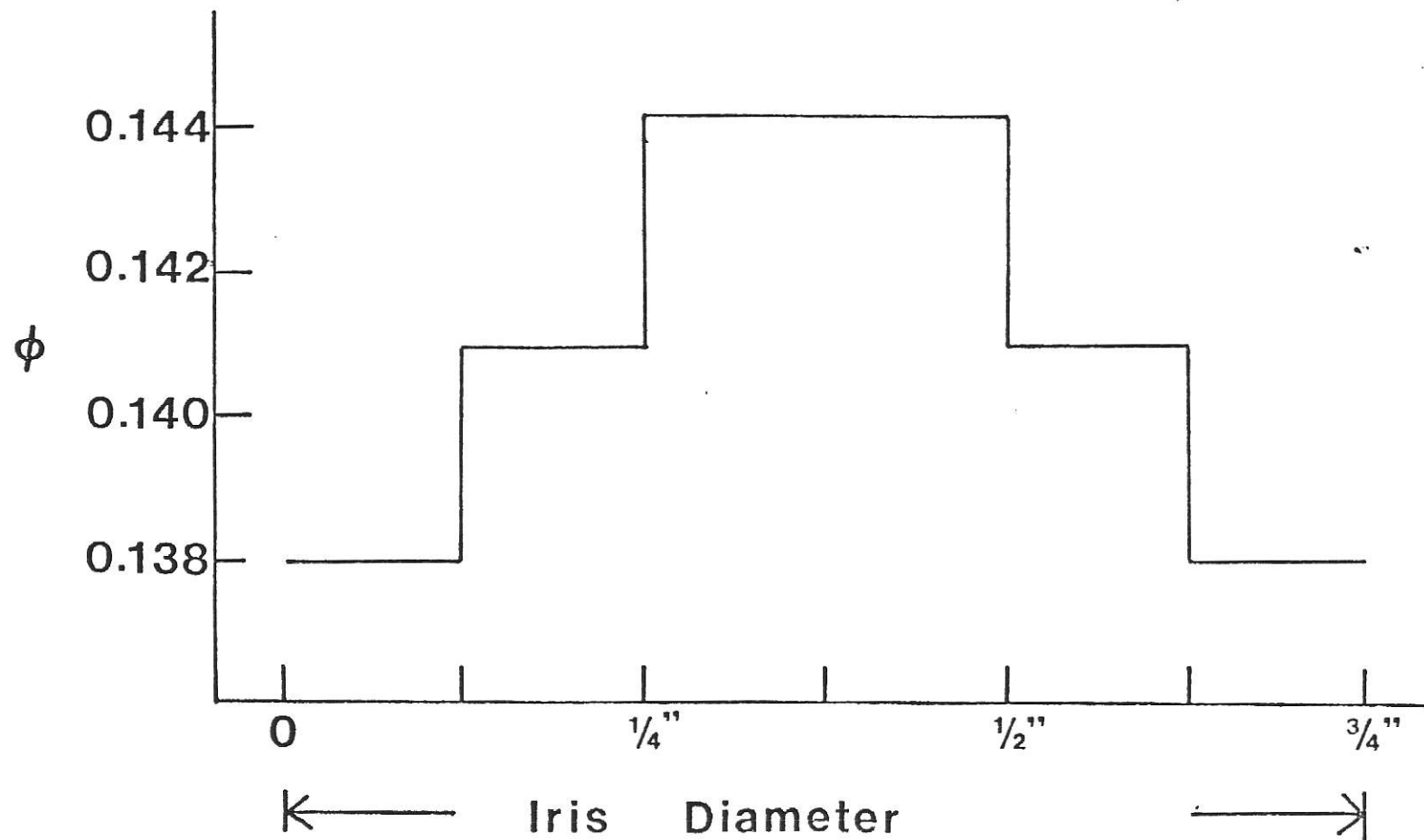
Figure 1 Measured spatial pattern of the CO_2 laser beam. The laser beam
profile was measured using a 1/8" diameter iris placed at
different positions across the 3/4" beam. The laser beam pattern
shows a superposition of several transverse modes.

(This diagram is copied from Clara Jang's Ph.D. thesis)

contained in a thin cell, was then placed at various positions to obtain various fluences. The maximum fluence used in this work was 5.3 J/cm^2, at higher fluence the cell windows were damaged.

II. Chemicals

All experiments were done in the gas phase. The starting material CF_3CH_2Cl (PCR Research Chemicals,Inc.) contained < 1% of CF_2Cl_2 was measured as GC-mass spectrometry (Finnigan 4000) and thermal conductivity(TCD) gas chromatography (Hewlett Packard 700 chromatograph). The b.p. of $CF_3CH_2Cl(6.9^oC)$ is higher than CF_2Cl_2 (-29.8^oC), so the impurity was removed by fractional distillation using a benzene slush bath at 5^oC. The slush was prepared by pouring liquid N_2 into benzene with stirring until a slush is formed, the temperature is maintained by periodically adding N_2 to maintain the slush, the purified sample was then degassed under vacuum, resulting in < 0.1 % CF_2Cl_2 impurity as determined by gas chromatography (TCD).

Samples of $CF_2=CHF$, $CF_2=CHCl$, $CF_2=CH_2$, $CHF=CHF$, C_2F_4, C_2F_6, SiF_4 (all of the above chemicals are from PCR Research Chemicals,Inc.), toluene (distilled, Fisher Scientific Co.), N_2 (Union Carbide Co.) and He (Air Products) were stored as gases in Pyrex vessels, which were attached to a vacuum system that was capable of achieving a pressure of 10^{-3} torr. The vessels were fitted with greaseless needle valves and teflon stopcocks that regulated the gas flow. Pressures were monitored with pre-calibrated MKS Baratron pressure transducers, type PDR-3. The minimum pressure that could be measured was 0.001 torr.

III. Measurement of Laser Absorption Cross-section, $\sigma_L(\emptyset)$

The $\sigma_L(\emptyset)$ were measured with a dual pyroelectric detector arrangement[5], as shown in Figures 2 and 3. A small fraction of the laser energy entering and leaving the reaction cell was reflected into two detectors, amplified and recorded by a microprocessor, and viewed on the screen of the oscilloscope. The dual detector arrangement is sensitive and can measure $\pm 1\%$ absorption. For unfocused laser beam experiments, the arrangement shown in Figure 3 was utilized. When energy fluences >1.5 J/cm^2 were required, the telescope arrangement shown in Figure 3 was added with the Ge flat being replaced by a NaCl flat; other parts of the detection system were the same as at low fluence. A fraction f_1 ($\sim 2\%$) of the laser energy was reflected by a NaCl flat into a detector (DET2). The laser beam with the reduced energy, E_1, then passed through the cell and a fraction of the transmitted beam, f_2, was reflected by a Ge or NaCl flat into the detector(DET1); $f_2 \sim 28\%$ by a Ge flat and $\sim 2\%$ by a NaCl flat. For low fluence experiments, the second beam splitter was removed and (DET1) was placed directly behind the sample cell.

The empty reaction cell was placed between two lenses as shown in Figure 4 and the preamplifier gains were adjusted so that the maximum values of peak 1 and peak 2 were 2-3 volts and the ratio of peak 2 to peak 1 was approximately 1.0 . The (peak 2 /peak 1)ratio for the empty cell is called R(vac). Then the cell containing the sample was placed in the sample position. The sample absorbs some of the laser energy and gives a ratio (peak 2/peak 1) = R(sample). The ratios can be expressed as[5]

Figure 2   Dual Detector arrangement for measurement of $\sigma_L(\phi)$ at low energy fluences
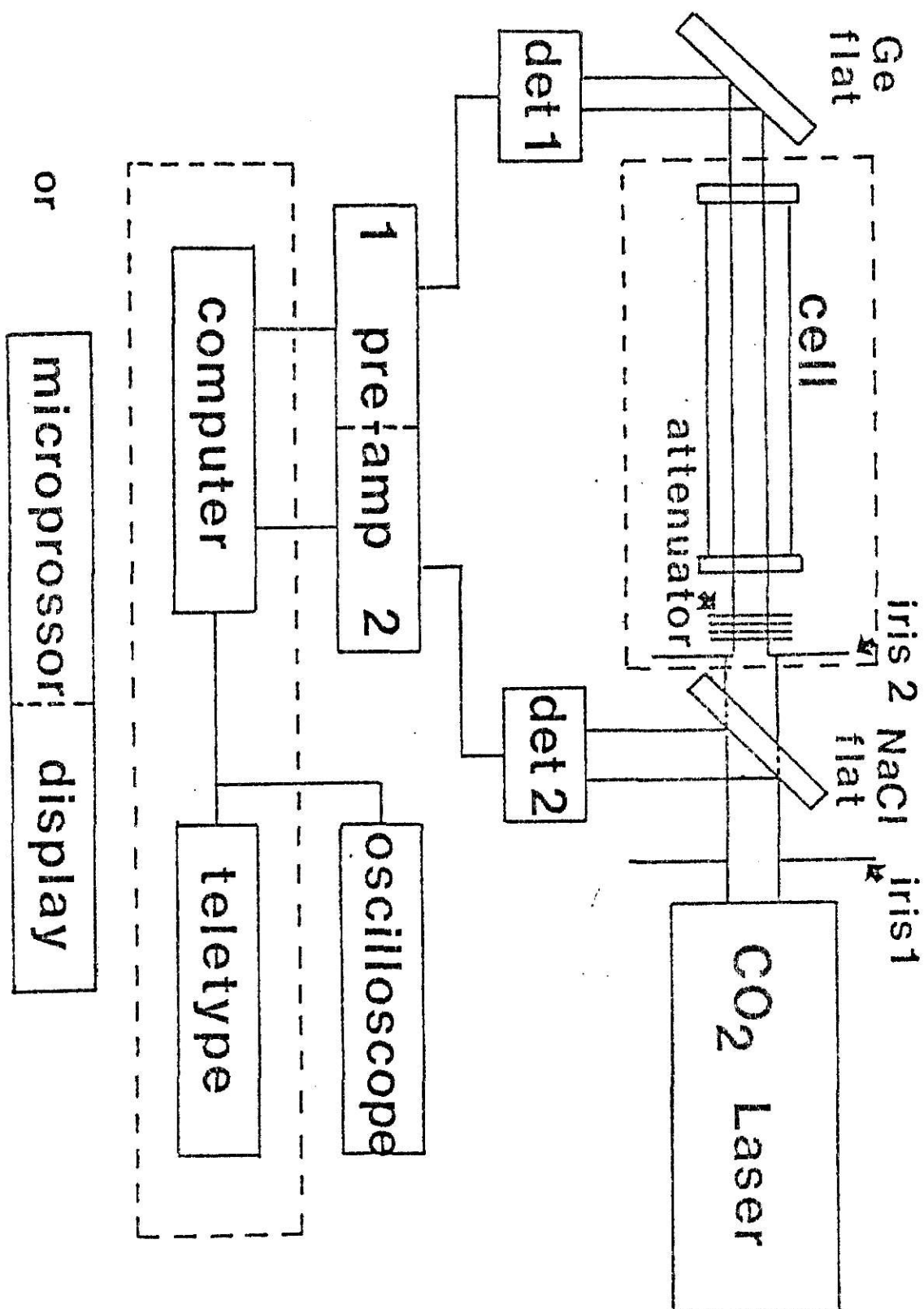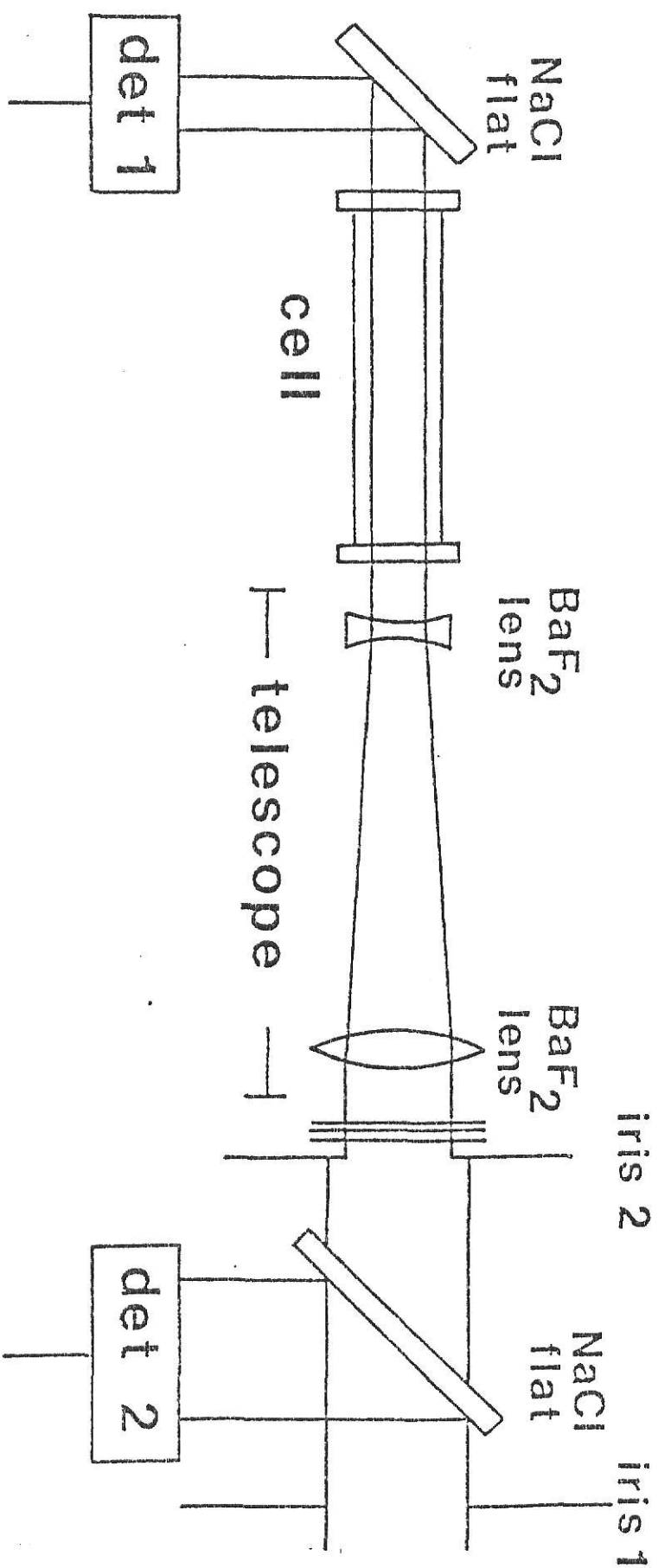
Figure 3 Arrangement for measuring $\sigma_L(\phi)$ at high energy fluences. Other parts of detection system were the same as shown in Figure 2

$$\left(\frac{peak2}{peak1}\right)_{vac.} = \frac{E_2(1-Lw)f_2\,\alpha}{E_1f_1\beta} = R(vac)$$

$$\left(\frac{peak2}{peak1}\right)_{sample} = \frac{T_2E_2(1-Lw)f_2\,\alpha}{E_1f_1\beta} = R(sample)$$

where $\quad E_1$ = energy before the first NaCl reflector

$\quad E_2$ = energy after the reaction cell

$\quad Lw$ = loss by the NaCl windows of the cell

$\quad f_1,f_2$ = fractions of reflected energy by the first

NaCl flat and second NaCl or Ge flat

$\quad \alpha,\beta$ = gains of preamp1 and preamp2

then

$$\frac{Rsample}{Rvac} = \frac{TE_2(1-Lw)f_2\,\alpha/E_1f_1\beta}{E_2(1-Lw)f_2\,\alpha/E_1f_1\beta} = T = Transmittance$$

From the ratio, we obtain the transmittance for the sample. Whenever the energy fluence and or the geometry were changed, R(vac) was reset. Even at the same energy fluence, R(vac) was checked several times to account for possible changes in the pulse-to-pulse energy.

The absorption cross-section, $\sigma_L(\emptyset)$, was calculated by the equation below from the transmittance values.

$$lnT = -\sigma_L(\emptyset)NX$$

X = length of cell,cm

N = concentration in molecules/cm^3

$\quad = 3.24 \times 10^{16}$ at 1 torr, 300°K

If the system follows Beer's law, the given pressure were used to obtain the best $\sigma_L(\emptyset)$.

IV.   Identification of Reaction Products

The reactant and products from the multiphoton laser induced unimolecular reaction were analyzed with a Varian Model 2700 Series gas chromatograph equipped with a H_2 flame ionization detector.   A 5´ long, 1/8" diameter copper column filled with Porapak Q and operated with a 55 ml/min flow rate of helium, carrier gas at 70-80°C was used to separate the components. Absolute gas chromatography calibrations were done for the reactant and the main products, $CF_2=CH_2$ $CF_2=CHF$, $CF_2=CHCl$. Whenever a new experimental series was started, new calibrations were made. Calibrations were done from carefully measured amounts of sample in a standard volume using the same GC conditions as for the laser experiments. · The GC detectivity was defined as the ratio of the peak height to the sample size (in torr units for the standard volume, 30.28 cm^3).

Figure 4 and 5 shows the calibration curve for CF_3CH_2Cl, $CF_2=CHF$ and $CF_2=CHCl$, in a 30.28 cm^3 cell. The peak area and peak height of all compounds showed linear responses versus sample size, since the peaks were narrow and symmetric with no significant tailing. The reproducibility of the calibration for 0.05 torr of CF_3CH_2Cl in the 30.28 cm^3 gas cell utilizing a gas chromatography Porapak Q column, temperature 80°C and a helium flow rate of 55 ml/min is ±0.001 torr.

The standard procedure for sample irradiation and analysis was the following. After a good vacuum was obtained, 0.05 torr of reactant was transferred to the 30.28 cm^3 irradiation cell and the pressure was carefully measured with the 0-10 torr MKS
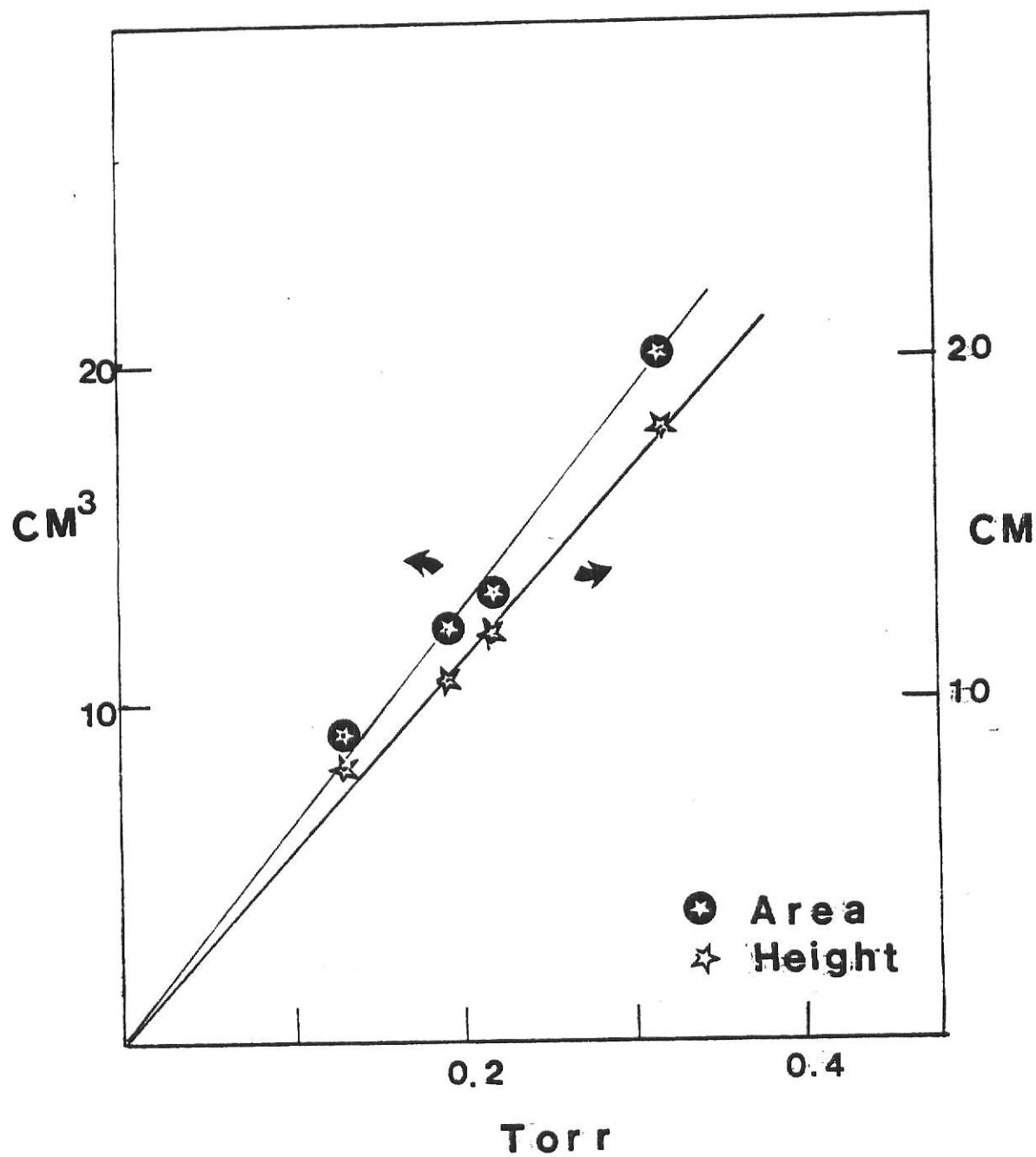
Figure 4   G. C. calibration curve for CF_3CH_2Cl of peak area and peak height. This calibration curve was obtained using a Porapak Q column at $80^{\circ}C$. The pressure axis is the pressure in a 30.28 cm^3 standard volume.
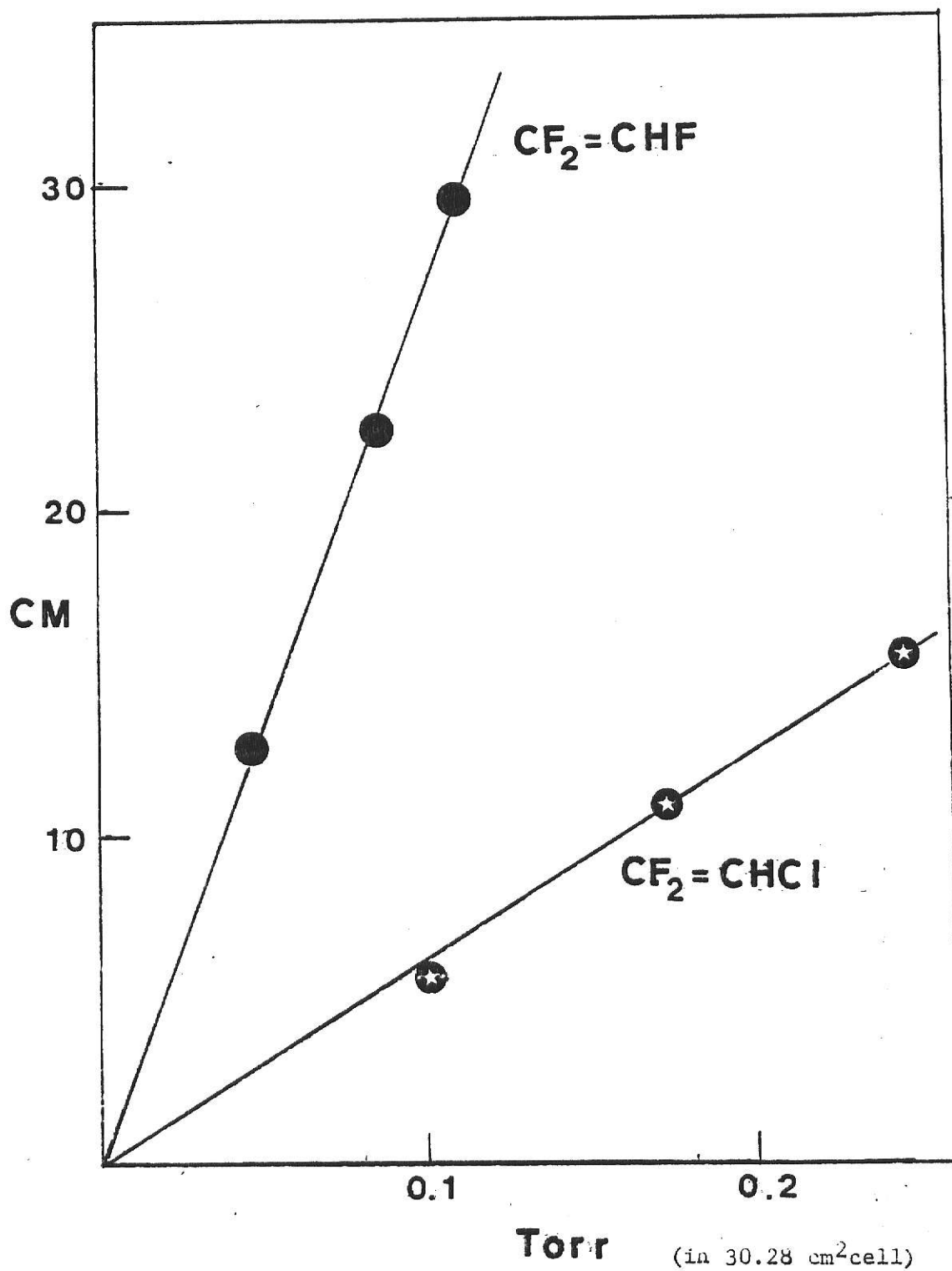
Figure 5   G.C. calibration curve for $CF_2 = CHF$ and $CF_2 = CHCl$. This calibration curve was obtaining using a Porapak Q column at 70°C.

Baratron pressure transducer. The cell was then placed in front of the CO_2 laser and irradiated with several pulses. The cell was then transferred to the vacuum unit of the gas chromatography. After a good vacuum (10^{-3} torr) was obtained, the injection loop was cooled with liquid nitrogen, the valve to the reaction cell was quickly opened to allow the sample to freeze into the injection loop, while the transfer was monitored by the pressure gauge. Once the transfer was complete, the injection loop was isolated and, while cooled with liquid nitrogen, it was pressurized with the He carrier gas. After being isolated again, the loop was heated with hot water and the sample was injected into the GC column by simultaneously opening two valves connected to the GC column and carrier gas column. This technique is very effective in quantitative transfer of small gas samples i.e., 0.05 torr gas sample in 30.28 cm^3 cell.

The products from laser irradiation of CF_3CH_2Cl were identified by GC-Mass spectrometer (Finnigan Model 4000). The sample from the 30.28 cm^3 reaction cell at 0.05 torr CF_3CH_2Cl was too low to be satisfactorily injected into the GC-Mass spectrometer; therefore, a 30 cm long cell with 2 torr of CF_3CH_2Cl was used to obtain sufficient reaction products. The sample was condensed by means of liq.N_2 into a small steel tube (Figure 6). The gas then was removed from the tube by a gas syringe (250 μl Hamilton company, gas tight) and inserted through a Teflon septum into the inlet of GC-Mass spectrometer.

TO VACUUM

TRAP WITH LIQ. N_2.
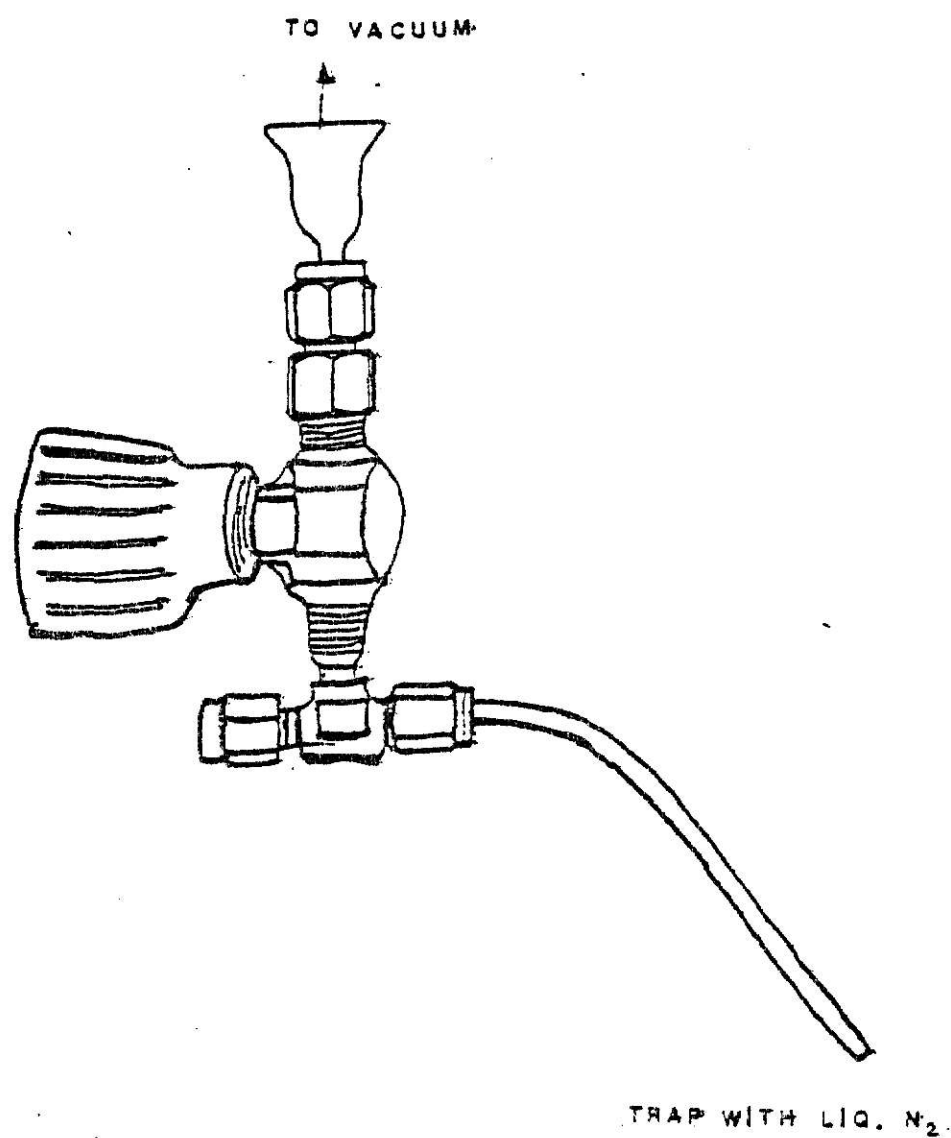
Figure 6   Steel tube for transferring sample from
vacuum system to GC-Mass

V. The P($\emptyset$) Measurements for Laser Induced Reaction

The reaction probability, P($\emptyset$), is defined as the fraction of molecules that react per laser pulse in the irradiated volume. For sample exposed to i pulses, the reaction probability is given by

$$P(\emptyset) = \frac{V_o}{G_o} [1 - (C_i/C_o)^{1/i}]$$

V_o = the total volume of the reaction cell

G_o = the irradiated volume

C_i = concentration of the reactant after i pulses

C_o = initial concentration of the reactant

i = number of pulses

The irradiated area, A, was measured with burn paper. If the burn paper appeared as in Figure 7, a and b were measured from blue edge to blue edge. The irradiated area is $A = (axb)\pi/4$ and the irradiated volume is $G_0 = A \times (cell\ length)$

Figure **7**
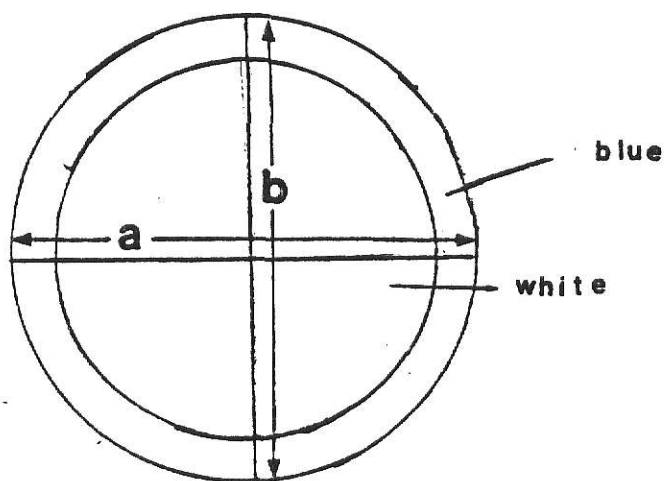
At some laser fluence, the irradiated area measured from the burn paper was smaller than the iris. If the iris is small, i.e., 0.74 cm^2 for $\emptyset$=0.2-0.4 J/cm^2 in sensitization reaction or in one focal lens high laser fluence experiment. Because of the inhomogeneous of the laser beam, the burn paper area is only 1/2 of iris area, this will increase the fluence measurement and reaction probability twice as it should be. But if the fluence is high(except the one lens experiment), the burn paper area is close to the iris, so we should choose the largest area as the irradiated area, A.

VI.   Quenching and Scavenging Experiments

Some experiments were done with CF_3CH_2Cl and added He, N_2 and toluene bath gases. Toluene acts as a scavenger for free radicals, as well as a deactivating bath gas. The CF_3CH_2Cl pressure was always 0.05 torr, and different amount of bath gas were used in making the gas mixture. The CF_3CH_2Cl/toluene mixture with certain composition was prepared and stored in a large vessel at least 30 minutes before the experiment for complete mixing. Toluene has very long retention time under the gas chromatography conditions used here and a very broad peak comes out after several injections. This necessitates raising the column temperature to $150^{o}C$ twelve hours after several analyses. The N_2/CF_3CH_2Cl mixture   was   made   in   the   same   way   as CF_3CH_2Cl/toluene mixture.

Instead of preparing the sample in a big vessel, the He/CF_3CH_2Cl mixture was taken from the He and CF_3CH_2Cl gas ves-sel directly each time. This is not a good way due to the slow speed of the gas diffusion, but, these experiments were not intended for quantitative interpretation.

VII. Procedure for the Sensitized Reaction Experiment

Sensitized reactions were done with 5 torr of SiF_4 and 0.4 torr of CF_3CH_2Cl; a fluence range of 0.2 to 0.6 J/cm^2 was used. The laser beam was used without focusing; plastic films were used to reduce the fluence. An aperture of 0.7 cm diameter was used to make the heated volume a small fraction (1:25) of the total cell volume. This ensures that "cooling" after the laser pulse is effective. Since the reaction cell never gets warm, the sensitized technique has been termed "cold pyrolysis"[13]. After several pulses, the gases were transferred to the injection loop of the GC and analyzed in the usual way.

The laser frequency should be strongly absorbed by the sensitizer, SiF_4, but not absorbed by the reactant, CF_3CH_2Cl. The P(40) line of 00^01-02^00 band at 1027.4 cm^{-1} matches this need. The pulse-to-pulse laser energy variation was ±10% and long term energy stability was ±10%. The gas mixture, 5 torr SiF_4 and 0.4 torr CF_3CH_2Cl, was prepared and allow to stand at least twenty minutes to make sure it was well mixed. Experiments were done at ϕ = 0.2 to 0.6 J/cm^2 range. There was no reaction for irradiation of 0.4 torr CF_3CH_2Cl alone, as shown by irradiating a cell at a fluence of 0.45 J/cm^2 with the P(40) line for 20 pulses.

Experiments also were done with toluene added as a radical scavenger in the sensitized reaction. The set-up was the same as for sensitized reactions, except that the gas mixture was 5 torr SiF_4, 0.4 torr CF_3CH_2Cl, and 0.14 torr Toluene. The experimental fluence range also was ϕ = 0.2-0.6 J/cm^2 for the sensitized experiments.

RESULTS

I. Spectroscopic Properties of CF_3CH_2Cl

The high resolution infrared spectrum of CF_3CH_2Cl shown in Figure 8 was taken with an FT-IR (IBM 98) instrument in the frequency region from 1070 cm^{-1} to 1130 cm^{-1} with resolution of 0.03 cm^{-1}, the rotational structure is just becoming observable at this resolution in the 1105 cm^{-1} region. Because of the declination of laser intensity as the wavelength moves toward the CF_3CH_2Cl absorption maximum. The frequency we chose for irradiation was 1084.6 cm^{-1}, the R(30) line of the $00^{\circ}1-02^{\circ}0$ band, which is on the low frequency side of this moderate strength absorption band.

The assignment[15] of the infrared frequencies for CF_3CH_2Cl is shown in Table 1.

Table 1   Vibrational Frequencies of CF_3CH_2Cl

A´ (totally symmetric vibrations)			A" (Non-totally symmetric vibrations)		
CH_2	ss	2294	CH_2	as	3044
CH_2	δ	1443	CF_3	as	1277
C-C	s	1339	CH_2	tw	1100
CF_3	as	1267			irradiate here
CH_2	w	1159			R(30),1085 cm^{-1}
CF_3	ss	855	CH_2	r	905
C-Cl	s	801	CF_3	aδ	541
CF_3	sδ	639	CF_3	r	355
CF_3	aδ	541	C-C	τ	109
CF_3	r	330			
C-C-Cl	δ	180			

ss : symmetric stretch   r : rock
s : stretch   δ : symmetric deformation
w : wag   aδ : asymmetric deformation
as : asymmetric stretch   tw : twist
                              τ : torsion
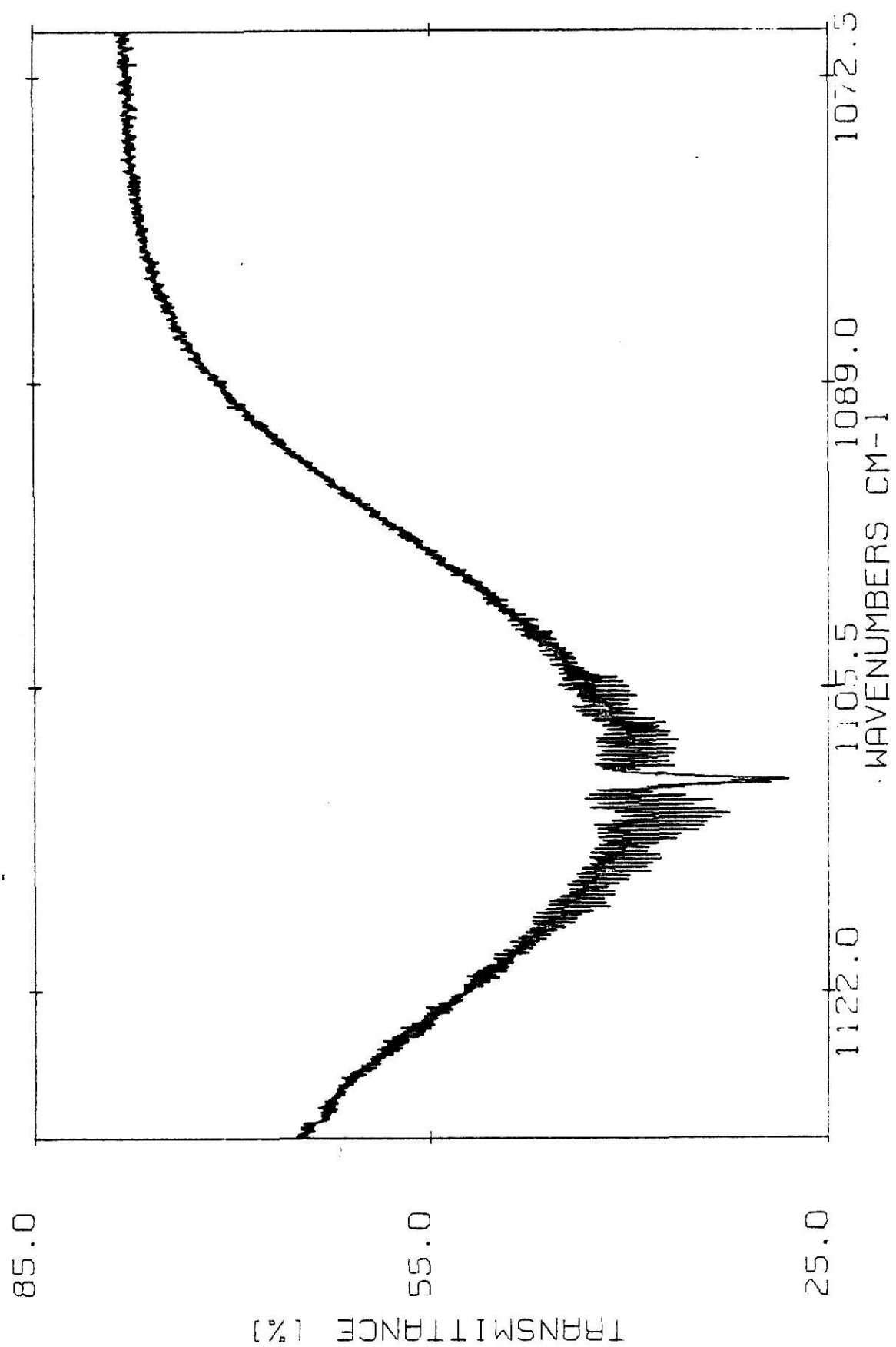
Figure **8**   Absorption spectrum of CF_3CH_2Cl at 0.03 cm^{-1} resolution

II. Laser Induced Chemical Reaction of CF_3CH_2Cl

1. Products from laser photolysis of CF_3CH_2Cl

Most samples were analyzed isothermally at 80°C with the Porapak Q column. Typical gas chromatograms are shown in Figures 9 and 10. The retention time for the three main products and the reactant are shown in table 2 for a carrier gas flow of 55 ml/min. :

Table 2

Substance	retention time 70°C	retention time 80°C
$CF_2=CH_2$	2 min	80 sec
$CF_2=CHF$	2 min 30 sec	100 sec
$CF_2=CHCl$	7 min	6 min
CF_3CH_2Cl	17 min	14 min

The three main products were identified by the retention times of the pure substances and by the GC-Mass spectra (described below).

After the analysis of the products by GC-mass spectra, a sample of the pure compound was injected directly to get a mass spectrum of the pure compound for comparison. The mass spectra of the reactant and main products are shown in Fig.11 , and the analysis of each compound is listed in Table 3.

The mass spectra of $CF_2=CH_2$ and $CHF=CHF$ are quite similar and the mass spectra can not distinguish between these isomers. However, isomers can be differentiated by the GC retention times. At 80°C and He=55 cm^3/min, the retention time of $CF_2=CH_2$ was 1.5 min while that for $CFH=CFH$ was 10 min (cis-trans isomers were not resolved).

A. $CF_2 = CH_2$

B. $CF_2 = CHF$

C. $CF_2 = CHCl$

D. CF_3CH_2Cl

E. CF_3CH_3

F. CF_2Cl_2
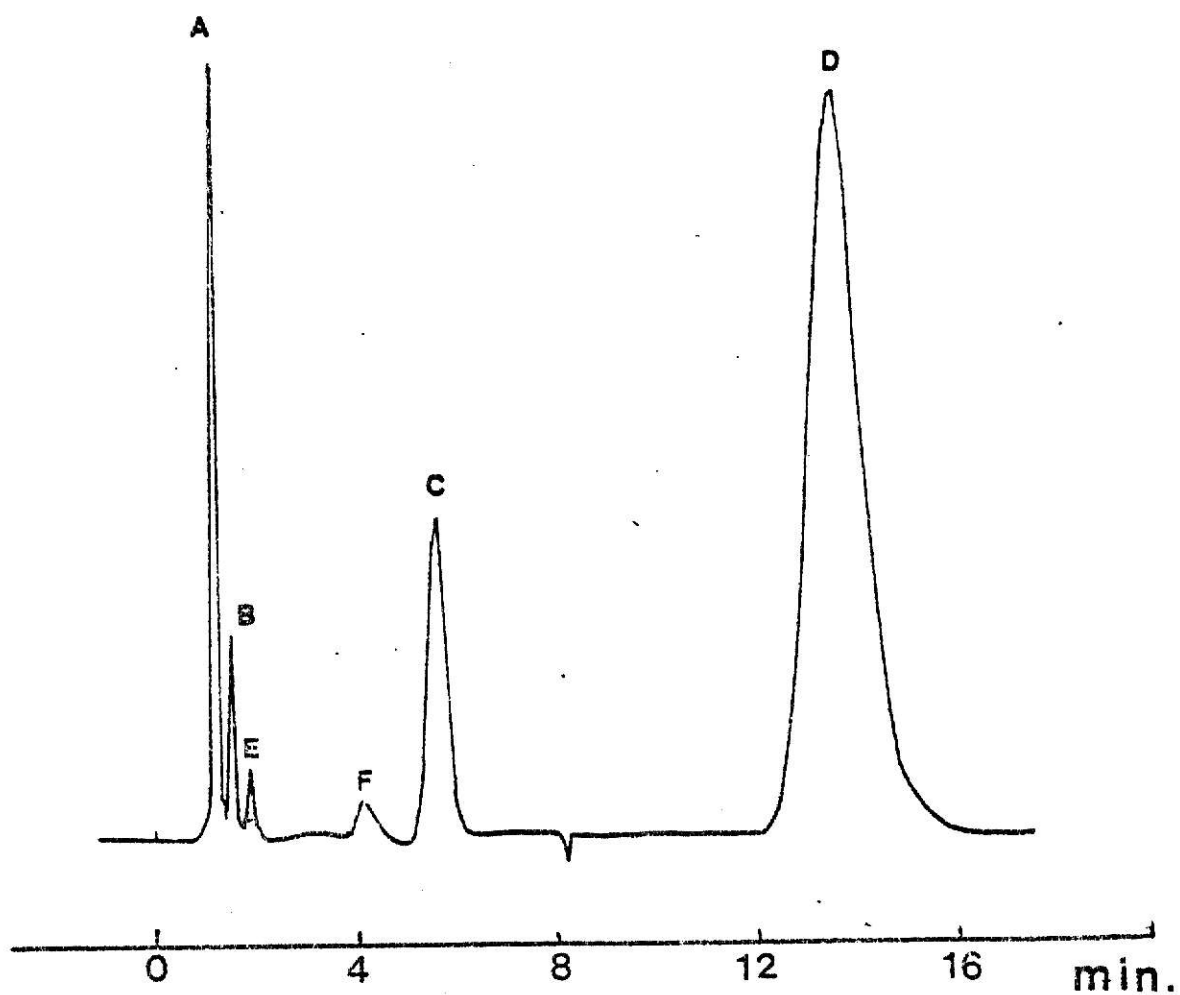
Figure 9   The G. C. spectrum of CF_3CH_2Cl laser induced reaction. (ϕ = 2.1 J/cm^2; $\kappa(30)$) for a Porapak Q column at $30^\circ C$.

A. $CF_2=CH_2$

B. $CF_2=CHF$

C. $CF_2=CHCl$
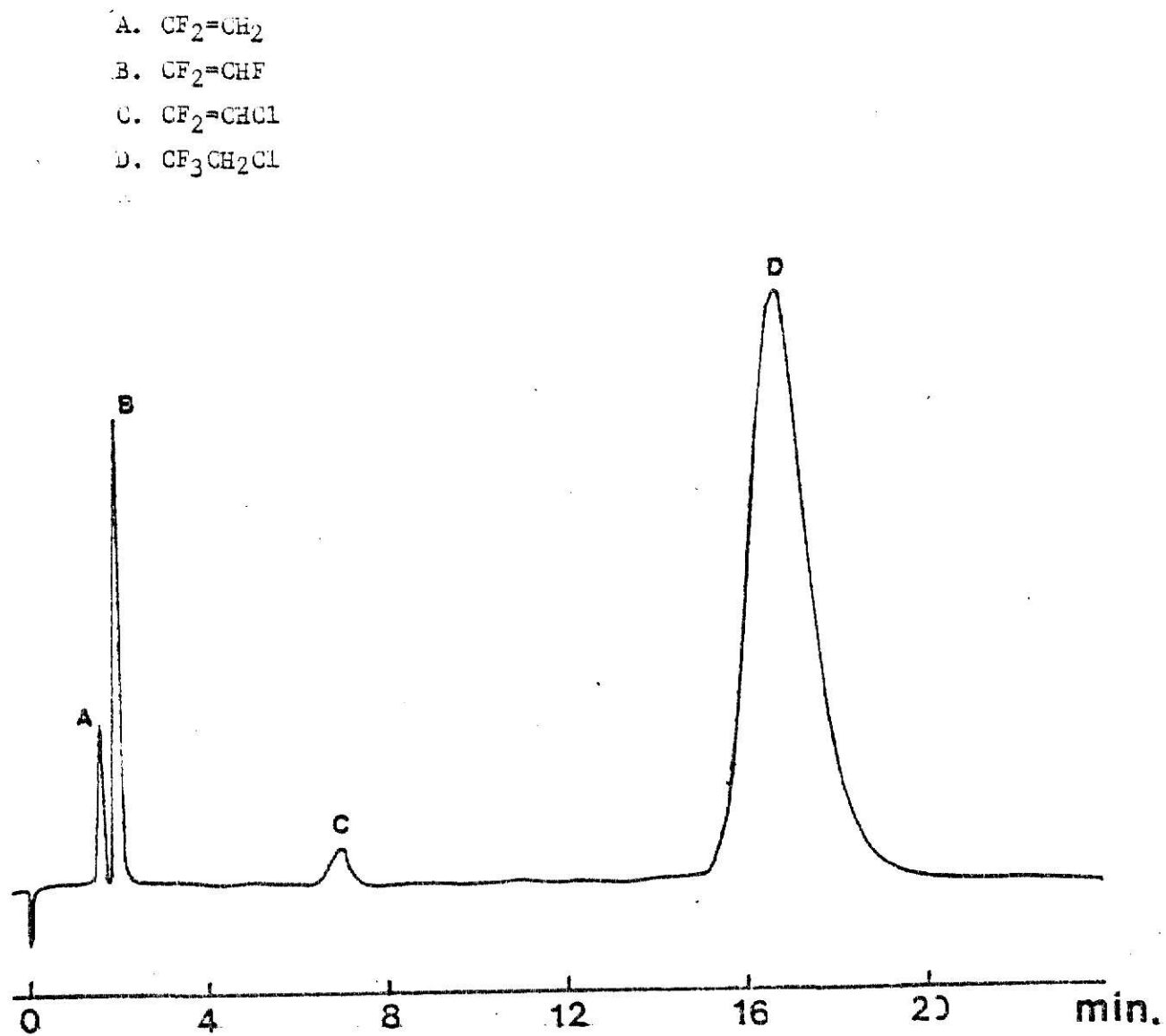
D. CF_3CH_2Cl

Figure 10   The G. C. spectrum of CF_3CH_2Cl laser induced reaction.

(R(30), $\phi = 0.5\,J/cm^2$) for a Porapak Q column at 70°C.

A. C_2F_6

B. C_2F_4

C. $CF_2 = CH_2$

D. $CF_2 = CHF$

E. CF_3CH_3

F. $CF_2 = CFCl$

G. $CF_3CH = CF_2$

H. CF_2Cl_2

I. $CF_2 = CHCl$
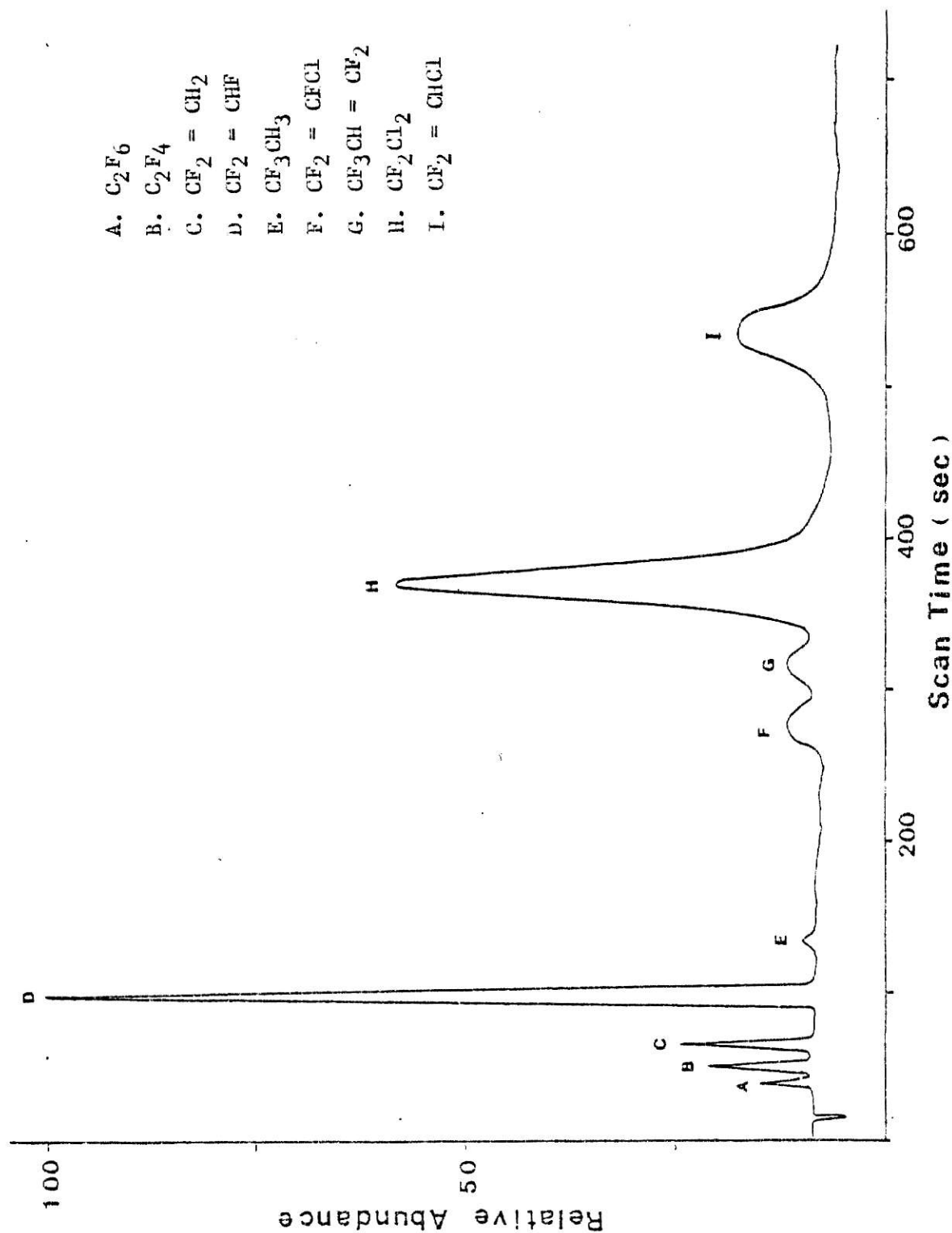
Figure 11   The G. C. spectrum from GC-Mass (Model Finnigan 4000) of CF_3CH_2Cl laser induced reaction (at $\phi = 1.6$ J/cm^2, R(30)) ; Porapak Q column.

Table 3

m/e	rel.abund.of std. sample	rel. abund. of product	ion
$CF_2=CH_2$			
44	50	47	$CFCH^+$
45	85	47	$CFCH_2^+$
50	4	4	CF_2^+
63	18	11	$CF_2=CH^+$
64	100	100	$..._H^+$
$CF_2=CHF$			
44	12		$CFCH^+$
50	12	7	CF_2^+
51	68	45	CF_2H^+
63	100	98	CF_2CH^+
82	72	100	$._+$
$CF_2=CHCl$			
48	12		
50	6	12	CF_2^+
63	12	22	CF_2CH^+
67	6	11	
69	3	5	
79	5	11	$CFCH^{35}Cl^+$
81	2	5	$CFCH^{37}Cl^+$
98	100	100	$CF_2CH^{35}Cl^+$
100	33	34	$CF_2CH^{37}Cl^+$
CF_3CH_2Cl			
49	47	34	$CH_2^{35}Cl^+$
51	20	11	$CH_2^{37}Cl^+$
69	27	26	CF_3^+
79	14	11	
83	98	69	$CF_3CH_2^+$
99	27	19	$CF_2CH_2^{35}Cl^+$
101	12	6	$CF_2CH_2^{37}Cl^+$
119	100	100	$CF_3CH_2^{35}Cl^+$
120	30	32	$CF_3CH_2^{37}Cl^+$

It was surprising to learn that $CF_2=CH_2$ is one of the main products. But, after careful comparison of the GC-Mass spectra and GC retention times, it was proven to be right. One of the products from laser induced reaction of CF_3CH_2Br also was $CF_2=CH_2$, which provides additional confirmation for identification of $CF_2=CH_2$ from MPR of CF_3CH_2Cl.

There are two minor products, C_2F_6 and C_2F_4, that appear on the gas chromatograms before the $CF_2=CH_2$ product for reactions induced at high fluence. Some minor products also appeared between the peaks for $CF_2=CHF$ and $CF_2=CHCl$; they were assigned as $CF_2=CFCl$, and $CF_3CH=CF_2$ from the GC-Mass spectra. There were also two components between the $CF_2=CHCl$ and CF_3CH_2Cl peaks; but, the peaks were too broad and too small to be identified by GC-Mass spectra. These minor products do not appear at low fluence (< 1.2 J/cm^2), When the laser fluence is > 1.2 J/cm^2, the minor products are observed; however, their total fractional contribution is between 2 % and 5 % at $\emptyset = 1.2 - 4.8$ J/cm^2. These were considered negligible compared to the main products and they were not studied. In the experiment with toluene, these minor products were reduced to only 1-2 % suggesting that some of the products are from radical reactions which were quenched by toluene.

No $CF_3CH=CHCF_3$, an expected product, from $CF_3CH:$ recombination was observed from GC and GC-mass spectra. We conclude that all of the carbene rearranged to $CF_2=CHF$.

The main products from the CF_3CH_2Cl reaction, $CF_2=CH_2$, $CF_2=CHF$ and $CF_2=CHCl$, were investigated in separate experiment

for laser induced reaction. Irradiations were done at high flu-
ence, i.e., 3.78 J/cm^2, for rather high pressure(0.5- 0.7 torr)
of each olefin at the same frequency, R(30), used in the
CF_3CH_2Cl reaction. In each case there was no reaction, which
eliminates the possibility of secondary MPD reactions of the
products.

Some laser work has been done with CF_2=CHCl[16] and
CF_2=CH_2[17]. They do undergo reaction, but for different frequen-
cies than used in this work. Excitation of CF_2=CHCl at 967.7
cm^{-1} with an energy fluence of 5-10 J/cm^2 in a molecular beam
experiment[16] gave both HCl and CF_2CH:. It was concluded that
two dissociation channels, namely C-Cl rupture and three-center
HCl elimination, must compete with comparable probabilities. No
HF four-centered elimination was reported.

$$CF_2=CHCl \longrightarrow C_2F_2 + HCl$$
$$\longrightarrow CF_2CH + Cl$$
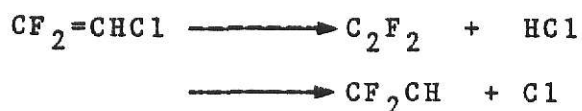
The IR photodissociation of CF_2=CH_2[17] at 944 cm^{-1} produces
vibrationally excited HF via collisionless molecular elimina-
tion.

From the IR spectrum of CF_2=CHF, there is no absorption
band around 1085 cm^{-1}, our selected laser frequency, accounting
for the lack of laser induced reaction of CF_2=CHF in our experi-
ments.

2. Dependence of Reaction Probability on Energy Fluence and
   Reactant Pressure

We define for unimolecular reactions the point at which the
deposited vibrational energy has reached equilibrium among all
degrees of freedom (including translations and rotations) of all
molecules within the irradiated volume as the differentiation
point between nonequilibrium laser-induced chemistry and the
onset of thermal chemistry. A relatively simple, but effective,
means of distinguishing between non-equilibrium unimolecular
laser process and a thermal reaction, as defined above, is to
introduce into the reaction cell a molecule which does not
absorb the laser radiation but which can undergo a unimolecular
thermal reaction with a threshold similar to the reactant molec-
ule. Such work has been done by Danen[2], et al. by using a
1 : 3 mixture of isopropyl bromide, a chemical thermometer, with
ethyl acetate. How low in total reactant pressure must one work
in order to avoid significant intermolecular V-T,R relaxation ?
Pressures of 0.1 torr or less are frequently found to be ade-
quate[2] . For pressures < 0.05 torr, thermal contribution to the
yields from irradiation of CF_3CH_2Cl should be negligible.

In the present work the $P(\emptyset)$ measurements were done with
0.05 torr of CF_3CH_2Cl. The laser beam was used either focused
(with telescope or long focal length lens) or unfocused using
the R(30), 1085 cm^{-1} line. The long laser pulse ($He:CO_2:N_2 =$
8.0:2.0:0.8 SCFH) consists of an initial spike of about 100
nsec at FWHM, followed by lower intensity tail of 1-2 μs, was
used in all experiments. Since << 5% of the laser radiation is

absorbed for a pressure of 0.05 torr, the incident fluence is virtually the same as the transmitted fluence and there are no significant fluence gradients within the cell.

The reaction probability, the ratio of $CF_2=CHCl/CF_2=CHF$, the fractional percentages of $CF_2=CH_2$, $CF_2=CHF$, $CF_2=CHCl$; Vo/Go, and the mass balance (major products) at a given energy fluence are shown in Table 4. Figure 12 shows the $P(\emptyset)$ vs. $\emptyset$ data for excitation of CF_3CH_2Cl with R(30). The threshold fluence for our experimental technique was around 0.4 J/cm^2 for 500 pulses. The high fluence region will be discussed in more detail in the following paragraph. $P(\emptyset)$ varies as $(\emptyset)^n$ with n = 3.

The reproducibility of the reaction probability data for 0.05 torr of CF_3CH_2Cl with R(30) was tested at $\emptyset = 2.3$ J/cm^2 ; the result was 0.13 ± 0.03 for three runs. The reproducibility is typical for reaction probability measurements at fixed 0. However the greatest uncertainty is in the fluence measurement. For the telescope experiment $\emptyset$ is uncertain by $\pm$ 0.15 J/cm^2. But, for the single lens experiment the laser beam was small and not homogeneous; so, the irradiated volume is not so well defined and the uncertainty in the area measurement raises the uncertainty in $\emptyset$ to $\pm$ 1 J/cm^2. Thus, for the $P(\emptyset)$ measurement, there is $\pm 5\%$ reproducibility for unfocused and for focusing with the telescope; the uncertainty increased to $\pm 20\%$ in the single lens region. The absolute error may be larger than the statistical reproducibility.

Great care is required for the high fluence experiments. For fluence higher than 3.7 J/cm^2, a single long focal length

Table 4   Reaction of CF_3CH_2Cl (0.05 torr) at
different laser fluences

A. (6-9-82)

i	Ci/Co	Ao cm^2	Vo/Go	Ø J/cm^2	P(Ø)
500	0.882	3.00	4.72	0.43	8.6×10^{-4}
200	0.860	3.00	4.72	0.55	2.5×10^{-3}
150	0.882	3.00	4.37	0.72	2.9×10^{-3}
150	0.850	3.00	4.37	0.72	3.9×10^{-3}
100	0.882	3.00	4.09	0.90	4.2×10^{-3}
100	0.882	3.00	4.09	0.90	6.7×10^{-3}
75	0.644	3.00	3.75	1.20	2.0×10^{-2}
75	0.725	3.00	3.75	1.20	1.5×10^{-2}
75	0.784	0.75	17.1	1.33	4.2×10^{-2}
75	0.792	0.75	17.1	1.33	4.2×10^{-2}
50	0.746	0.75	16.3	1.77	7.9×10^{-2}
50	0.780	0.75	16.3	1.77	6.6×10^{-2}
20	0.792	0.75	15.1	2.31	1.5×10^{-1}
20	0.829	0.75	15.1	2.31	1.3×10^{-1}
15	0.804	0.75	14.4	2.87	2.0×10^{-1}
15	0.746	0.75	14.6	3.33	2.6×10^{-1}
15	0.659	0.75	14.6	3.33	3.7×10^{-1}
10	0.792	0.75	13.6	3.73	3.1×10^{-1}
10	0.730	0.75	13.6	3.73	4.1×10^{-1}
20	0.755	0.33	35.2	3.34	4.3×10^{-1}
10	0.794	0.33	33.6	4.13	3.9×10^{-1}
10	0.820	0.33	33.6	4.13	4.5×10^{-1}
8	0.870	0.33	32.6	4.62	6.1×10^{-1}
10	0.850	0.33	32.6	4.62	6.3×10^{-1}
4	0.870	0.33	32.6	4.82	1.1×10^{0}
4	0.920	0.33	30.6	5.30	9.8×10^{-1}
5	0.880	0.33	30.6	5.30	8.2×10^{-1}
10	0.720	0.33	30.6	5.30	1.0×10^{0}

(continued)

Table 4   Continued   X = CF_2=CHCl/CF_2=CHF

ϕ_2 J/cm^2	CF_2=CH$_2$ fract.%	CF_2=CHF frac.%	CF_2=CHCl frac.%	X	mass balance
0.55					86.8%
0.72					90.0%
					87.0%
0.90		3.4	94.0	27.6	91.0%
					87.0%
1.20	5.0	5.4	86.0	15.9	85.0%
	4.2	4.8	87.7	18.3	86.3%
1.33	10.7	6.0	79.7	13.3	87.5%
	9.4	5.2	82.6	15.9	86.2%
1.77	18.8	7.8	70.2	9.0	90.4%
	17.4	7.3	72.1	9.9	92.3%
2.31	28.1	8.7	63.3	7.3	93.0%
	26.2	8.2	65.6	8.0	96.3%
2.87	38.3	10.3	51.4	5.0	99.0%
	38.5	10.6	50.9	4.8	98.0%
3.63	40.5	10.9	48.6	4.5	92.3%
	44.3	9.9	45.8	4.6	92.2%
3.73	40.9	9.0	50.1	5.6	97.6%
	40.0	9.7	50.4	5.2	97.6%
3.34	44.4	11.1	44.4	4.0	90.6%
4.13	48.2	8.5	43.3	5.1	89.0%
	48.8	8.5	42.7	5.0	90.0%
4.82	50.3	8.9	40.7	4.6	91.2%
5.30	65.8	13.5	20.7	1.5	96.3%
	62.8	8.0	29.1	3.6	97.2%
	59.5	8.7	31.7	3.6	98.1%

Condition:
laser line : R(30), 1085 cm^{-1}
upper part: unfocused condition
middle part: focused by the telescope
lower part: focused by one lens (f=75 cm)
cell length : 3 cm
Ao is the laser beam area in the cell, Vo and Go are total
reaction cell volume and irradiated volume, respectively.
i is the number of irradiations. Ci/Co is the ratio of the
remaining after i irradiations and initial conditions of the
reactant.

Figure 12   Reaction probability vs. laser energy fluence for
CF$_3$CH$_2$Cl (0.05 torr) irradiated at R(30)
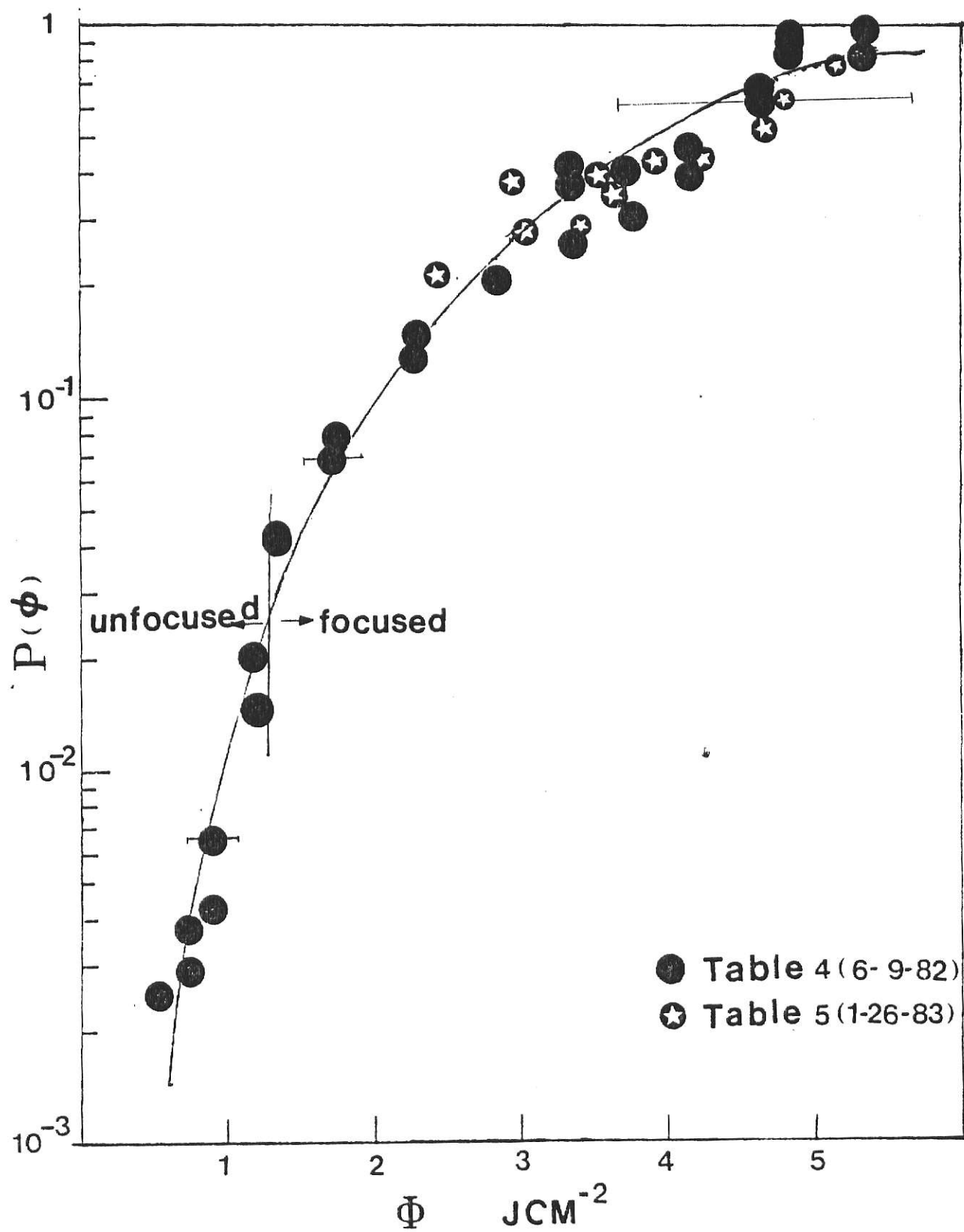
(f=75 cm) lens was used and each laser pulse damaged the NaCl window, necessitating changing the position at which the beam entered the cell after each pulse. If the same spot was irradiated, the NaCl window was broken. The experimental error could be reduced if more laser pulses were used but, due to the damage to the window at such a high fluence, it is inconvenient to use too many pulses or the window has to be replaced. The largest number of pulses used was 10 pulses at fluence 4.1 J/cm^2 and 4 pulses at 4.8 J/cm^2, and 10 pulses at 5.3 J/cm^2. The C_i/C_o ratio was 0.82 and 0.87, respectively. That means more than 10% undergo reaction, so the GC results should be more reliable than the irradiated volume measurements.

Experiment were done to check $P(\emptyset)$ at high laser energy fluence. For these experiments 0.025 torr toluene was added to 0.05 torr CF_3CH_2Cl; this pressure of toluene cause no quenching but should remove from radical processes. The result was similar with the experiments done seven months earlier. This demonstrated two things: First, the experimental results are good. Second, because the addition of toluene reduced the minor products, C_2F_4, CF_3CH_3, C_2F_6, but did not affect $P(\emptyset)$, the radical reactions are not important for the three main reaction channels even at high laser fluence.

In order to compare the results for the telescope and single lens experiments, data for both were collected from 2 to 4 J/cm^2. The overlap of the data points in Figure 12 between 2-4 J/cm^2 showed no obvious difference. The one lens experiment for 2-4 $J.cm^2$ did not raise the $P(\emptyset)$ systematically, so the $P(\emptyset)$

measured at $4 - 5$ J/cm^2 should be reliable. The second set of experimental results are shown in table 5. In these experiments, instead of changing the number of plastic films, the reaction cell position was changed every time to get the desired laser fluence, so the irradiated areas were not constant.

Table 5 Reaction Probability Measurement of CF_3CH_2Cl
at High Laser Fluence (1-26-83)

i	Ci/Co	Ao cm^2	Vo/Go	Ø J/cm^2	P(Ø)
5	0.848	0.91	11.09	3.63	35.0×10^{-2}
5	0.833	0.71	14.22	4.65	51.0×10^{-2}
5	0.793	0.70	14.42	4.72	65.5×10^{-2}
3	0.852	0.65	15.53	5.10	81.0×10^{-2}
10	0.654	1.13	8.93	2.91	37.0×10^{-2}
5	0.860	1.08	9.35	3.04	27.8×10^{-2}
10	0.747	1.36	7.42	2.42	21.0×10^{-2}
5	0.869	0.98	10.30	3.35	28.7×10^{-2}
3	0.901	0.79	12.86	4.21	44.3×10^{-2}
5	0.834	0.94	10.74	3.51	38.3×10^{-2}
3	0.889	0.84	12.02	3.92	44.0×10^{-2}

(All data for single focusing lens)

From Table 5, the reaction probability did not really go to 100% reaction, P(Ø)~80% at Ø=5 J/cm^2. In Table 4 the old P(Ø) data raised gradually but, suddenly jumped up from 60% to 100% in Ø=4.6-4.8 J/cm^2 region(in fact only 4 laser pulses was not reliable). This was not common, the recheck experiment gave a more reasonable result, from Figure 12, we drew a smooth curve and concluded that P(Ø)=80%, instead of 100% occurred at Ø=5.3 J/cm^2. More discussion will be in discussion section.

The $[CF_2=CHCl]/[CF_2=CHF]$ ratio vs. Ø plot is shown in Figure 13. The $CF_2=CHCl$ yield is always larger than for $CF_2=CHF$, i.e., HF elimination is faster than HCl elimination. The product distribution vs. Ø is shown in Figure 14, it is similar for toluene-added data (see Figures 14,19,20). All products increase with fluence, but the relative fractions of $CF_2=CH_2$ and $CF_2=CHF$ increase with increasing fluence. Mainly one sees that $CF_2=CH_2$ increases at the expense of $CF_2=CHCl$. At Ø = 1.0, the C-Cl rupture was the slowest channel. A crossing with HCl elim-
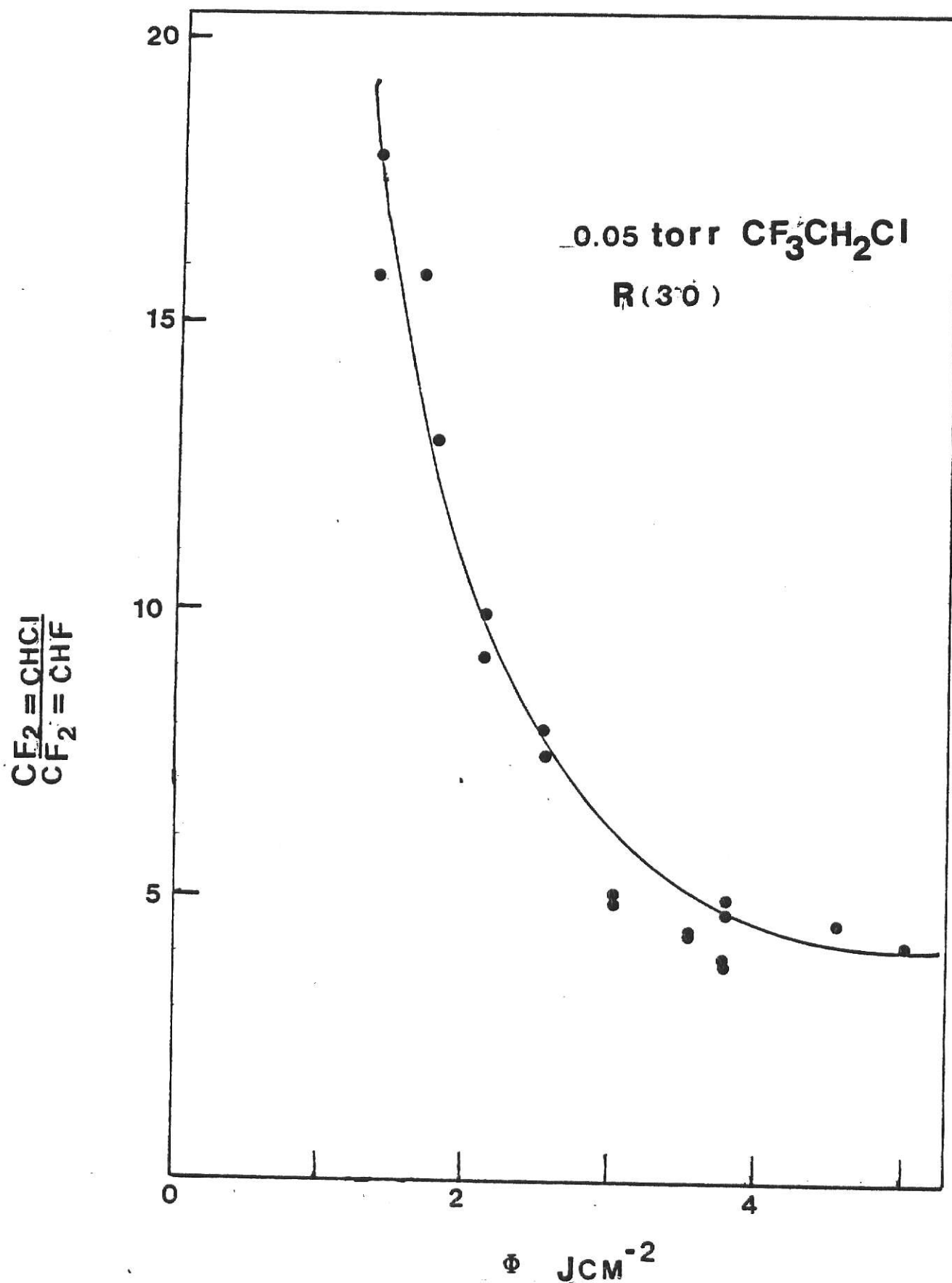
Figure 13 The ratio of CF_2CHCl / CF_2CHF vs. laser energy fluence for CF_3CH_2Cl (0.05 torr) irradiated at R(30)

Figure 14   The   percentages   ' of three main
products, $CF_2 = CH_2$, $CF_2 = CHF$, $CF_2 = CHCl$
vs. laser energy fluence for CF_3CH_2Cl
(0.05 torr) irradiated at R(30).
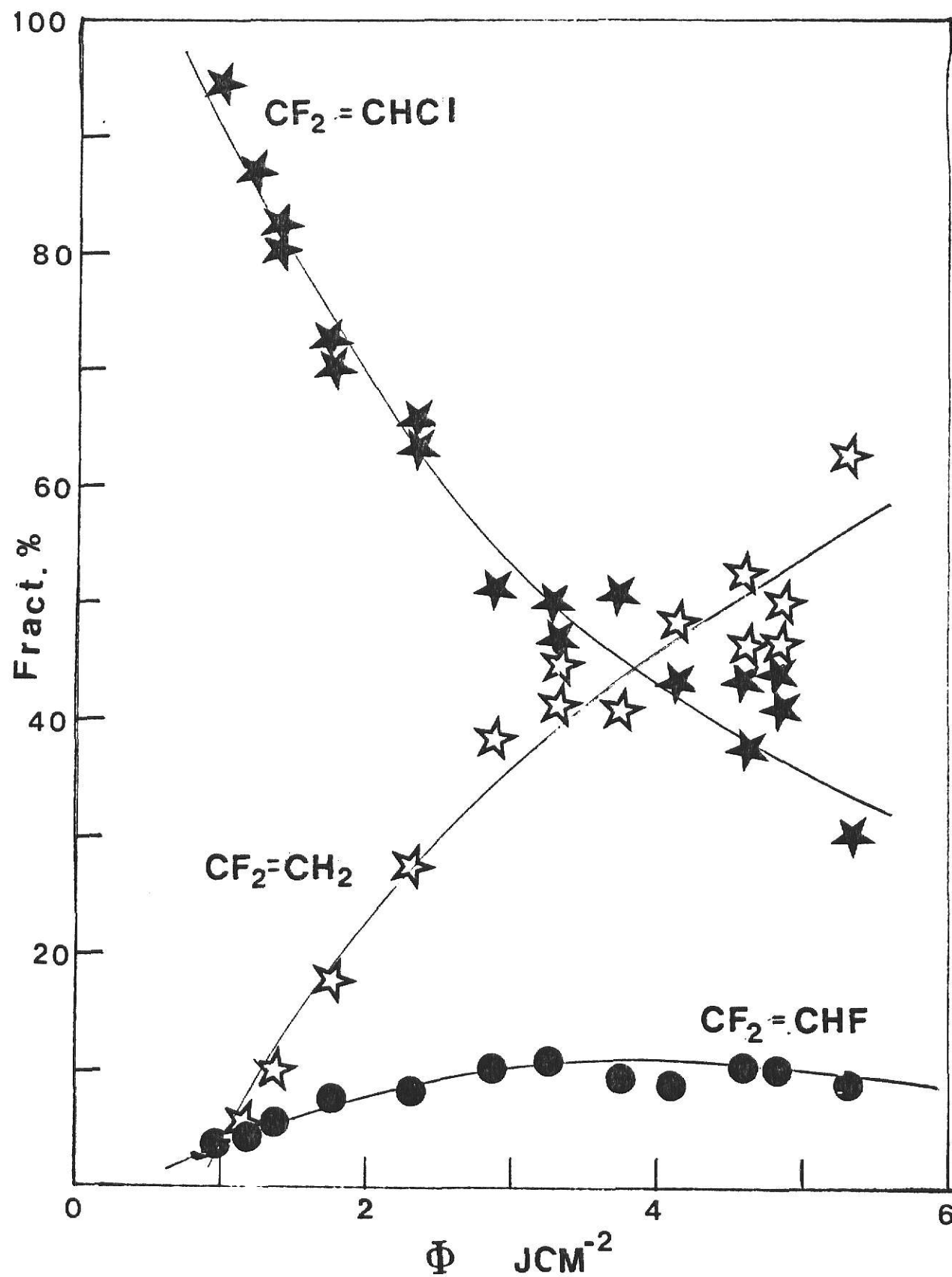
ination occurs at $\emptyset$ = 1.0 J/cm^2 and another crossing with HF elimination occurs at $\emptyset$ = 3.3 J/cm^2.

A set of experiments were conducted with different CF_3CH_2Cl pressures at constant laser fluence (table 6). The pressure was varied from 0.05, 0.1, 0.2, 0.4, 0.8, 1.6, to 3.2 torr. Four sets of experiments were performed at fluences of 1.55, 2.17, 2.33, and 2.55 J/cm^2. The P($\emptyset$) was constant with reagent pressure for P < 0.8 torr. For higher pressure P($\emptyset$) increased. These data are consistent with onset of enhanced reaction because of thermal contribution at the higher pressure. The thermal effects onset at lower $\emptyset$ for higher pressure and this is shown in Figure 15.

Plots showing the product distribution (CF_2=CHCl/CF_2=CHF, and fractional percentage distribution of CF_2=CH_2, CF_2=CFH, CF_2=CHCl) vs. reactant pressure at different fluences are shown in Figure 16,17,18. Clearly the relative product distributions change with increasing pressure at constant $\emptyset$, and CHF=CF_2 grows at the expense of CHCl=CF_2 as pressure increases. When the pressure is > 1.5 torr, CF_2=CHF predominates, which is similar to the shock tube[10] and laser sensitized result (with no added toluene). But the ratio of CF_2=CFH/CF_2=CHCl in this work is 1-2 in the 2 to 3 torr region, and 3-4 for sensitization reactions. They are both much lower than that in shock tube experiment, i.e., 9-13 for 2610 to 3350 torr CF_3CH_2Cl at ~1200°K. The product distributions change with pressure in a much different way than with $\emptyset$ (see Figure 13), for laser induced reaction, CF_2=CH_2 is the main product at high $\emptyset$.

Fig.15 Reaction probability vs. CF_3CH_2Cl pressure
irradiated with laser at R(30).
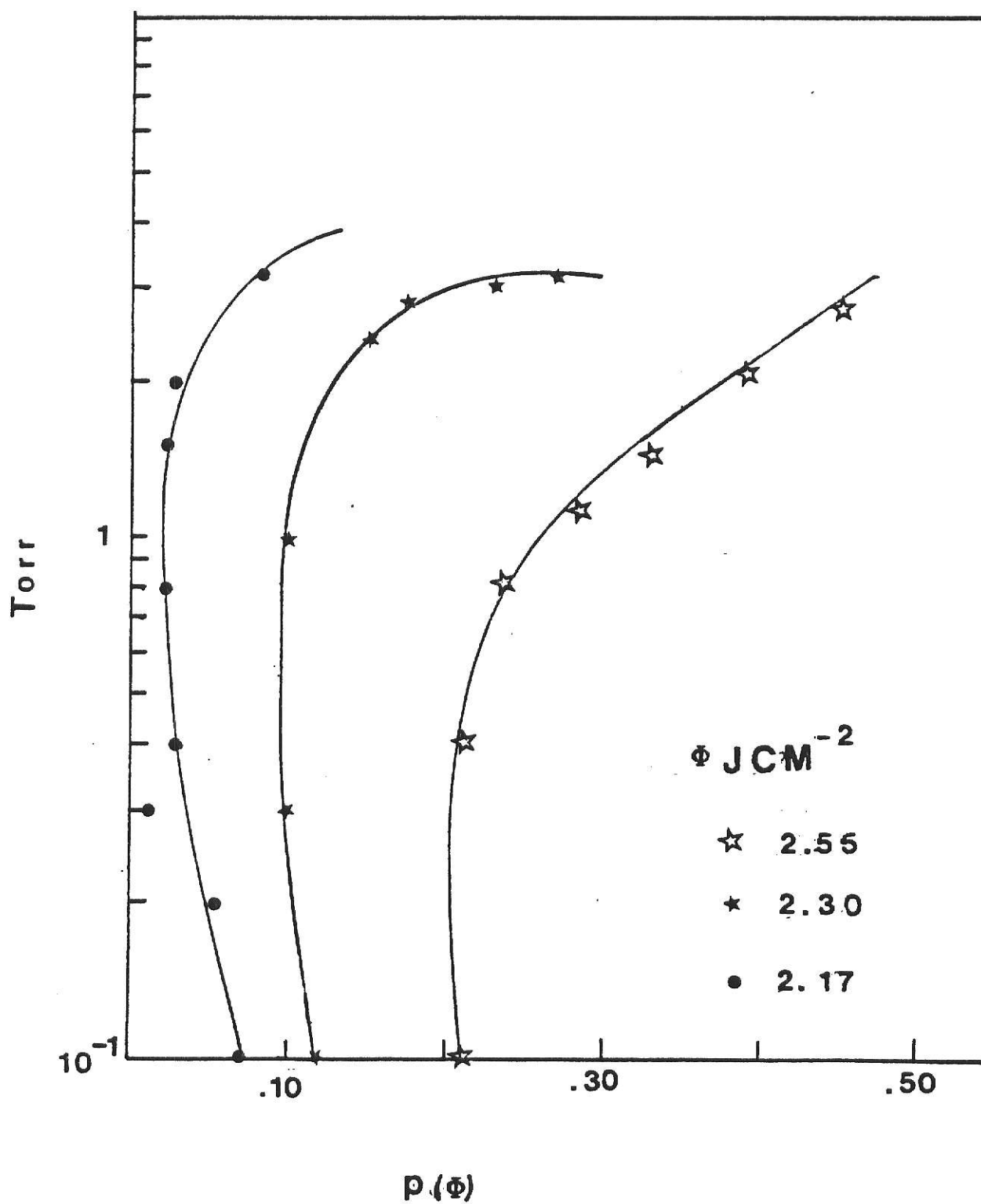
Table 6   MPR for Different CF_3CH_2Cl Pressure

A.

Co	C_i/C_o	$P(\emptyset)$	$CF_2=CH_2$	$CF_2=CHF$	$CF_2=CHCl$	$\dfrac{CF_2=CHCl}{CF_2=CHF}$	mass balance
torr			frac.%	frac.%	frac.%		
0.1	0.887	2.87%	8.0	5.2	87.0	16.7	85.3%
0.4	0.905	2.38%	5.4	1.8	92.8	17.0	90.8%
1.0	0.901	2.50%	15.6	12.5	72.0	5.8	91.1%
2.1	0.867	3.43%	19.4	40.9	39.7	0.9	87.8%
2.9	0.888	2.84%	19.5	46.0	34.6	0.8	90.6%

condition:
laser line : $R(30), 1085$ cm^{-1}
$\emptyset = 1.55$ J/cm^2 Ao = 0.75   i = 75
Vo/Go = 18.02   focused by telescope

B.

Co	C_i/C_o	$P(\emptyset)$	$CF_2=CHCl/CF_2=CHF$
torr			
0.05	0.840	9.7×10^{-2}	11.00
0.10	0.874	7.5×10^{-2}	11.17
0.20	0.900	5.9×10^{-2}	11.30
0.30	0.949	1.3×10^{-2}	11.00
0.40	0.943	3.3×10^{-2}	9.81
0.80	0.962	2.2×10^{-2}	4.44
1.62	0.951	2.8×10^{-2}	0.87
2.00	0.948	3.0×10^{-2}	0.72
3.20	0.859	8.5×10^{-2}	0.39

(continued)
condition:
laser line : $R(30), 1085$ cm^{-1}
$\emptyset = 2.17$ J/cm^2 Ao = 0.75   i = 30
Vo/Go = 16.82   focused by telescope

Table 6, continued.
C.

Ci	Ci/Co	P($\emptyset$)	$CF_2=CH_2$	$CF_2=CHF$	$CF_2=CHCl$	Y	mass balance
torr			frac.%	frac.%	frac.%		
0.1	0.758	20.78%	20.5	19.7	58.9	5.52	88.0%
0.4	0.750	21.06%	28.2	16.1	55.8	3.47	87.3%
0.7	0.725	23.40%	27.0	29.6	43.4	1.43	88.3%
1.2	0.679	28.40%	21.6	45.0	33.4	0.79	94.0%
1.5	0.637	32.89%	22.3	51.8	25.9	0.57	87.0%
2.9	0.541	44.90%	21.5	53.4	21.9	0.41	81.6%

condition:
laser line : R(30),1085 cm^{-1}
$\emptyset$ = 2.55 J/cm^2 A = 0.75 cm^2 i = 20
focused by telescope   Vo/Go = 14.84
Y : $CF_2=CHCl/CF_2=CHF$
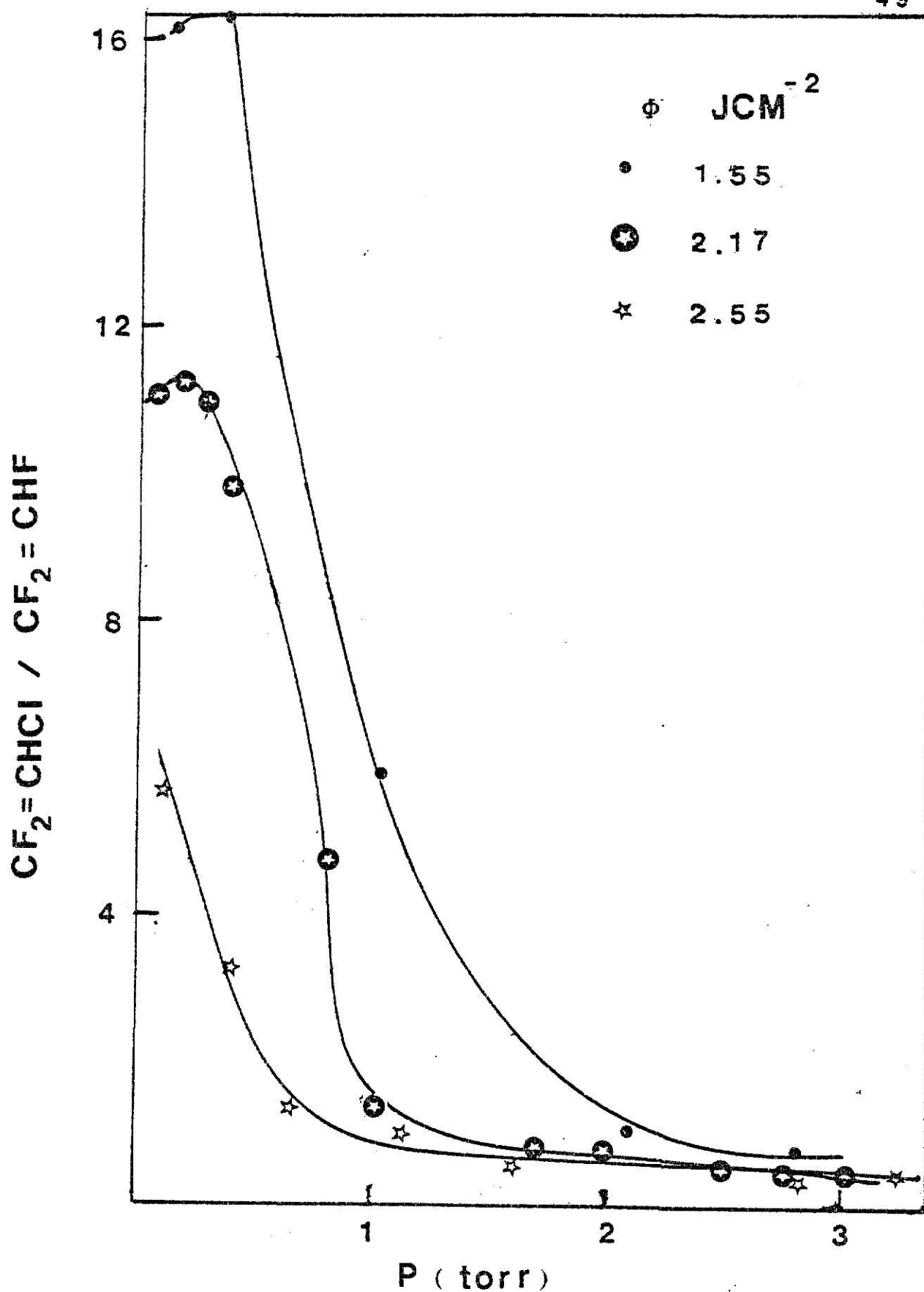
Figure 16   Product ratio $CF_2 = CHCl$ / $CF_2 = CHF$ ratio vs. CF_3CH_2Cl pressure irradiated by laser at R(30).
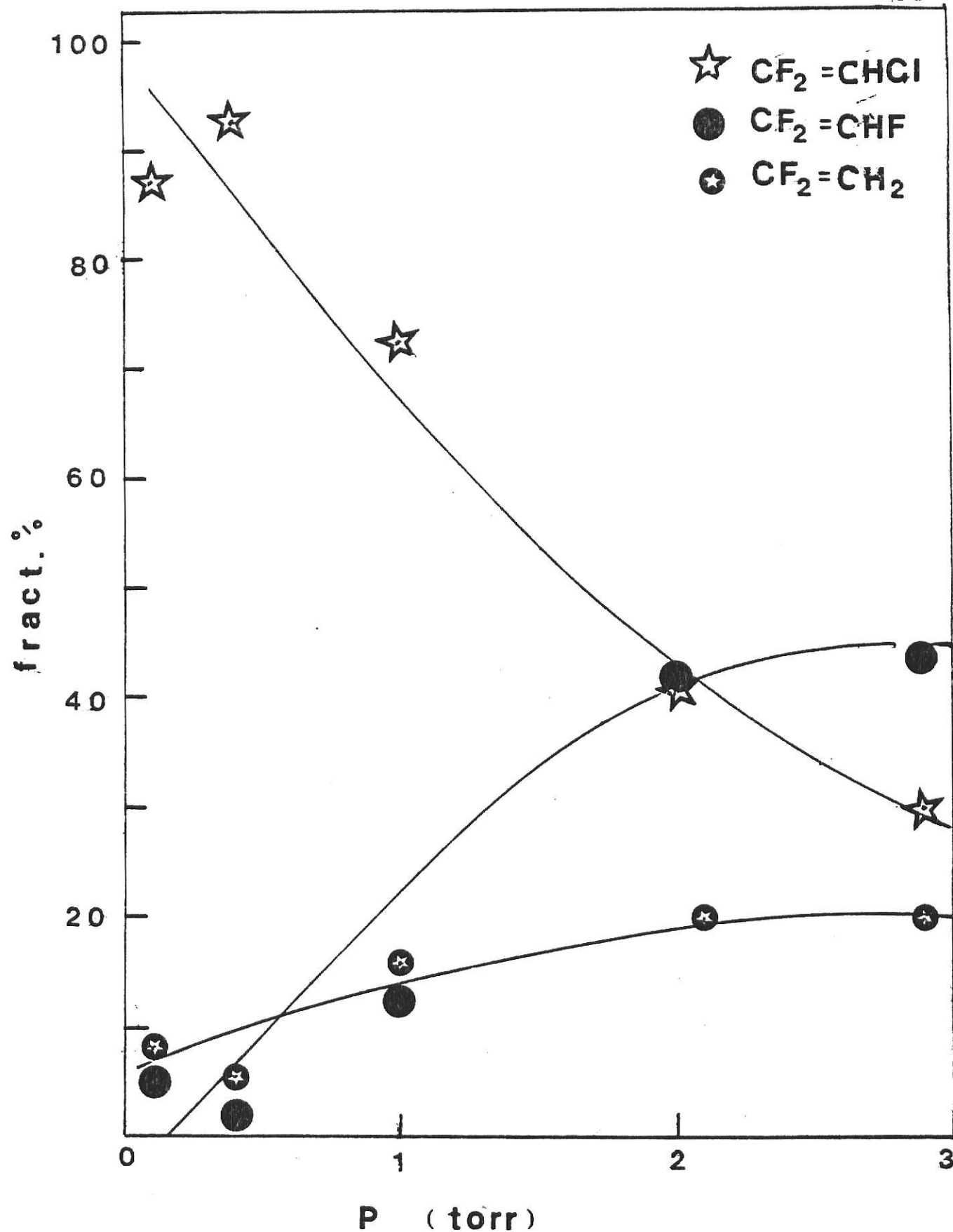
Figure 17   Fractional percentage of products of CF_3CH_2Cl
reaction irradiated by R(30) laser beam, with
fluence 1.55 J/cm^2
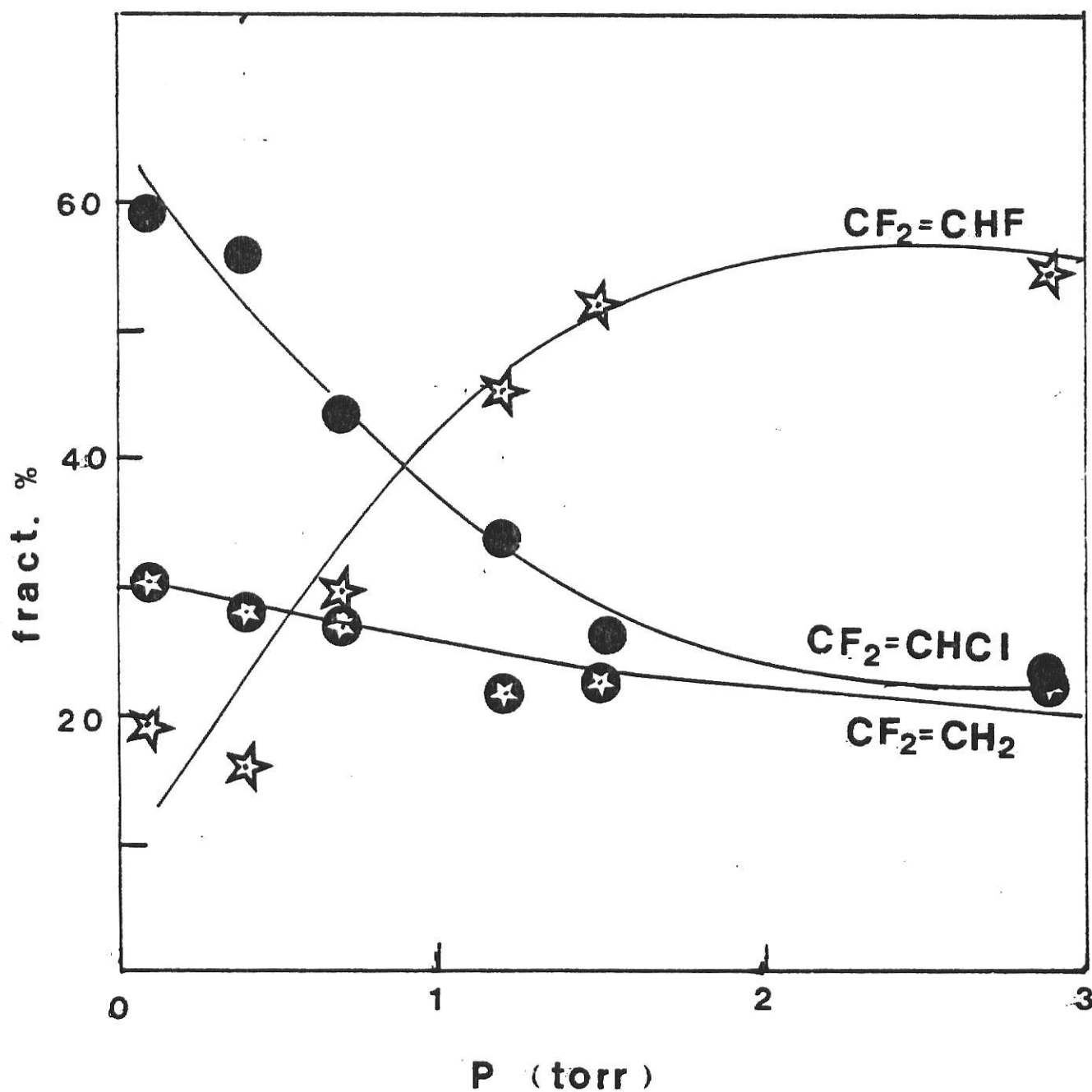
Figure **18**   Fractional percentage of products of CF_3CH_2Cl
reaction irradiated by R(30) laser beam with
fluence 2.55 J/cm^2

3. Reaction Probability and Product Distribution with Added

   Inert and Scavenger Gases

a. Inert gases

MPD of CF_3CH_2Cl in the presence of He and N_2 was studied. The pressure of bath gas was high enough so that the temperature of the reaction cell does not increase. Experiments with 0,1,2,3,4,5 torr of He , $\emptyset$ = 2.05 J/cm^2 and 0,1,2,3 torr of N_2, $\emptyset$ = 2.44 J/cm^2 mixed with 0.05 torr CF_3CH_2Cl were performed. The fractional product distributions are shown in table 7. There was no enhancement of reaction probability with addition of He or N_2, in contrast to the frequently observed enhancement for laser irradiation of small molecules, i.e., CF_3CH_3[5]. Some quenching effect was observed for 3.5 torr of N_2. The product distribution with N_2 appears different from the pure CF_3CH_2Cl LID at 2.05 J/cm^2. The toluene experiment below did not change the product distribution. The result here might come from the experiment error, but comment will be made without any further proof.

The retention time of CF_4 is the same as CF_3CH_2Cl, so no experiments could be done with CF_4 as a bath gas.

b. Toluene

Toluene was used as both a radical scavenger and a quenching gas. The uniform fluence cell was used with the long laser pulse to study the dependence of reaction probability upon toluene pressure. All experiments were done with 0.05 torr of CF_3CH_2Cl and added toluene. The two sets of experiments at $\emptyset$ =

Table 7 Reaction of CF_3CH_2Cl (0.05 torr) with different pressures of N_2 bath gas

N_2 (torr)	Ci/Co	P(∅)	$CF_2=CH_2$ frac.%	$CF_2=CHF$ frac.%	$CF_2=CHCl$ frac.%	Y	mass balance
0	0.68	17.4%	17.0	8.0	70	26	87.5%
1	0.84	11.8%	38.8	10.2	51	5	96.3%
2	0.81	13.8%	43.0	14.0	43	3	100%
3.5	0.86	10.6%	43.0	11.4	46	4	100%

condition:
laser line : R(30),1085 cm^{-1}
∅ = 2.05 J/cm^2 i = 20 A = 0.74 cm^2 Vo/Go = 13.64
focused condition Y : $CF_2=CHCl/CF_2=CHF$

Reaction of CF_3CH_2Cl (0.05 torr) with different pressures of He Bath gas.

He torr	$CF_2=CH_2$ frac.%	$CF_2=CHF$ frac.%	$CF_2=CHCl$ frac.%	Y
0	32.8	10.6	54.0	5.1
1	36.8	10.5	52.6	5.0
2	40.9	9.7	49.4	5.1
5	37.3	10.8	51.9	4.8
10	33.9	11.9	54.2	4.6

condition:
laser line : R(30),1085 cm^{-1}

∅ = 2.44 J/cm^2 A = 0.73 i = 20 Vo/Go = 13.83
focused condition Y : $CF_2=CHCl/CF_2=CHF$

Table 8 Laser induced reaction with toluene

A. fluence 1.61 J/cm^2
Po$(\emptyset)$=1.44 x 10^{-1} A = 2.9 cm^2

i	toluene(torr)	Ci/Co	P$(\emptyset)$	Po$(\emptyset)$/P$(\emptyset)$
25	0	0.860	1.22 x 10^{-1}	1.00
25	0.05	0.862	8.44 x 10^{-2}	1.70
20	0.05	0.892	8.10 x 10^{-2}	1.77
80	0.50	0.924	1.40 x 10^{-2}	10.25
100	0.50	0.916	1.24 x 10^{-2}	11.57
100	0.55	0.923	1.13 x 10^{-2}	12.70
150	0.55	0.896	1.04 x 10^{-2}	13.80
100	0.70	0.962	5.52 x 10^{-3}	26.00
150	0.70	0.940	5.87 x 10^{-3}	24.45
100	0.84	0.970	4.20 x 10^{-3}	34.20
150	0.84	0.961	3.77 x 10^{-3}	38.10

(continued)

toluene torr	i	$CF_2=CH_2$ fract.%	$CF_2=CHF$ fract.%	$CF_2=CHCl$ fract.%
0	25	7.5	4.2	88.5
0.05	25	8.3	4.6	87.0
0.05	20	8.6	4.1	87.3
0.50	80	7.4	3.9	88.7
0.50	100	7.2	3.8	89.0
0.55	100	7.3	4.0	88.7
0.55	150	6.4	4.0	89.6
0.70	100	6.1	2.3	91.6
0.70	150	6.2	3.6	90.3
0.84	100	5.7	3.4	91.0
0.84	150	6.5	3.2	90.3

B. fluence = 3.42 J/cm^2
   $Po(\emptyset) = 2.65 \times 10^{-1}$ $A = 0.73 \; cm^2$

toluene(torr)	i	Ci/Co	P($\emptyset$)	Po($\emptyset$)/P($\emptyset$)
0	15	0.760	2.65×10^{-1}	1.00
0.8	20	0.788	1.69×10^{-1}	1.78
0.8	20	0.799	1.59×10^{-1}	1.67
1.0	20	0.813	1.46×10^{-1}	1.81
1.0	25	0.758	1.57×10^{-1}	1.69
1.5	20	0.849	1.16×10^{-1}	2.28
2.0	20	0.873	9.64×10^{-2}	2.75
3.0	15	0.922	7.68×10^{-2}	3.45
4.0	10	0.957	6.18×10^{-2}	4.29
5.0	10	0.965	5.13×10^{-2}	5.16
6.0	20	0.949	3.72×10^{-2}	7.11
7.0	20	0.946	3.90×10^{-2}	6.80
8.0	20	0.960	2.89×10^{-2}	9.17
9.0	20	0.965	2.50×10^{-2}	10.61
10.0	25	0.969	1.79×10^{-2}	14.77

(continued)

table 8, B.continue

toluene torr	i	$CF_2=CH_2$ fract.%	$CF_2=CHF$ fract.%	$CF_2=CHCl$ fract.%
0	15	46.7	7.1	46.2
0.8	20	42.2	4.2	53.6
1.0	20	41.8	3.0	55.2
1.5	20	42.4	4.3	53.3
2.0	20	41.4	4.5	54.1
3.0	15	43.0	5.8	51.2
4.0	10	45.5	4.2	50.3
5.0	10	43.8	5.4	50.8
6.0	20	42.5	5.0	52.5
7.0	20	41.5	5.1	53.5
8.0	20	38.0	4.8	57.1
9.0	20	40.7	5.0	54.3
10.0	25	34.4	6.6	59.0

Figure 19   Reaction probability and product distribution
with added toluene.

$\phi = 1.61 \text{ J/cm}^2$

$\Phi = 1.61$

$CF_2=CHCl$

$CF_2=CH_2$

$CF=CHF$

$P_o(\Phi) / P(\Phi)$

fract. %

Toluene (torr)
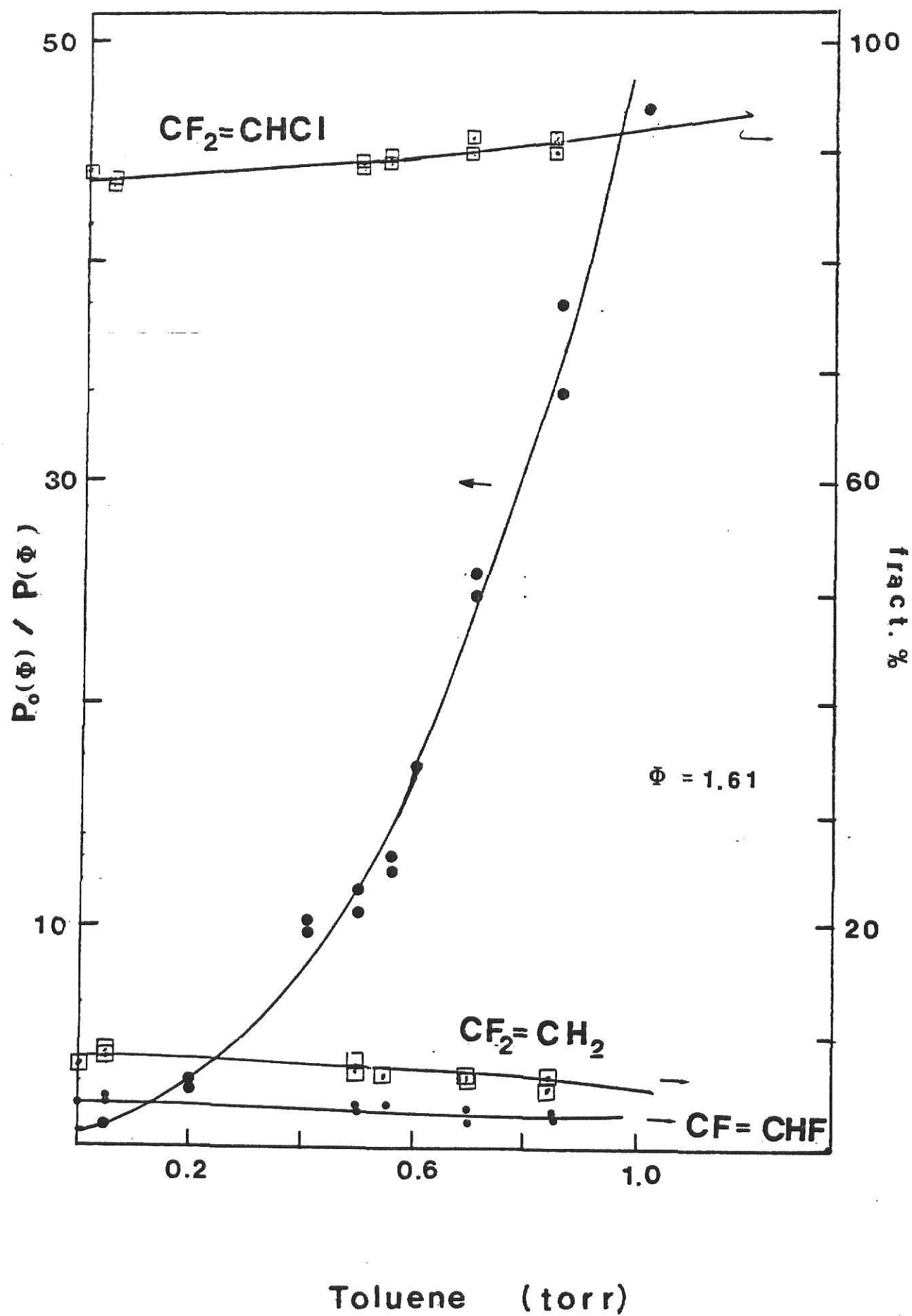
Figure 20   Reaction probability and product distribution
             with added toluene.
             $\phi = 3.42 \ J/cm^2$

$\Phi = 3.42$

$CF_2 = CHCl$

$CF_2 = CH_2$

$CF_2 = CHF$

Toluene (torr)
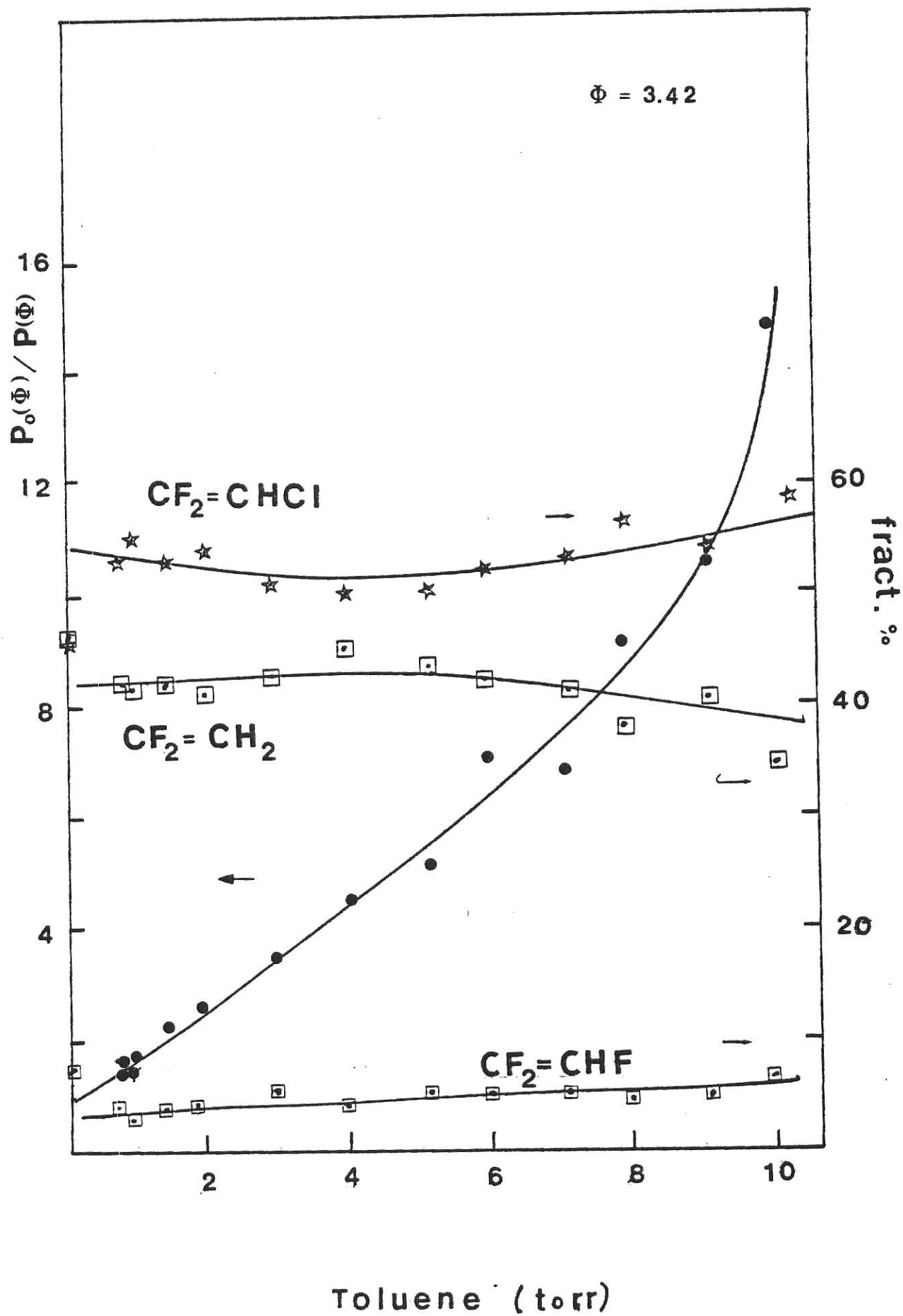
1.61 and 3.42 J/cm^2 both show quenching effects. The degree of quenching depends upon the pressure of toluene and on fluence. The effect of added toluene on product yield and ratios are illustrated in Figures 19, 20 and Table 8. The data are presented as Stern-Volmer type plots, i.e., graphs of the ratio of the reaction probability in the absence of the added gas, $P_0(\emptyset)$, to that in the presence of toluene, $P(\emptyset)$, vs. pressure of added toluene. At higher fluence one needs a higher pressure of toluene to get the same quenching, for example, at $\emptyset = 1.61$, it only took 0.5 torr toluene to have $Po/P = 10$, but at $\emptyset = 3.42$ J/cm^2, 9 torr of toluene was needed.

The fractional distribution of the three main products were not affected by adding the toluene; even though the absolute reaction yield may be reduced dramatically. These toluene data conclusively demonstrate the absence of bimolecular radical pathways for the $CF_2=CH_2$ channel. As mentioned before, the minor products for these experiments are only 1-2% fractional percentage. The addition of toluene did reduce the minor products which come from radical reactions.

III. SiF_4 Sensitization Reactions of CF_3CH_2Cl

1. Experiments Without Toluene

Multiphoton excitation of a sensitizer gas followed by collisional energy transfer may be used to produce high temperature thermal excitation for other added molecules[13]. In this work, a purely thermal excitation of CF_3CH_2Cl was produced by CO_2 laser MPE of a non-reactive sensitizer molecule, SiF_4.   Rapid energy transfer among vibrational, rotational and translational degrees of freedom thermalized the gas on a microsecond time scale and yielded a Boltzmann energy distribution in the irradiated volume. After about 50 μs the thermal reaction will be quenched by cooling of the irradiated volume.

All reaction probability measurements were done with 0.4 torr of CF_3CH_2Cl and 5 torr of SiF_4. The laser beam was unfocused and plastic films reduced the laser fluence to a range of 0.2 to 0.6 J/cm^2. The long laser pulse was used in all experiments, and a small iris diameter of 0.74 cm was employed.   As described before, SiF_4 caused no trouble in analysis. However, since a large amount of SiF_4 was utilized, it affected the GC column and the sensitivity was reduced, resulting in deleterious effects on the product separation and quantitative analysis. To solve this problem, the column was cleaned by raising column temperature to 150°C and using a higher flow rate of carrier gas after 2 or 3 days of experiments. New calibrations were necessary after this treatment.

There was no reactions for SiF_4 sensitized mixtures of $CF_2=CHF$ or $CF_2=CHCl$ in separate experiments. The experiments

were done for 20 pulses of $\mathscr{O}$ = 0.36 J/cm^2, SiF$_4$, 5 torr, CF$_2$=CHF, 0.4 torr and 30 pulses of 0.36 J/cm^2 of CF$_2$=CHCl, 0.4 torr, SiF$_4$, 5 torr. Since CF$_2$=CH$_2$ has equally high threshold energies, secondary reaction from the products of the CF$_3$CH$_2$Cl reaction need not be considered.

Table 9 lists the reaction probability, P($\mathscr{O}$), ratio of products, and fractional percentage of CF$_2$=CH$_2$, CF$_2$=CHF, CF$_2$=CHCl vs energy fluences, the plots of these data are shown in Figures 21, 22 and 23. As shown in Figure 21, the P($\mathscr{O}$) range from 10^{-3} to 0.3 can be conveniently covered. The product distribution from the sensitized reaction is very similar to the shock tube results and the high reactant pressure laser induced reaction, i.e., at high fluence the CF$_2$=CHF product becomes the most important one, another important point is that CH$_2$=CF$_2$ is also a major product. In addition to the three major products, there is a 2-5% contribution of minor products. They are C$_2$F$_6$, C$_2$F$_4$, CF$_2$=CFCl and CF$_3$CH=CF$_2$, as in the laser induced reactions.

2. Experiments with Toluene

The gas mixture CF$_3$CH$_2$Cl : SiF$_4$: Toluene = 0.4 : 5 : 0.14 was used for these experiments. The data are shown in Table 10 and Figures 21, 24 and 25. Separate experiments with toluene and SiF$_4$ showed no reaction under the same experimental condition. If toluene is added as a radical scavenger, the reaction should be simplified to approximately the primary reaction channels. Indeed the results are similar to the laser-induced reaction except sensitization has a higher reaction probability.

Table 9   Sensitized Reaction of CF_3CH_2Cl

i	C_i/C_o	$\varnothing$ J/cm^2	$P(\varnothing)$	mass balance
8	0.86	0.57	3.3×10^{-1}	95.0%
10	0.87	0.50	2.3×10^{-1}	95.8%
15	0.90	0.47	1.3×10^{-1}	99.7%
20	0.90	0.41	8.7×10^{-2}	99.4%
40	0.91	0.34	4.1×10^{-2}	95.6%
40	0.92	0.32	4.0×10^{-2}	96.0%
40	0.95	0.31	3.6×10^{-2}	97.4%
50	0.98	0.27	9.0×10^{-3}	99.0%
100	0.99	0.20	2.0×10^{-3}	99.4%

(continued)

X : $CF_2=CHCl/CF_2=CH_2$,   Y : $CF_2=CHCl/CF_2=CHF$

$\varnothing$ J/cm^2	$CF_2=CH_2$ frac.%	$CF_2=CHF$ frac.%	$CF_2=CHCl$ frac.%	X	Y
0.57	24.8	53.2	16.5	0.67	0.31
0.50	23.0	56.8	16.0	0.70	0.28
0.47	22.5	57.7	16.2	0.72	0.28
0.41	24.0	56.5	16.5	0.69	0.29
0.34	20.1	59.4	20.5	1.02	0.35
0.32	20.0	60.2	19.8	1.08	0.38
0.31	20.6	56.2	23.0	1.12	0.41
0.27	19.6	47.3	33.1	1.69	0.70
0.20	15.4	29.0	55.4	3.60	1.91

condition:
laser line : $_2$P(40),1027 cm^{-1}
A = 0.44 cm^2 Vo/Go = 25.23
amount used: CF_3CH_2Cl 0.4 torr
sensitizer: SiF_4 5   torr
(All the symbols used are the same as table 4)

Table 10   Sensitized Reaction of CF_3CH_2Cl with toluene

i	C_i/C_o	$\emptyset$ J/cm^2	$P(\emptyset)$	mass balance
80	0.964	0.19	5.4×10^{-3}	96.5%
40	0.954	0.25	1.3×10^{-2}	96.0%
30	0.898	0.37	4.1×10^{-2}	90.7%
20	0.934	0.43	4.5×10^{-2}	97.3%
10	0.910	0.56	2.7×10^{-1}	96.4%
5	0.910	0.59	2.8×10^{-1}	95.0%

(continued)
     X : $CF_2=CHCl/CF_2=CH_2$,   Y : $CF_2=CHCl/CF_2=CFH$

$\emptyset$ J/cm^2	$CF_2=CH_2$ frac.%	$CF_2=CHF$ frac.%	$CF_2=CHCl$ frac.%	X	Y
0.19	22.8	10.7	66.4	2.90	6.2
0.25	30.0	12.0	57.9	1.93	4.8
0.37	36.3	16.8	46.8	1.29	2.8
0.43	46.9	19.5	33.6	0.72	1.7
0.56	47.6	24.3	28.1	0.59	1.2
0.59	49.9	22.0	28.1	0.56	1.3

condition:
     laser line ; P(40), 1027 cm^{-1}
     A = 0.44 cm^2
     amount used:
     CF_3CH_2Cl : 0.40 torr
     Sensitizer SiF_4 : 5   torr
     Radical scavenger Toluene : 0.14 torr
(All the symbols used are the same as table 4)

Figure 21   Reaction probability for sensitized reaction
of CF_3CH_2Cl vs. laser energy fluence.

sensitizer	:	SiF_4
radical scavenger	:	toluene
irradiated frequency	:	P(40)

CF_3CH_2Cl with

• SiF_4

✪ SiF_4 + Toluene

$P(\Phi)$

$\Phi \quad JCM^{-2}$
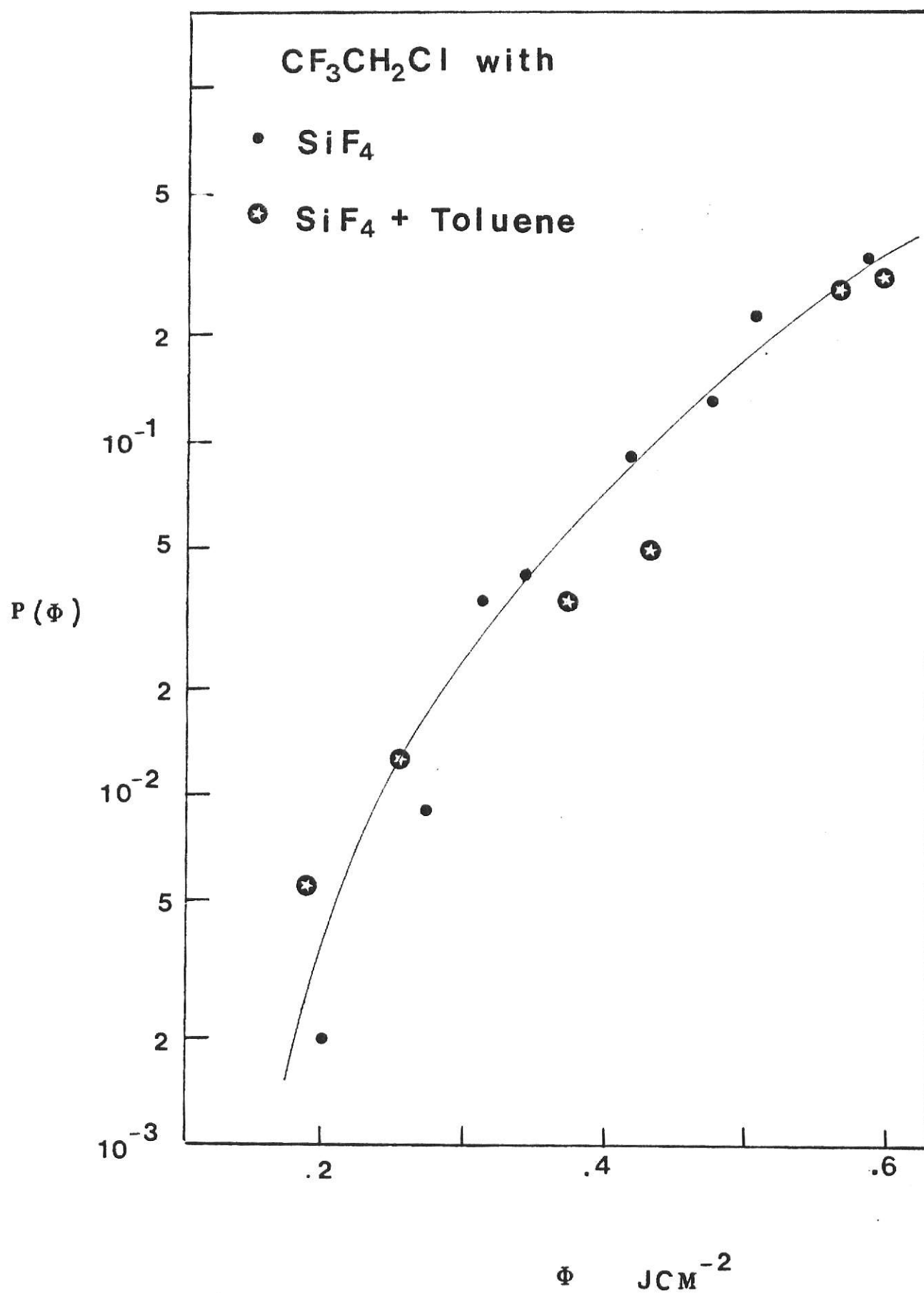
Figure 22   Fractional percentage of the main products for
             CF_3CH_2Cl sensitized reaction vs. laser energy fluence.
             CF_3CH_2Cl :   0.4 torr
             SiF_4 :   5   torr

$CF_3CH_2Cl + SiF_4$

$CF_2=CHF$

$CF_2=CH_2$

$CF_2=CHCl$

fract %

60

50

30

10

.2   .4   .6

Φ $J CM^{-2}$
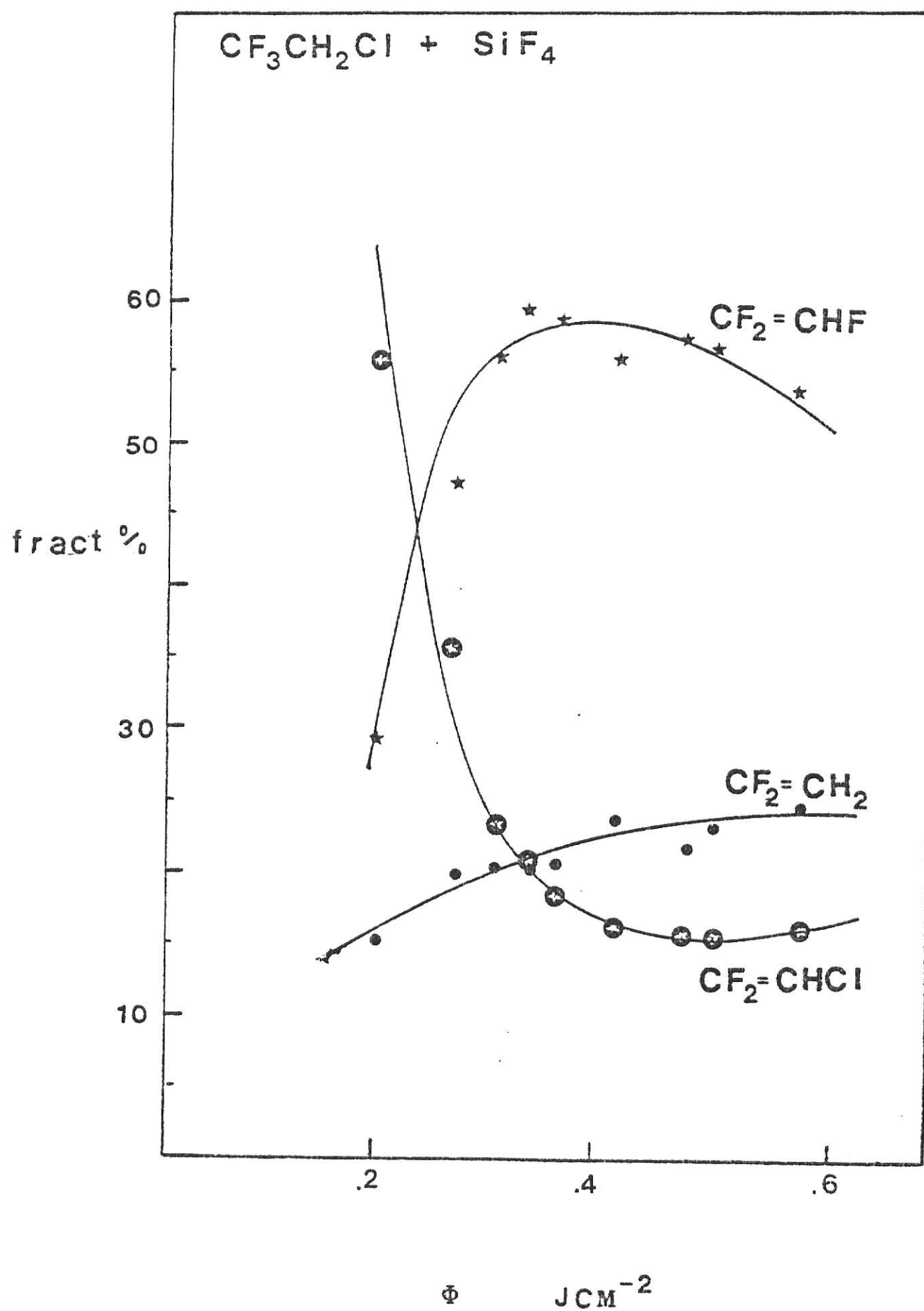
Figure 23   The product ratio vs. laser energy fluence
for sensitized reaction of CF_3CH_2Cl.

sensitizer SiF_4 :   5   torr
CF_3CH_2Cl :   0.4 torr

Legend:
- $CF_2=CHCl / CF_2=CH_2$
- $CF_2=CHCl / CF_2=CHF$

Y-axis: Product Ratio

X-axis: $\Phi \quad JCM^{-2}$
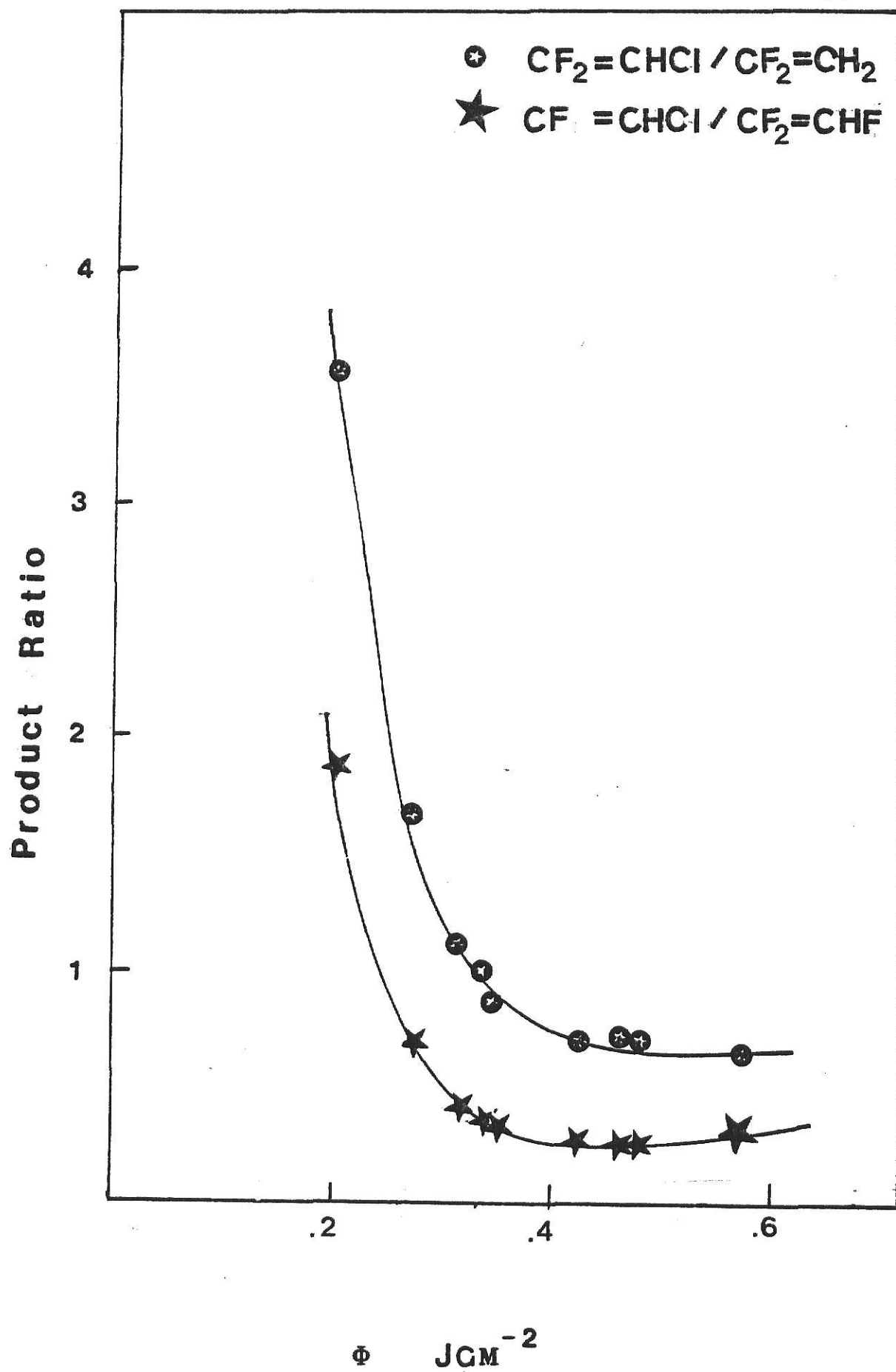
Figure **24**   Fractional percentage of the main products

for sensitized reaction of CF_3CH_2Cl with toluene

Sensitizer SiF_4 :   5   torr

Radical scavenger   toluene   :   0.14   torr

CF_3CH_2Cl :   0.05   torr

Figure axis labels: fract. % (y-axis), Φ JCM^{-2} (x-axis)

Legend:
+ Toluene
○ $CF_2=CHCl$
★ $CF_2=CH_2$
● $CF_2=CHF$
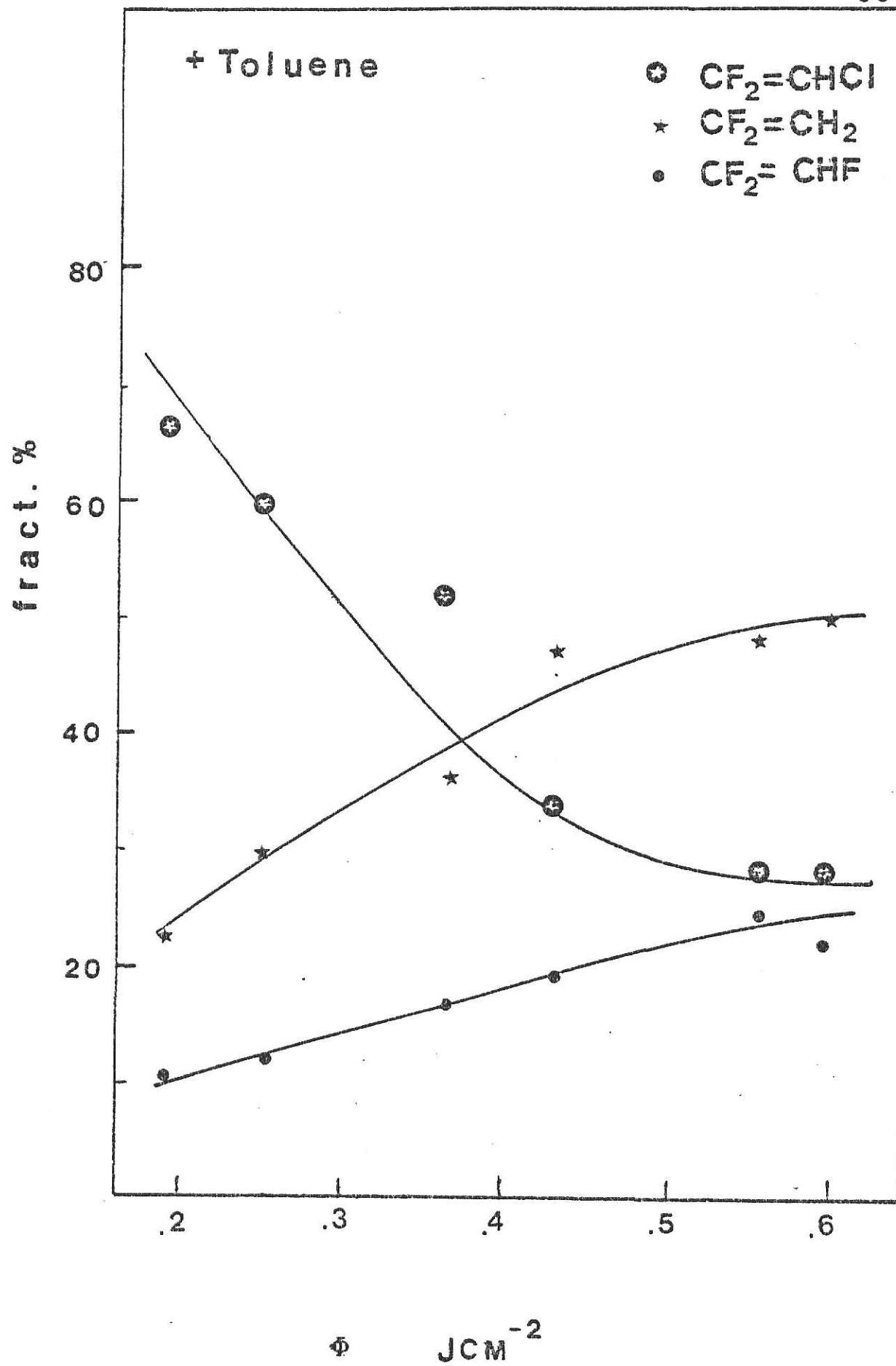
Figure 25 The ratio of main products vs. laser energy

fluence for CF_3CH_2Cl sensitized reaction.

sensitizer $\qquad$ SiF_4 : 5.0 torr

radical scavenger toluene : 0.14 torr

$\qquad\qquad\qquad$ CF_3CH_2Cl : 0.40 torr

Φ $J C M^{-2}$
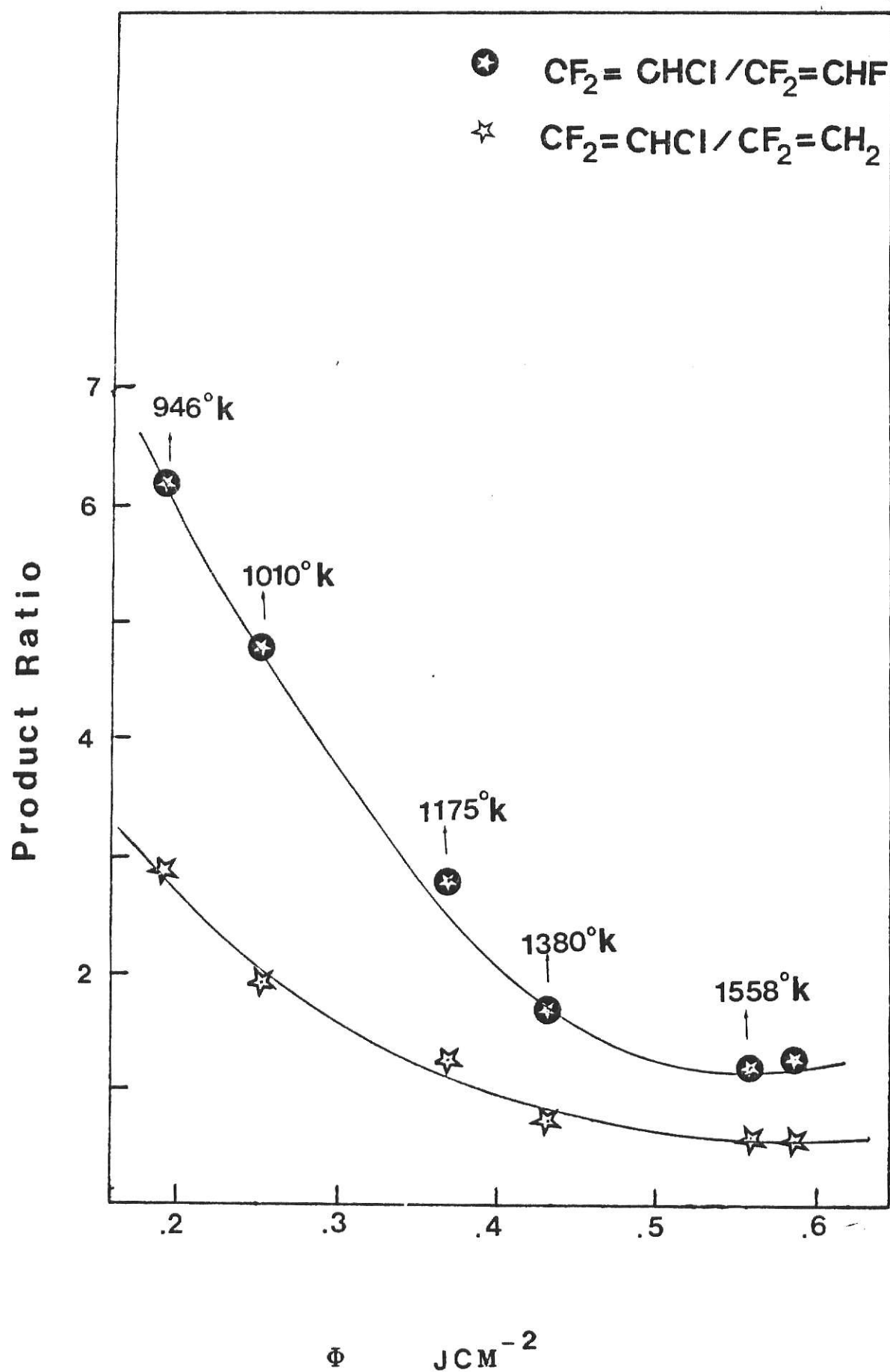
We now compare the experimental product distributions of (1) laser induced reaction, and (2) sensitization with toluene as a scavenger. From the viewpoint of the reaction probability at the same fluence, the sensitization reaction has 100 times higher reaction probability than for the laser-induced reaction because of the thermal nature of the reaction and the large cross-section of SiF_4. The product distribution at $\emptyset$ = 2-5 J/cm^2 in Figure 13 matches well with $\emptyset$ = 0.2-0.4 J/cm^2 in Figure 24. The C-Cl rupture was the main reaction channel at $\emptyset$ > 4 J/cm^2 in reaction (1) and $\emptyset$ > 0.4 J/cm^2 in reaction (2).

In the discussion section, the $\sigma_L(SiF_4)$ will be estimated in order to find the temperature for these reaction conditions; then the sensitized results can be discussed in terms of the pre-exponential factors and threshold energies.

IV.   Laser Energy Absorption Measurements for CF_3CH_2Cl

The broad band cross-sections, σ_o, of CF_3CH_2Cl was measured with a Perkin Elmer 180 IR spectrophotometer at 1 cm^{-1} resolution. Spectra were taken for different pressures of CF_3CH_2Cl with background correction for an empty cell. The absorption was calculated directly from the transmittance. Some sample spectra are shown in Figure 26, and a high resolution (0.03 cm^{-1}) was shown in Figure 8. The results of the broad band experiment are shown in Figure 27 as pressure vs. ln T. The broad band cross-section σ_o was calculated from the slope of this plot, i.e., ln T = $-\sigma_o NX$. Two sets of experiments were done at different times. The data were listed in Tables 11A and 11B; the agreement is satisfactory. Experiments also were done for CF_3CH_2Br at 1082 cm^{-1} to compare to that of CF_3CH_2Cl. The broad band cross sections are 6.2 x 10^{-19} cm^2/molecule for CF_3CH_2Br at 1082 cm^{-1}. The mean results for CF_3CH_2Cl are (9.4 ± 1.7) x 10^{-20} at 1085 cm^{-1}; (1.30 ± 0.06) x 10^{-19} at 1088 cm^{-1}, (1.87 ± 0.07) x 10^{-19} at 1090 cm^{-1} and (2.3 ± 0.2) x 10^{-19} at 1092 cm^{-1}.

The absorption cross-sections corresponding to laser fluence of ~0.5 J/cm^2 are tabulated in Table 11C. In doing these experiments nothing was changed in the laser system except to turn the micrometer to get the highest energy for each laser line. From the laser gain curve, it is obvious that the laser energy declines from R(30) to R(44) since the fluence changed from 0.66 to 0.39 J/cm^2 (Table 11C). The comparison of broad band cross-section and laser cross-section at $\emptyset$~0.5 J/cm^2 at
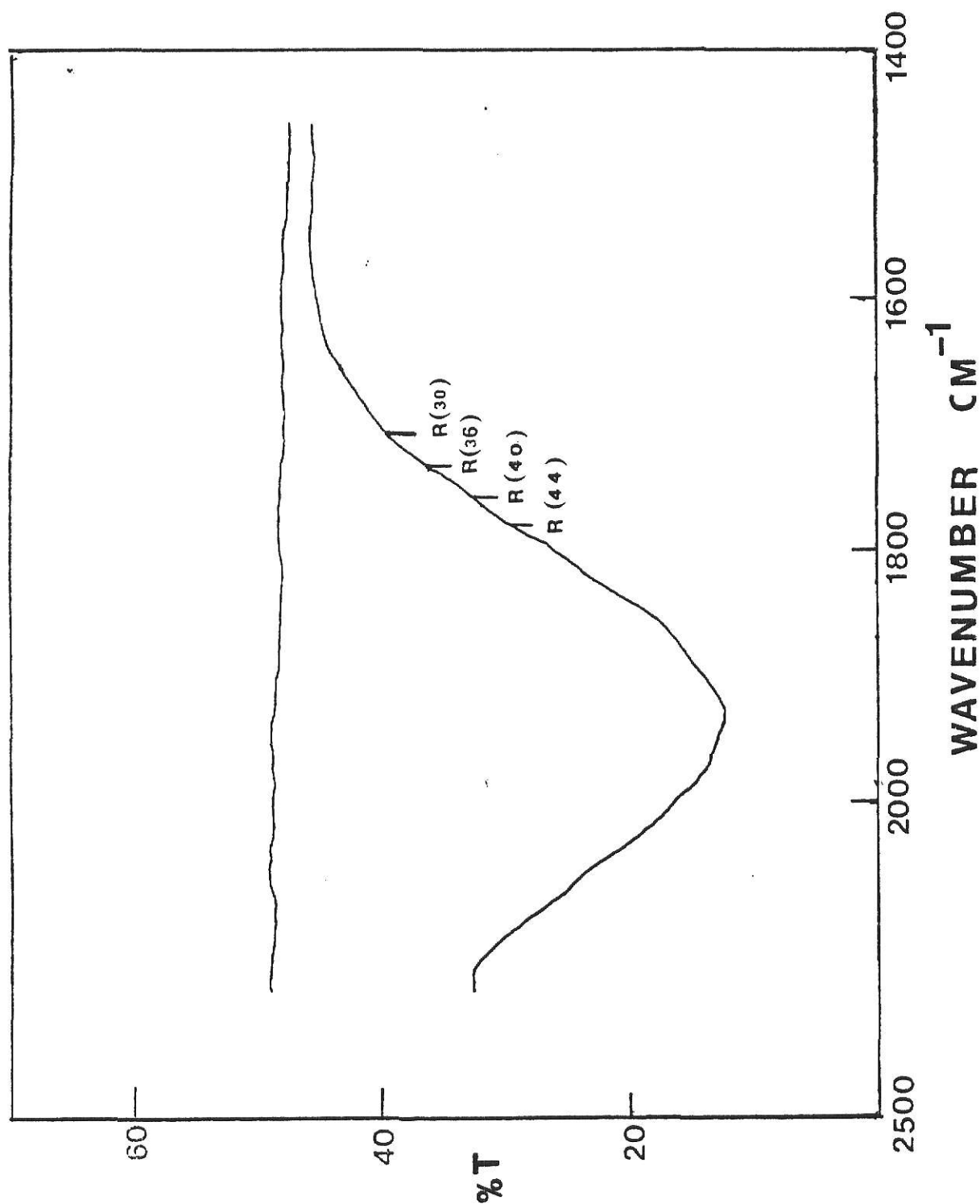
Figure 26   Absorption spectrum of CF_3CH_2Cl was taken from a Perkin Elmer 180 infrared spectrophotometer at 1 cm^{-1} resolution. Pressure was 5 torr and cell length was 20 cm. The four laser lines were indicated.

Table 11   Broad Band Cross Section Measurement of
           CF_3CH_2Cl from IR spectrometer at frequencies
           corresponding to the laser lines

A.

P(torr)	R(30) ln T	R(36) ln T	R(40) ln T	R(44) ln T
1	-0.080	-0.129	-0.158	-0.182
3	-0.187	-0.282	-0.405	-0.481
4	-0.210	-0.340	-0.473	-0.580
5	-0.240	-0.431	-0.580	-0.720
6.3	-0.322	-0.530	-0.730	-0.840
7.6	-0.390	-0.620	-0.883	-1.026
10.0	-0.463	-0.730	-1.040	-1.274
σ ($\times 10^{-20}$)	7.7	12.5	18.1	20.8

B.

P(torr)	R(30) ln T	R(36) ln T	R(40) ln T	R(44) ln T
1	-0.040	-0.095	-0.134	-0.150
3	-0.197	-0.240	-0.305	-0.405
5	-0.360	-0.460	-0.660	-0.790
σ ($\times 10^{-20}$)	11.0	13.6	19.4	24.2

Table 11 Laser absorption cross-section of CF_3CH_2Cl
C.   at different frequencies.

| 1085 cm^{-1} R(30) | | R(36) 1088 cm^{-1} | |
| $\emptyset = 0.66$ J/cm^2 | | $\emptyset = 0.53$ J/cm^2 | |
P(torr)	ln T	P(torr)	ln T
0.500	−0.008	0.500	−0.037
1.000	−0.042	1.000	−0.093
2.000	−0.095	2.000	−0.186
3.000	−0.140		
$\sigma = 1.1 \times 10^{-19}$		$\sigma = 1.36 \times 10^{-19}$	

| 1090 cm^{-1} R(40) | | R(44) 1092 cm^{-1} | |
| $\emptyset = 0.44$ J/cm^2 | | $\emptyset = 0.39$ J/cm^2 | |
P(torr)	ln T	P(torr)	ln T
0.570	−0.070	0.500	−0.094
1.500	−0.170	1.000	−0.170
2.000	−0.310	1.520	−0.262
2.510	−0.235	2.000	−0.320
$\sigma = 1.94 \times 10^{-19}$		$\sigma = 2.44 \times 10^{-19}$	

Figure 27   Beer's law (ln T vs. pressure) from
1 cm^{-1} resolution spectra for CF_3CH_2Cl
and CF_3CH_2Br at certain laser lines.

The σ_o for each line is : (cm^2/molecule)

CF_3CH_2Cl	R(30)	$9.4 \pm 1.7 \times 10^{-20}$
	R(36)	$1.3 \pm 0.06 \times 10^{-19}$
	R(40)	$1.9 \pm 0.07 \times 10^{-19}$
	R(44)	$2.3 \pm 0.17 \times 10^{-19}$
CF_3CH_2Br	R(26)	6.2×10^{-19}
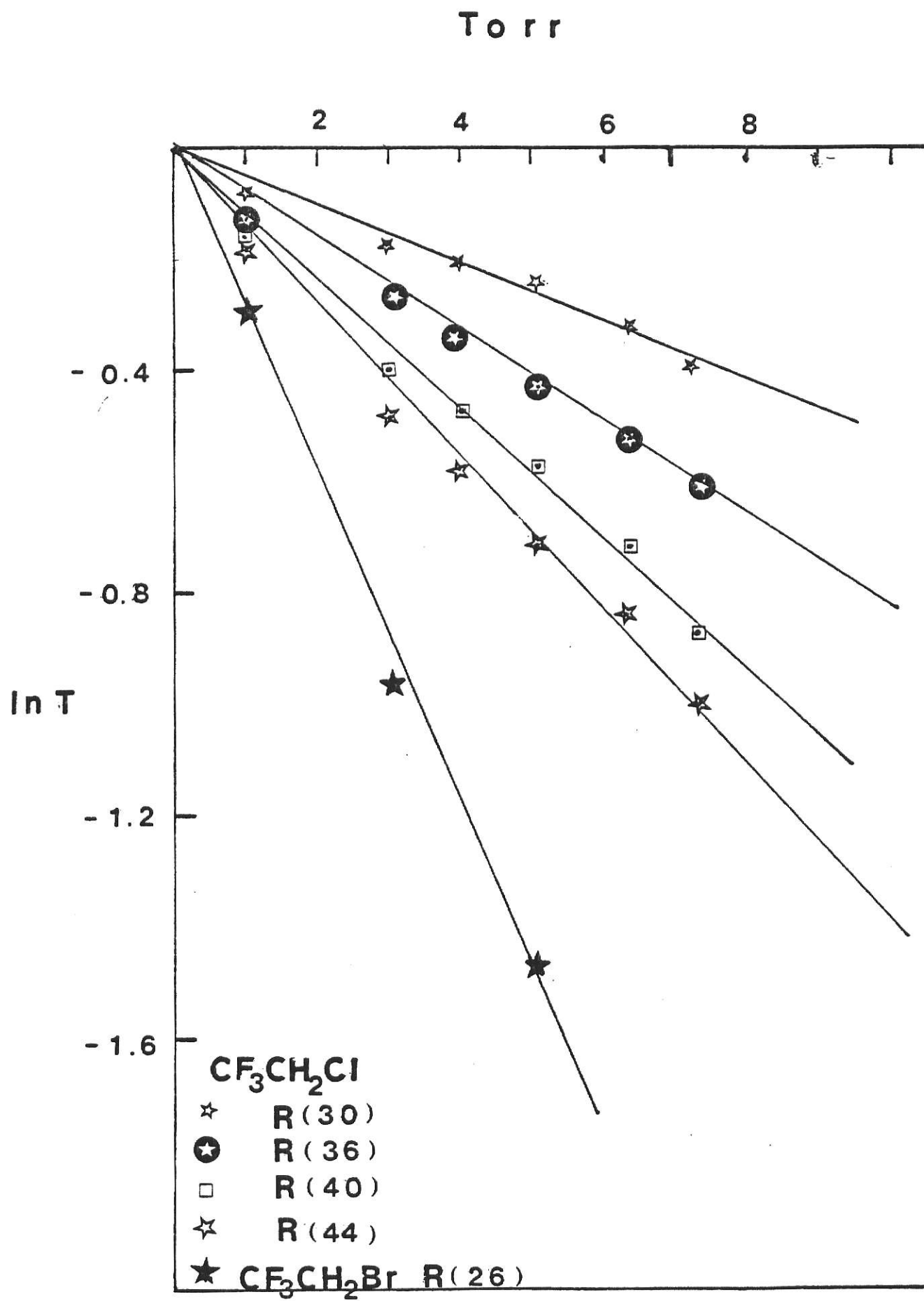
these frequencies is shown in Figure 28. The CF_3CH_2Cl has highest absorption value at 1092 cm^{-1} laser line since this frequency is the one close to the IR maximum absorption region (Figure 26); but, the laser line at this frequency is too weak for laser induced chemistry, so all the experiments for $P(\emptyset)$ were done with R(30).

Two laser frequencies, R(30)-1085 cm^{-1} and R(44)-1092 cm^{-1}, were selected for systematic study of the multiphoton absorption cross-section of CF_3CH_2Cl. The long laser pulse (He : CO_2 : N_2 = 8.0 : 2.0 : 0.8) was used in all experiments. The energy absorption measurements were done by the dual detector method up to $\emptyset$=3.5 J/cm^2. As a check on methodology, experiments also were done with CF_3CH_3 with the same setup. Excellent agreement with the earlier experimental data of CF_3CH_3 at R(16) line 973 cm^{-1} was obtained[5]. The CF_3CH_3 data are shown in Table 12.

Table 12

this work $\emptyset = 1.5$ J/cm^2		Jang's work[5] $\emptyset = 1.88$ J/cm^2	
P(torr)	ln T	P(torr)	ln T
0.403	-0.042	0.20	-0.009
0.710	-0.097	0.40	-0.052
1.105	-0.183	0.50	-0.057
		0.70	-0.106
		1.00	-0.164
$\sigma = 3.6 \times 10^{-19}$ cm^2/molecule		$\sigma = 3.6 \times 10^{-19}$ cm^2/molecule	

The $\sigma_L(\emptyset)$ of CF_3CH_3 decline with $\emptyset$ and become constant for $\emptyset > 0.63$ J/cm^2 in Jang's work[5].

Because of the low cross-section for CF_3CH_2Cl, we worked at higher pressure (0.3 to 4 torr) to avoid large experimental

Figure 28   The comparison of broad band cross-sections
with laser cross-section ($\phi \simeq 5$ J/cm^2).   75
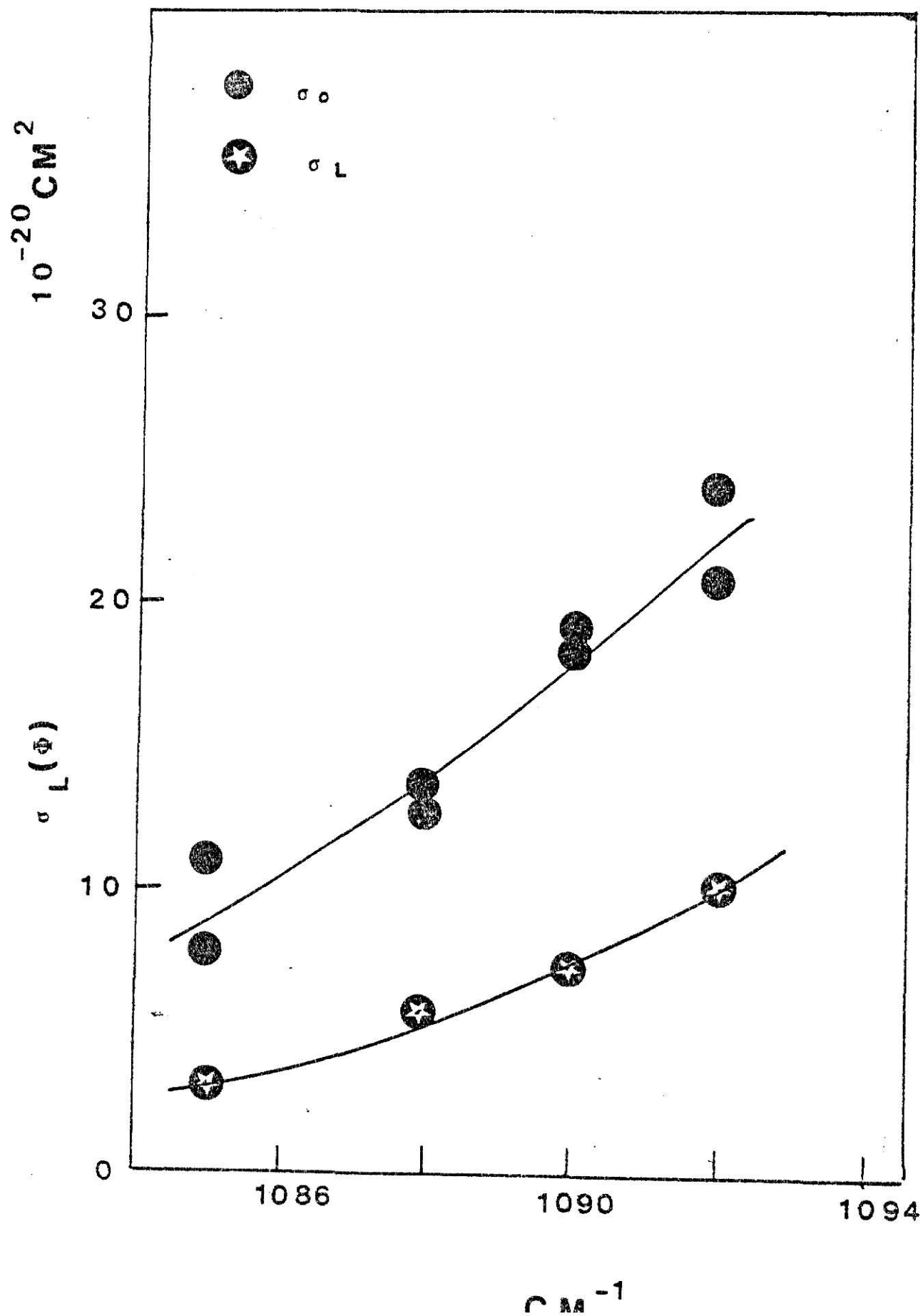
errors associated with low absorption signals. The energy absorption by CF_3CH_2Cl appeared to obey Beer's law except for part of the low cross-section region. (i.e. the plot of P vs. ln T was not linear, rather the $\sigma(\emptyset)$ increases with CF_3CH_2Cl pressure). The linear behavior is shown in Figure 29 for 1 - 8 torr of CF_3CH_2Cl at $\emptyset = 1.70$ J/cm^2 at 1085 cm^{-1}. The ln T vs. P(torr) data and cross-sections are listed in Tables 13, 14 and Figures 30,31,32 and 33. For 1085 cm^{-1}, excitation from $\emptyset = 0.195$ to $\emptyset = 3.46$ J/cm^2 and 1092 cm^{-1} excitation from $\emptyset = 0.062$ to 0.354 J/cm^2. The $\sigma_L(\emptyset)$ were calculated from the slopes of ln T vs. pressure plot. For the data which do not follow Beer's law, the cross-section was obtained by extrapolating the $\sigma(\emptyset)$ calculated from each point to zero pressure to obtain the laser absorption cross-section in the absence of collision. All the $\sigma_L(\emptyset)$ results are plotted vs $\emptyset$ in Figure 34.

The results demonstrate that Beer's law (with some exception at low cross-section region, $\emptyset=0.30\pm0.05$ J/cm^2) describes the multiphoton process for CF_3CH_2Cl at 1085 cm^{-1} line and that the bulk laser absorption cross-section is a molecular property independent of pressure (< 4 torr is normal) at higher fluence. For a small molecule (i.e., CF_3CH_3) $\sigma_L(\emptyset)$ depends on pressure and does not follow Beer's law. So CF_3CH_2Cl seems to be a compound that exhibits behavior intermediate between a large molecule and small molecule, since at certain low $\emptyset$ the cross-sections are pressure dependent. The cross-sections increased and then declined with increasing $\emptyset$ for CF_3CH_2Cl at 1085 cm^{-1}. At $\emptyset > 2.2$ J/cm^2 , $P(\emptyset) > 0.10$, the $\sigma_L(\emptyset)$ values may

Figure **29**   Beer's law plot (ln T vs. pressure of CF_3CH_2Cl)
for R(30) irradiation of CF_3CH_2Cl

Torr

CF_3CH_2Cl

ln T

$\Phi = 1.70$ $J CM^{-2}$
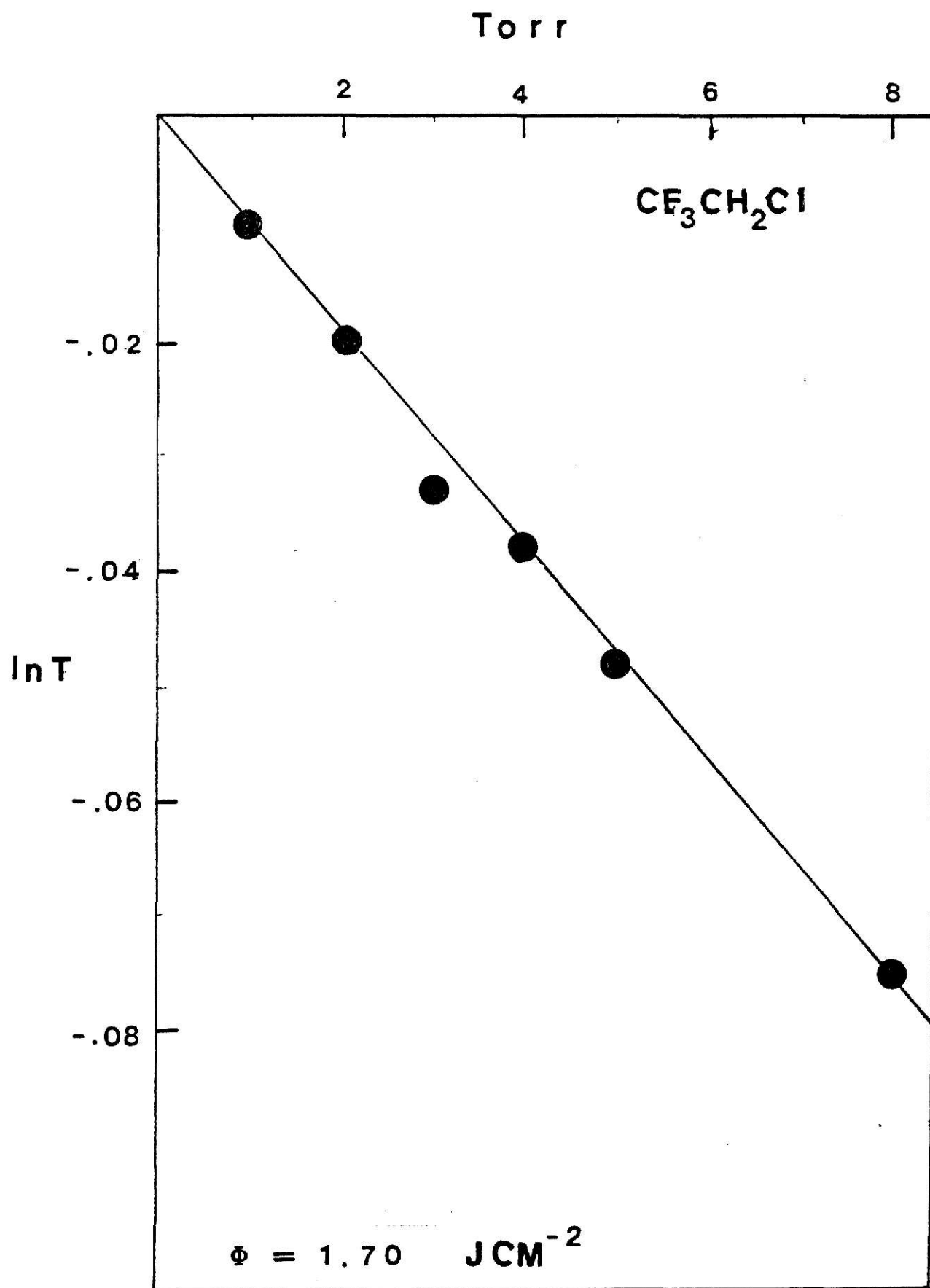
Table 13   Laser Absorption cross section of CF_3CH_2Cl
for R(30) excitation (1085 cm^{-1})

$\emptyset$ = 1.65 J/cm^2		$\emptyset$ = 2.31 J/cm^2	
P(torr)	ln T	P(torr)	ln T
0.935	-0.124	0.948	-0.149
0.600	-0.077	0.600	-0.088
0.302	-0.025	0.292	-0.045
σ = 8.02 x 10^{-20}		σ = 9.69 x 10^{-20}	

$\emptyset$ = 2.55 J/cm^2		$\emptyset$ = 0.644 J/cm^2	
P(torr)	ln T	P(torr)	ln T
1.000	-0.160	0.341	-0.023
0.600	-0.097	0.603	-0.038
0.300	-0.037	0.940	-0.060
σ = 9.07 x 10^{-20}		σ = 3.83 x 10^{-20}	

$\emptyset$ = 2.98 J/cm^2		$\emptyset$ = 2.17 J/cm^2	
P(torr)	ln T	P(torr)	ln T
0.900	-0.145	0.460	-0.072
0.600	-0.083	0.840	-0.134
0.360	-0.039	0.353	-0.067
0.750	-0.100	0.504	-0.100
1.000	-0.160		
σ = 8.15 x 10^{-20}		σ = 9.88 x 10^{-20}	

$\emptyset$ = 1.73 J/cm^2		$\emptyset$ = 0.82 J/cm^2	
P(torr)	ln T	P(torr)	ln T
0.353	-0.067	0.465	-0.022
0.504	-0.100	0.932	-0.057
		1.390	-0.083
σ = 1.23 x 10^{-19}		σ = 3.52 x 10^{-20}	

$\emptyset$ = 1.00 J/cm^2		$\emptyset$ = 1.40 J/cm^2	
P(torr)	ln T	P(torr)	ln T
0.520	-0.035	1.000	-0.110
0.800	-0.059	0.610	-0.065
0.950	-0.065	0.300	-0.026
σ = 4.32 x 10^{-20}		σ = 6.79 x 10^{-20}	

$\emptyset$ = 0.20 J/cm^2		$\emptyset$ = 0.27 J/cm^2	
P(torr)	ln T	P(torr)	ln T
0.500	-0.030	0.890	-0.037
1.500	-0.045	1.200	-0.050
2.500	-0.097	1.600	-0.077
4.000	-0.166		
σ = 2.56 x 10^{-20}		σ = 2.00 x 10^{-20}	

(continued)

table 13, continue

ϕ = 0.18 J/cm^2		ϕ = 0.08 J/cm^2	
P(torr)	ln T	P(torr)	ln T
0.640	-0.031	1.160	-0.051
0.980	-0.044	1.810	-0.092
1.676	-0.069	1.500	-0.076
σ = 2.84 x 10^{-20}		σ = 3.21 x 10^{-20}	

ϕ = 1.40 J/cm^2		ϕ = 1.01 J/cm^2	
P(torr)	ln T	P(torr)	ln T
1.000	-0.100	1.000	-0.060
3.000	-0.315	2.000	-0.144
5.000	-0.490	3.000	-0.220
8.000	-0.750	4.000	-0.286
σ = 6.04 x 10^{-20}		σ = 5.86 x 10^{-20}	

ϕ = 0.63 J/cm^2		ϕ = 0.46 J/cm^2	
P(torr)	ln T	P(torr)	ln T
1.000	-0.050	2.000	-0.120
3.000	-0.174	1.000	-0.007
4.000	-0.220	2.800	-0.170
σ = 3.40 x 10^{-20}		σ = 3.79 x 10^{-20}	

ϕ = 0.33 J/cm^2		ϕ = 0.27 J/cm^2	
P(torr)	ln T	P(torr)	ln T
0.750	-0.024	0.840	-0.057
1.500	-0.043	1.600	-0.081
2.500	-0.116	3.520	-0.205
3.500	-0.183	0.500	-0.022
		σ = 3.59 x 10^{-20}	

Table 14   Laser Absorption cross section of CF_3CH_2Cl
for R(44) excitation (1092cm^{-1})

$\phi = 0.354$ J/cm^2			$\phi = 0.315$ J/cm^2	
P(torr)	ln T		P(torr)	ln T
0.565	-0.057		0.760	-0.117
1.029	-0.128		0.440	-0.051
1.500	-0.190		0.550	-0.068
0.777	-0.100		1.200	-0.173
			1.890	-0.273
$\sigma = 7.8 \times 10^{-20}$			$\sigma = 8.95 \times 10^{-20}$	

$\phi = 0.256$ J/cm^2			$\phi = 0.172$ J/cm^2	
P(torr)	ln T		P(torr)	ln T
0.600	-0.100		0.400	-0.054
1.000	-0.156		0.890	-0.124
1.520	-0.236		1.680	-0.240
$\sigma = 9.82 \times 10^{-20}$			$\sigma = 8.70 \times 10^{-20}$	

$\phi = 0.123$ J/cm^2			$\phi = 0.108$ J/cm^2	
P(torr)	ln T		P(torr)	ln T
0.500	-0.053		0.860	-0.072
1.010	-0.130		1.400	-0.141
1.340	-0.167		2.000	-0.245
$\sigma = 7.53 \times 10^{-20}$				

$\phi = 0.097$ J/cm^2			$\phi = 0.062$ J/cm^2	
P(torr)	ln T		P(torr)	ln T
0.520	-0.058		0.530	-0.040
1.130	-0.130		1.080	-0.100
2.000	-0.240		2.120	-0.242
$\sigma = 2.16 \times 10^{-20}$				

decline because of depletion of molecules by chemical reaction during the laser pulse. The onset of this trend is expected to occur at $P(\emptyset) \sim 0.1$ if all molecules absorb energy. Another possibility is that the cross-section are intrinsically increase with 0, so that the two trends balance.

The broad band cross-section, σ_o, at 1085 cm^{-1} and 1092 cm^{-1} are $(9.4 \pm 1.7) \times 10^{-20}$ and $(2.3 \pm 0.2) \times 10^{-19}$ cm^2/molecule, respectively. The density of rotational states is high and the $\sigma_L(\emptyset)$ value at low $\emptyset$ might be expected to be the same as a broad band cross-section. But the limiting σ_L are below the broad band cross-sections for R(30), $\sigma = 2.56 \times 10^{-20}$ cm^2/molecule at $\emptyset = 0.20$ J/cm^2, and R(44), $\sigma = 7.53 \times 10^{-20}$ at $\emptyset = 0.12$. The reason we studied R(44) at low fluence was because we thought there might be some effect related to the apparent structure in the band, (Figure 8). From Figure 28, the CF$_3$CH$_2$Cl has higher cross-section at R(44), whether $\sigma(\emptyset)$ will increase at low laser fluence at R(44) was tried, and no enhancement was observed down to $\emptyset = 0.06$ J/cm^2. We concluded that σ_o and $\sigma_L(\emptyset \sim 0)$ do not concide for CF$_3$CH$_2$Cl. The same result was found for CF$_3$CH$_3$ with $= 2 \times 10^{-19}$ cm^2/molecule at $\emptyset = 0.02$ J/cm^2, which is lower than the broad band cross-section, 4.63×10^{-19} cm^2/molecule[5]. In contrast the CF$_3$CH$_2$Br molecule acts as a normal big molecule with $\sigma_L(\emptyset)$ becoming equal to the broad band cross-section at low fluence as shown in Figure 34.

Plots of P(<E>) vs. <E> inherently should be more informative[5] than P($\emptyset$) vs. $\emptyset$, since the extent of reaction is directly related to the absorbed energy. With the availability of the
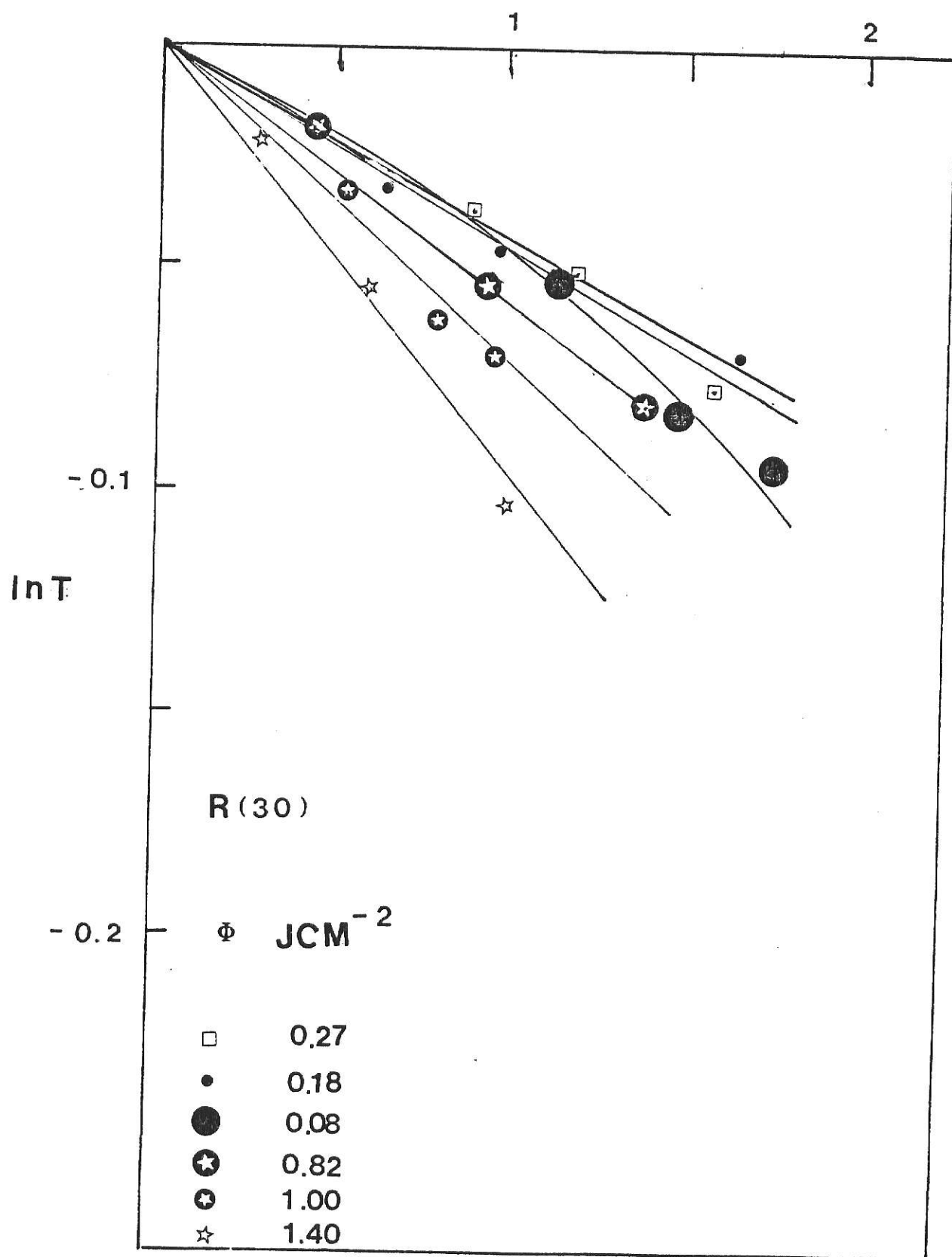
Figure **30**   Plot of ln T vs. CF_3CH_2Cl pressure for R(30)
(001-020) excitation of CF_3CH_2Cl
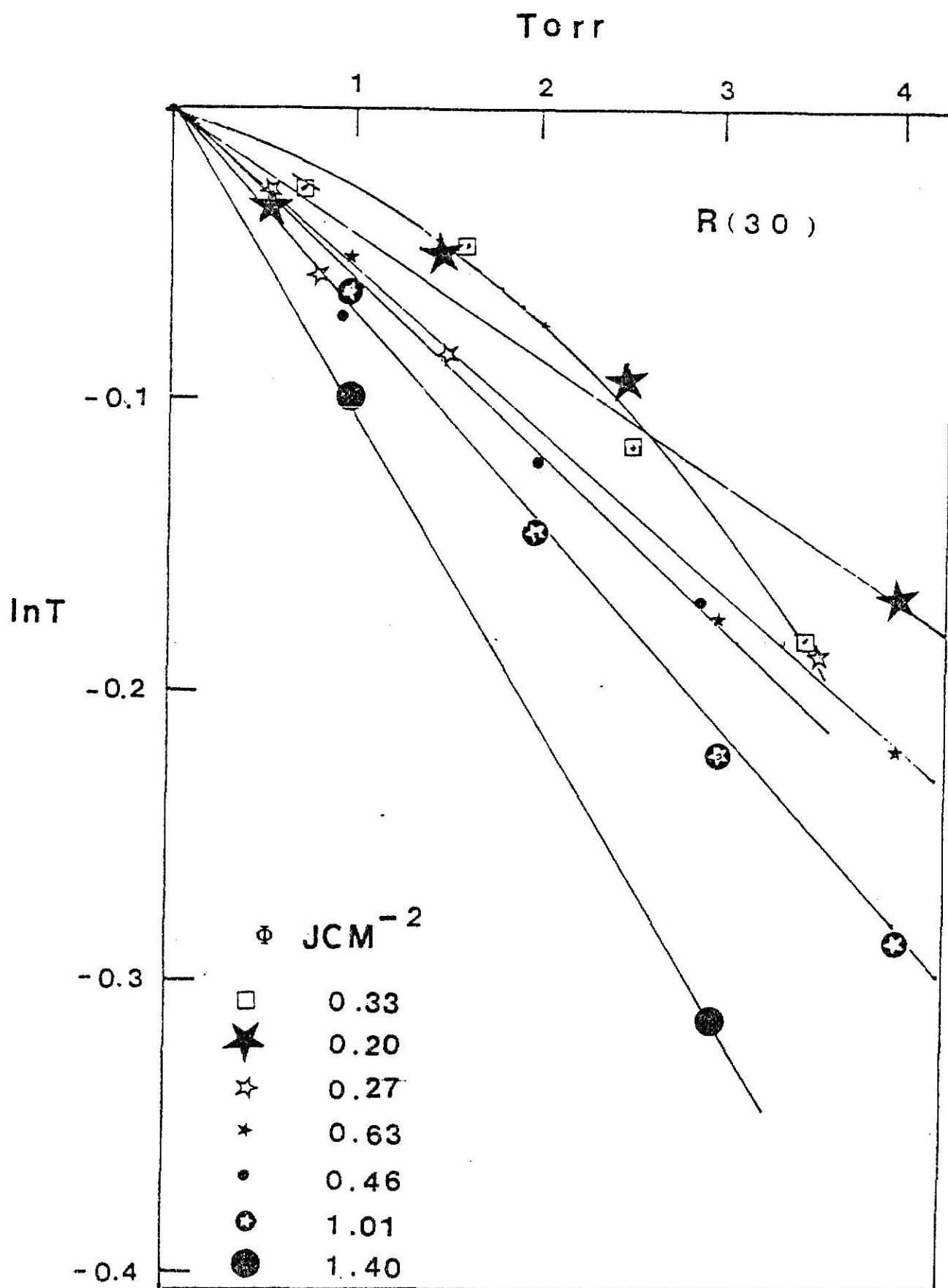
Figure 31   Plot of ln T vs. CF_3CH_2Cl pressure for R(30)
(001-020) excitation of CF_3CH_2Cl
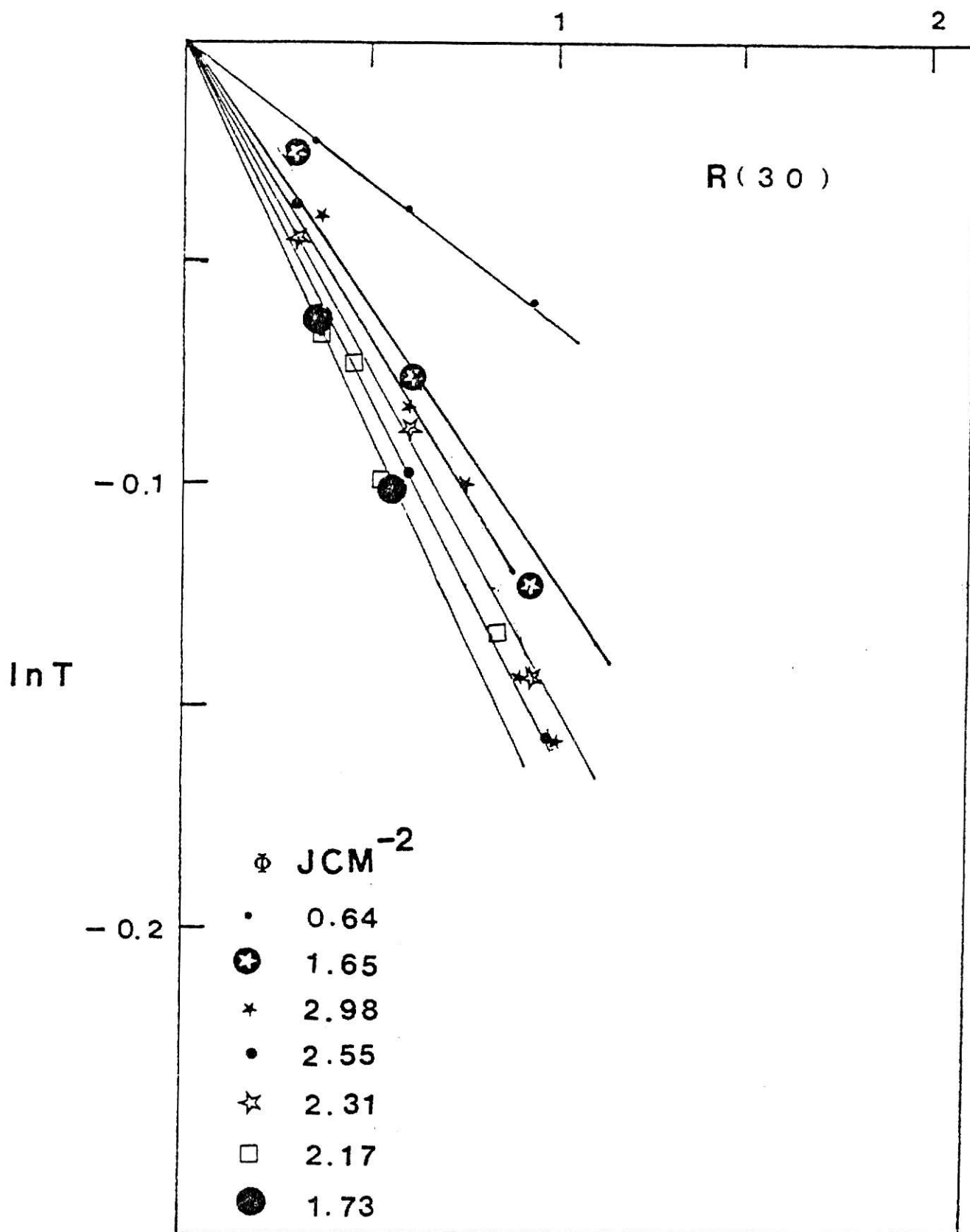
Figure 32   Plot of ln T vs. CF$_3$CH$_2$Cl pressure for R(30)
(001-020) excitation of CF$_3$CH$_2$Cl

R(44)

lnT

1   2

-0.1

-0.2

-0.3

Φ JCM^{-2}

★ 0.062
□ 0.108
✪ 0.354
☆ 0.123
✩ 0.315
✦ 0.172
▫ 0.256
● 0.097
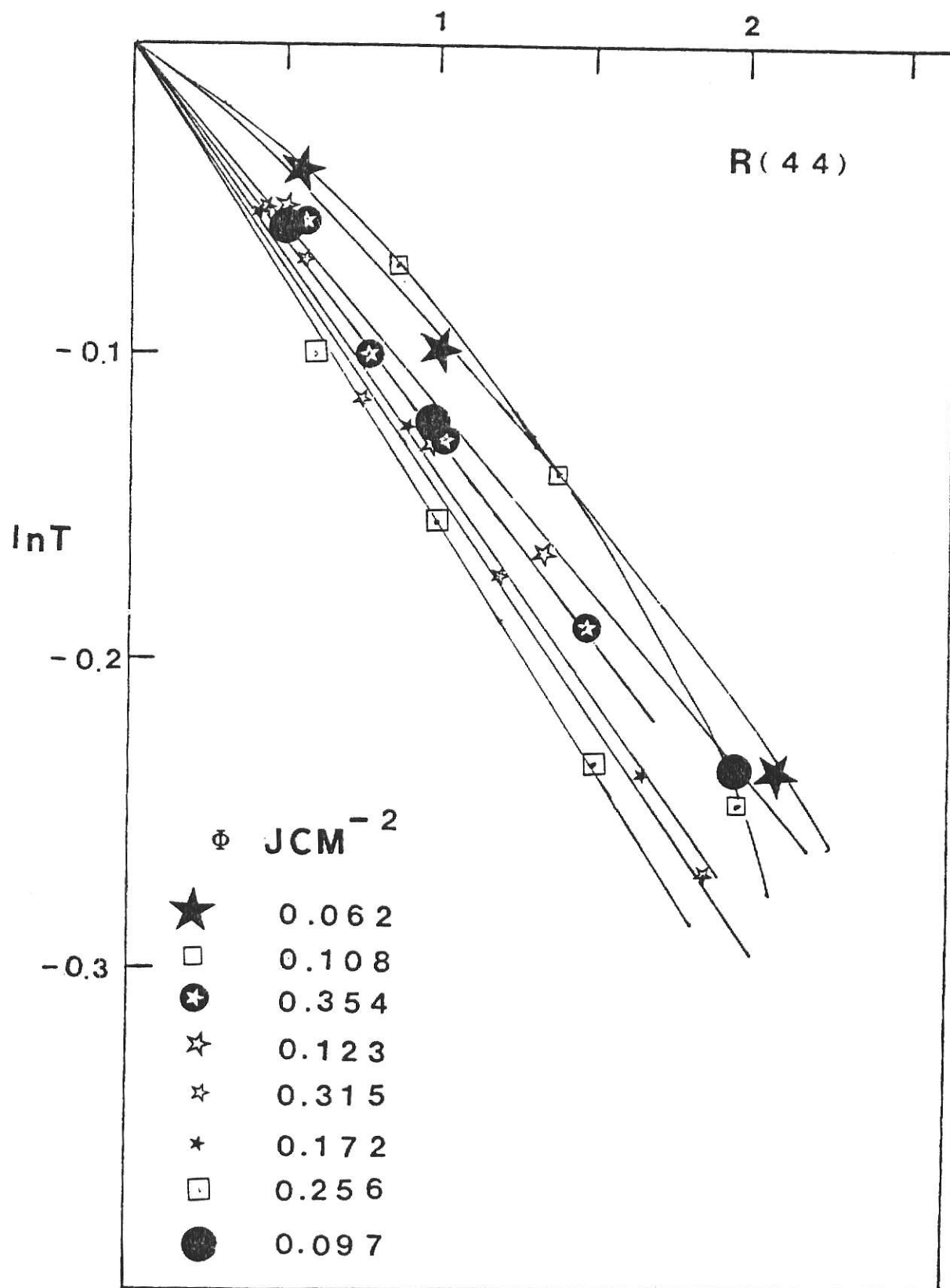
Figure 33   Plot of ln T vs. CF_3CH_2Cl pressure for R(44)
(001-020) excitation of CF_3CH_2Cl

Figure 34   Bulk laser absorption cross-section, $\sigma_L(\phi)$, vs. laser energy fluence, ϕ, for R(30) and R(44) irradiation of CF_3CH_2Cl, R(26) for CF_3CH_2Br and R(16) for CF_3CH_3
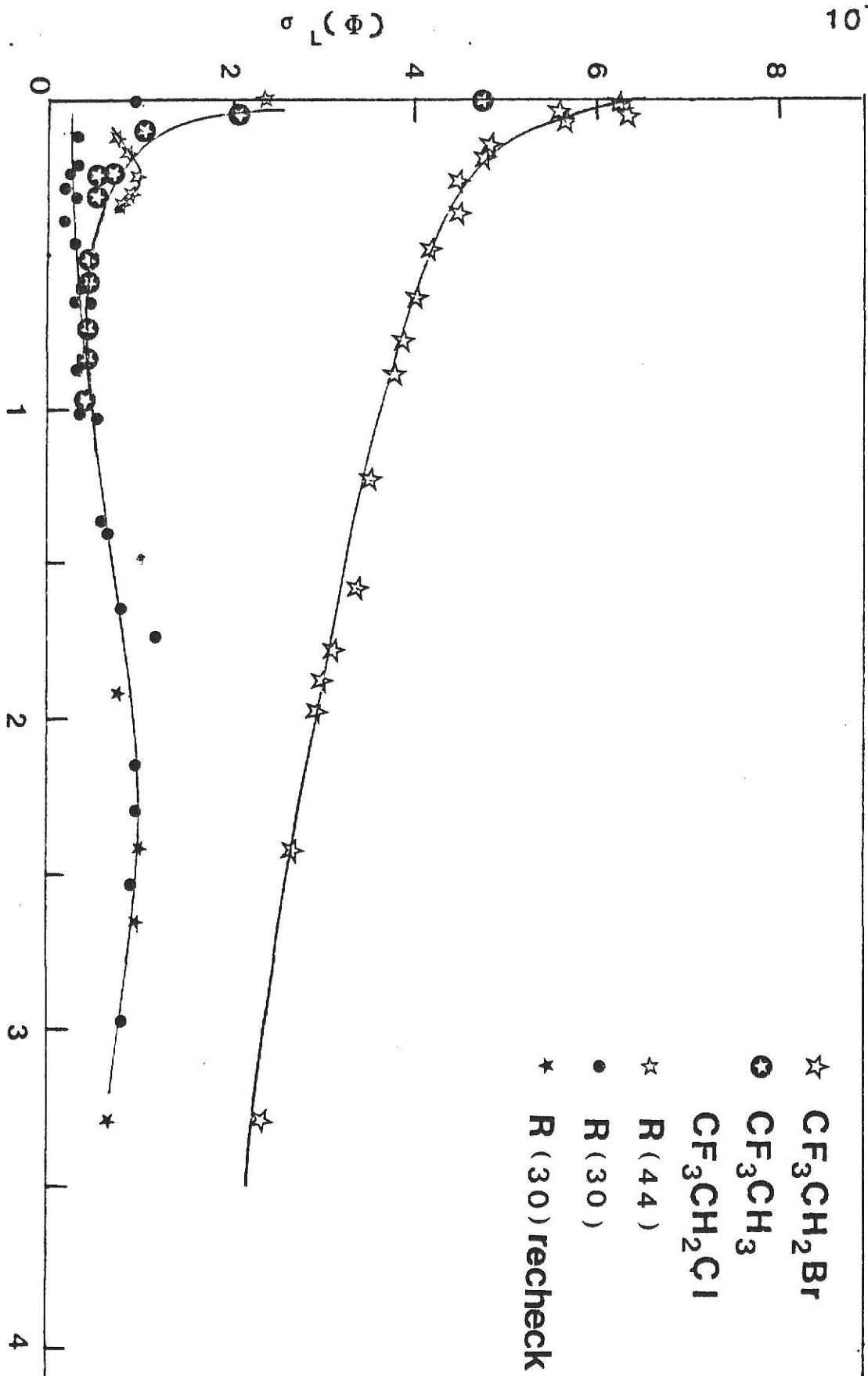
$\sigma_L(\emptyset)$ values such graphs can be constructed. If all molecule absorb the energy , the average energy absorbed per molecule in the irradiated volume, $\langle E \rangle$, is given by $\langle E \rangle = \emptyset \times \sigma_L(\emptyset)$. The $\langle n \rangle$, $\langle E \rangle$ and reaction probability at each fluence for these three compounds are listed in table 15. For ease of comparisons plots were made but they are placed in the discussion section. They are labeled Figure 35 and Figure 36. In the $P(\emptyset)$ vs $\emptyset$ plot, CF_3CH_2Cl reached the $P(\emptyset) = 0.8$ at $\emptyset > 5$ J/cm^2 and CF_3CH_2Br has the highest reaction probability at a given fluence (for $\emptyset < 3.5$ J/cm^2). CF_3CH_2Cl is second and CF_3CH_3 is third. But different relationships are found for the $P(\langle E \rangle)$ vs. $\langle E \rangle$ plot. A detailed discussion will be provided in the discussion section.

The $P(\emptyset)$ and $\sigma_L(\emptyset)$ data for CF_3CH_2Cl, CF_3CH_2Br, and CF_3CH_3 were obtained with considerable care by three different workers in the same laboratory. They are believed to be as accurate as achievable with the available instrumentation. One exception may be the $P(\emptyset)$ results for CF_3CH_2Br at higher laser fluence after Br_2 was formed.

Because of the low mean energy at higher laser fluence for CF_3CH_2Cl, the recheck experiment of absorption measurement at high laser fluence was done from 0.2-0.6 torr CF_3CH_2Cl. The results are shown below:

Table 16A

$\emptyset(J/cm^2)$	ln T	σ (cm^2/molecule) $\times 10^{-20}$
3.3	-0.072	7.5
2.7	-0.08	9.2
2.4	-0.09	9.3
1.9	-0.07	7.1

A good agreement with earlier experiment can be seen from Figure 34.

The absorption measurements of CF_3CH_2Cl with added He were also done at high laser fluence. The result is shown below.

Table 16B $\emptyset$ = 2.9 J/cm^2

CF3CH2C1 = 1 torr		CF3CH2C1 = 0.6 torr	
He	ln T	He	ln T

0	-0.16	0	-0.14
1	-0.12	1	-0.13
2	-0.08	3	-0.01
3	-0.06	5	-0.09
4	-0.04		

As the He pressure increase, the absorption was lowered due to collisional deactivation. No enhancement was observed.

From the two experiments above, the cross-section of CF_3CH_2Cl at high fluence region should be reliable, the cross-section does not seem to increase for $\emptyset$ > 3 J/cm^2.

Table 15   The reaction probability , absorption cross-section $\langle n \rangle$, and $\langle E \rangle$ of CF_3CH_3, CF_3CH_2Br and CF_3CH_2Cl laser induced reaction

A. CF_3CH_3 R(16), 973.3 cm^{-1}

$\emptyset$ J/cm^2	$P(\emptyset)$	$\sigma(\emptyset)$ $cm^2/molecule$ $\times 10^{-20}$	$\langle n \rangle$ photon	$\langle E \rangle$ kcal/mole
1.8	6.9×10^{-3}	3.6	3.35	9.33
2.3	2.2×10^{-2}	3.6	4.32	11.93
2.7	4.0×10^{-2}	3.6	5.04	14.00
3.1	7.0×10^{-2}	3.6	5.76	16.07
3.5	2.0×10^{-1}	3.6	6.42	17.88
4.4	2.0×10^{-1}	3.6	8.19	22.81
4.5	2.0×10^{-1}	3.6	8.37	23.33

B. CF_3CH_2Br R(26), 1082 cm^{-1}

$\emptyset$ J/cm^2	$P(\emptyset)$	$\sigma(\emptyset)$ $cm^2/molecule$ $\times 10^{-19}$	$\langle n \rangle$ photon	$\langle E \rangle$ kcal/mole
0.50	5.3×10^{-3}	4.20	9.77	30.38
0.65	2.0×10^{-2}	4.00	12.10	37.44
0.80	2.9×10^{-2}	3.85	14.30	44.35
	3.6×10^{-2}			
0.90	3.7×10^{-2}	3.75	15.70	48.67
1.25	1.3×10^{-1}	3.45	20.00	62.06
1.60	1.4×10^{-1}	3.25	24.20	74.88
1.80	2.0×10^{-1}	3.10	26.00	80.35
1.85	2.9×10^{-1}	3.00	25.80	79.92
2.00	3.2×10^{-1}	2.95	27.40	84.96
2.47	3.3×10^{-1}	2.70	31.00	96.05
3.34	3.7×10^{-1}	2.30	33.90	105.00

C. CF_3CH_2Cl R(30), 1085 cm^{-1}

$\emptyset$ J/cm^2	P($\emptyset$)	σ($\emptyset$) cm^2/molecule x 10^{-20}	<n> photon	<E> kcal/mole
0.55	1.5 x 10^{-3}	3.8	0.97	3.0
0.72	3.9 x 10^{-3}	4.4	1.50	4.6
0.90	9.0 x 10^{-3}	5.0	2.11	6.5
1.20	2.0 x 10^{-2}	6.0	3.38	10.4
1.33	3.5 x 10^{-2}	6.5	3.96	12.2
1.77	8.0 x 10^{-2}	8.2	6.79	20.9
2.31	1.5 x 10^{-1}	9.7	10.49	32.3
2.87	2.5 x 10^{-1}	9.6	12.89	39.7
3.33	3.5 x 10^{-1}	9.1	14.16	43.6
3.73	4.5 x 10^{-1}	9.0	15.68	48.3
4.13	6.0 x 10^{-1}	8.9	17.18	52.9
4.82	8.0 x 10^{-1}	8.8	19.83	61.1
5.30	8.0 x 10^{-1}	8.8	21.71	67.2

V. Survey of Products for CF_3CH_2Br Laser Photolysis

The properties of CF_3CH_2Br are similar to those of CF_3CH_2Cl, except the C-Br bond (69 kcal/mole) is weaker than the C-Cl bond (82 kcal/mole). If $CF_2=CH_2$ is one of the main products from the secondary reaction of CF_3CH_2 radical, it should be favored even more for the CF_3CH_2Br reaction.

The samples were irradiated and analyzed isothermally at $80^{o}C$ with a carrier gas He flow rate of 55 ml/min in a Porapak Q column. The G.C. trace is shown in Figure 37. Only five out of more than eleven products were identified by GC-Mass spectra, (i.e., $CF_2=CH_2$, $CF_2=CHF$, $CF_3CH=CF_2$, $CF_3CH=CH_2$ and $CF_2=CHBr$). Three of them ($CF_2=CH_2$, $CF_2=CHF$, $CF_2=CHBr$) were verified by injecting the pure sample and observing the same retention time in the GC(FID). The retention time for these five products and the reactants are listed in Table 17A.

Table 17A

substance	retention time
$CF_2=CH_2$	30 sec
$CF_2=CHF$	40 sec
$CF_3CH=CF_2$	2 min 20 sec
$CF_3CH=CH_2$	3 min 10 sec
$CF_2=CHBr$	9 min
CF_3CH_2Br	22 min

From the experiments, we can see that $CF_2=CH_2$ is one of the products. It was assumed that the CF_3CH_2 radical is produced with a sufficient excess of vibrational energy to be in the quasicontinuum. It absorbs additional photons and undergoes a secondary reaction to form $CF_2=CH_2$.

Three experiments were done to check the quenching of the CF_3CH_2Br reaction by toluene. In pure CF_3CH_2Br experiment, $P(\emptyset)$

A. $CF_2 = CH_2$ D. $CF_3CH = CH_2$

B. $CF_2 = CHF$ E. $CF_2 = CHBr$

C. $CF_3CH = CF_2$ F. CF_3CH_2Br
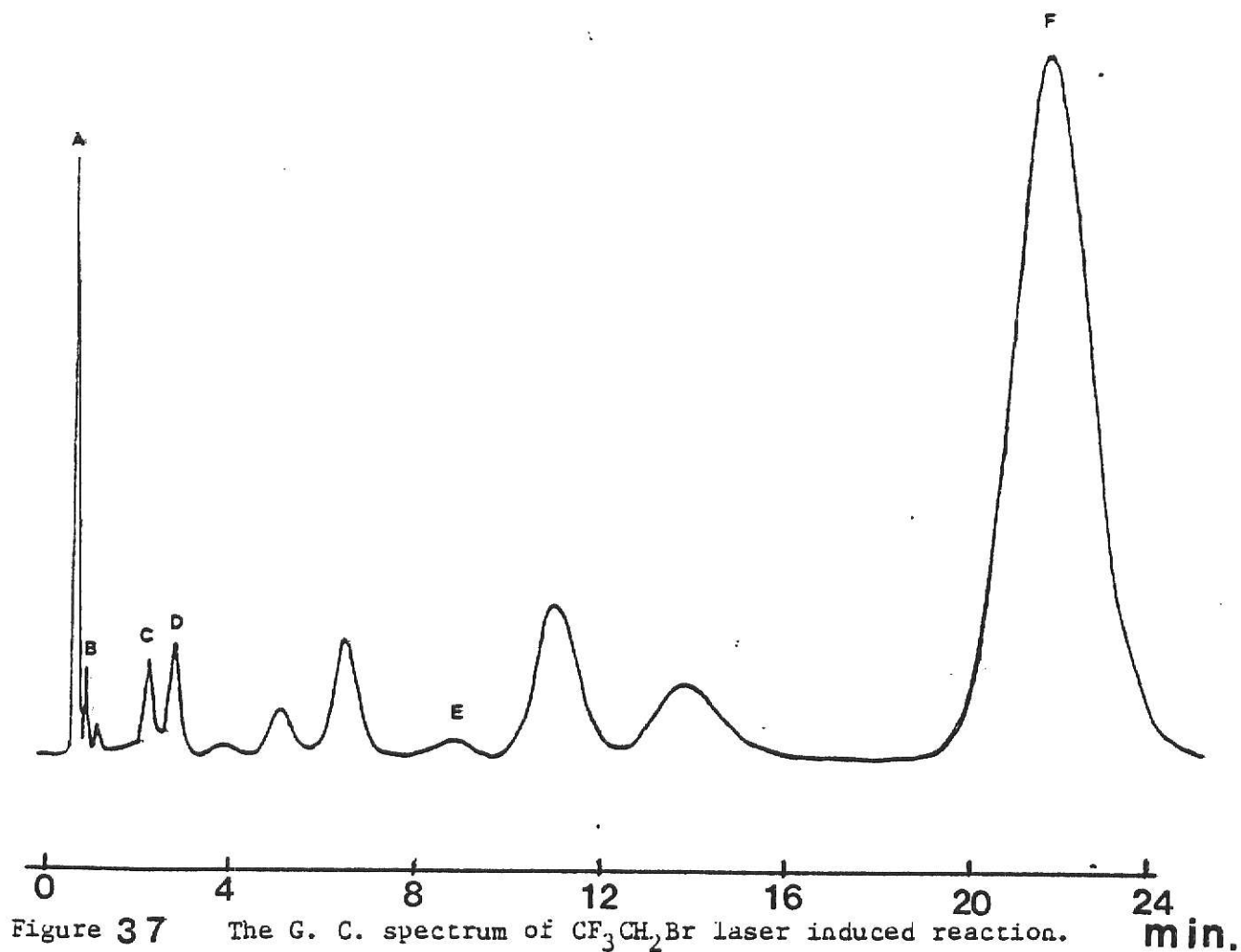
Figure 37   The G. C. spectrum of CF_3CH_2Br laser induced reaction.
The laser beam was R(26), $\phi = 1.35$ J/cm^2, the Porapak
Q column temperature was 85° C.

= 0.148 at $\emptyset$ = 1.35 J/cm^2, this correlates very well with the old data in Table 16, where P($\emptyset$)= 0.13 at $\emptyset$ = 1.25 J/cm^2. There is obvious quenching of the reaction probability with added toluene, i.e., the products were reduced, but the main product distribution didn't change significantly. This is consistent with CF_3CH_2Cl experiments. The experimental conditions and results are listed in Table 17B.

Table 17B $\quad\quad$ $\emptyset$ = 1.35 J/cm^2 $\quad\quad\quad\quad$ A = 2.97 cm^2

Vo/Go = 10.2 $\quad\quad\quad\quad$ CF_3CH_2Br = 0.05 torr

toluene torr	i	P($\emptyset$)	$CF_2=CH_2$ fract.%	$CF_2=CHF$ fract.%	$CF_2=CHBr$ fract.%
0	20	1.48 x 10^{-1}	70.4	10.7	18.9
0.15	15	9.96 x 10^{-2}	80.2	6.0	13.6
0.50	10	3.20 x 10^{-2}	82.4	5.4	12.3

We are not sure about the whole mechanism, however, HF elimination, HBr elimination and C-Br rupture are occuring with CF_3CH_2Br. Because of the lower C-Br bond energy, more C-Br rupture products are expected than for the CF_3CH_2Cl C-Cl rupture reaction. Also the larger number of Br and F atoms will lead to more secondary reactions.

DISCUSSION

I. Literature review of Multiphoton Induced Reactions of Fluor-
inated Methanes and Ethanes[1].

The possibility that a polyatomic molecule in an intense
field of an infrared laser could absorb enough photons to disso-
ciate in a very short time span was first suggested in 1971 by
Isenor and Richardson[18] based on their experimental observation
of luminescence from irradiation of some small molecules, CH_3Cl,
CF_4, CF_2Cl_2, SiF_4, NH_3, etc. Infrared multiphoton
dissociation(MPD) was shown to be isotopically selective in 1974
by Lyman et al[19]. By 1980, it has been shown to occur in a wide
variety of molecules in many different types of experiments. In
the measurements of product yields, it is desirable to obtain
information on the identity and yield of the products and the
energy distribution of the reacting molecules as a function of
frequency, power, and energy fluence of the laser, as well as
other experimental parameters. These results are necessary for
understanding the important aspects of the dynamics of unimolec-
ular dissociation and for obtaining information concerning the
multiphoton excitation of the molecules prior to dissociation.

The molecular beam method gives collisionless conditions.
Coggiola et al[20] were the first to demonstrate the collisionless
multiphoton dissociation of polyatomic molecules, they also
measured the translational energy distributions of the fragments

from SF_6 in a crossed laser-molecular beam arrangement. The Berkeley group has used this technique to study MPD of a variety of other molecules including N_2F_4, and a number of halogenated methanes, ethanes, and ethylenes. In all cases unimolecular reaction proceeds according to the statistical theory of unimolecular reaction. Three molecules closely related to the work here (CHF_2Cl, $CHFCl_2$, and CH_3CCl_3), gave either three-centered or four-centered elimination of HCl as the lowest reaction channel.

There are numerous examples of time-resolved spectroscopic detection of products in the literature for MPD. Quick and Wittig[17] measured infrared spontaneous emission from vibrationally excited HF produced in MPD of vinyl fluoride and other fluorinated ethanes and ethylenes. A linear dependence of fluorescence intensity with $\emptyset < 30$ J/cm^2 was observed. Wurzberg[21] et al used LIF to monitor production of CF_2 from MPD of CF_3Br and CF_3I. They argue that the CF_2 arises from secondary dissociation of the primary CF_3 product during the laser pulse. This may be possible even though CF_3 is only "born" with a few kcal/mole of internal energy, since it absorbs around the same frequency as CF_3Br and CF_3I.

While MPD tends to proceed via the lowest energy channel or the channel that is statistically more favorable, if a molecule has two (or more) dissociation channels close in energy, the molecule may be excited to above the thresholds of all these channels. In such cases there will be competition between the various channels and the branching ratio may depend on the laser pumping rate, as well as the k_E for each channel. Such competi-

tion is expected to occur within the framework of statistical unimolecular rate theory . The situation is somewhat analogous to a pyrolysis experiment where at higher temperatures additional dissociation pathways may open up and branching ratios may change with temperature. Using the LIF technique mentioned earlier, King and Stephenson[22] estimated that for CF_2Cl_2 about 15% of the decomposition yields Cl_2 and 85% yields Cl. Using a differentially pumped, beam sampling mass spectrometer and energy fluences of 10-140 J/cm^2, Hudgens measured the branching ratio of Cl versus Cl_2 elimination[23] from CF_2Cl_2 to be greater than 33 : 1. In the molecular beam experiments of Sudbo[24] et. al., energy fluences of 5 - 10 J/cm^2 were used and again the atomic elimination channels were found to be the major channels for both CF_2Cl_2 and CF_2Br_2. The implication of the experiments is that the atomic dissociation becomes more important relative to three-center molecular elimination as the energy fluence is increased. This is consistent with the threshold energies and the pre-exponential factors for the competing channels.

We will now consider briefly a few examples of MPD studied in gas cell at relatively high pressures (> 1 torr), for which thermal chemistry will dominate the yields. Dever and Grunwald[25] irradiated CF_3Cl and $CFCl_3$ as pure gases at 60 torr and in the presence of 0 - 60 torr of H_2. Energy densities between 0.1 and 0.4 J/cm^2 were used. On the basis of the reaction products they concluded that the primary processes are $CF_3Cl \longrightarrow CF_3 + Cl$ and $CFCl_3 \longrightarrow CFCl + Cl_2$. However, the results of Hudgens[23] and Sudbo et al[24] clearly

demonstrate that under collisionless conditions $CFCl_3$ primarily dissociates into $CFCl_2 + Cl$ rather than $CFCl + Cl_2$. This illustrates the danger of drawing conclusions about the primary collisionless dissociation process from high pressure gas cell experiments.

Hanh Nguyen[26] studied the of CO_2 laser-induced reaction of ethyl 3-cyclohexene-carboxylate. This large organic ester,which has two reaction channels differing by 13 kcal/mole in threshold energies, was studied over the 0.02- 0.20 torr pressure range, $P(\emptyset)=10^{-3}-1.0$. The reaction product ratio was very dependent on the incident laser energy but almost independent of the laser pulse duration (intensity) at constant fluence. The former can be explained for low fractional reaction by a postpulse model using RRKM rate constants and a broad distribution function with mean energy equal to the absorbed laser energy. Studies of ethyl vinyl ether done by Brenner[25] showed that the product ratio follows the RRKM expectation; however the product ratio is dependent on laser intensity and fluence. This suggests the presence of a bottleneck in the vibrational manifold of levels.

A series of organic esters[7] have been studied using multi-photon, pulsed, infrared laser excitation. The dependence of the reaction probability and absorption cross-sections on the laser fluence, laser frequency, reactant pressure, and bath gas pressure was determined. A master equation formulation which matched the reaction yield and absorbed energy without bottlenecks was used to explain both general and specific features[6(b)]. The postpulse reaction and quenching, which that

is very important in bulb experiments for large molecules, was elucidated. These organic acetates provide a conclusive body of data illustrating the MPD behavior of large molecules without serious bottlenecks for multiphoton absorption.

Setser et. al.,[7,26] have extensively studied the vibrational deactivation of chemically activated $CF_3CH_3^*$ and $C_2H_5F^*$. The experimental technique was the measurement of the ratio of the unimolecular decomposition product to the collisionally stabilized product over a wide range of pressure. By fitting the pressure variation of this ratio with model calculations, the average vibrational energy ,<E>, removed from the reactants per collision was assigned. These results are useful for understanding collisional deactivation of buffer gases in MPD experiments.

The laser-induced unimolecular reaction probability and absorption of CF_3CH_3[5] has been studied[5]. The multiphoton absorption of CF_3CH_3 does not follow Beer's law, rather the absorption increases with CF_3CH_3 pressure. This can be explained by collisional rotational relaxation during the laser pulse. The $\sigma_L(\emptyset)$ also was measured with the short laser pulse and compared with the $\sigma_L(\emptyset)$ obtained with long laser pulse. Because anharmonicity and saturation occured, the absolute value of $\sigma_L(\emptyset)$ was smaller for the short pulse. The $\sigma_L(\emptyset)$ decreases very sharply with an increase of $\emptyset$ at low fluence and becomes constant at high fluence region. The saturation in the reaction probability seems to occur above 3 J/cm^2 and reaches $P(\emptyset) = 0.20$. Ethylfluoride behaved in much the same way as CF_3CH_3 for

laser absorption. Experiments also were done to study collisional effects in IR multiphoton induced unimolecular reactions of fluorethane and trifluoroethane[7(a)]; A good correlation existed with the collisional quenching from chemical activation data. Also a correlation between laser pulse length and extent of collisional quenching and/or collisional enhancement was observed.

The CF_3CH_2Br molecules[9] do follow Beer's law for the $\sigma_L(\emptyset)$ measurements and rotational hole burning was not observed. However, a saturation in the reaction probability still did occur above 3 J/cm^2 with $P(\emptyset) \sim 0.40$.

From the description above, we can see the difference shown between CF_3CH_3, C_2H_5F and CF_3CH_2Br molecules. That is why we chose to study CF_3CH_2Cl in some detail. The experimental work is discussed in the following sections. The elementary unimolecular reactions of CF_3CH_2Cl are first characterized and then the laser induced reaction is compared to the results for CF_3CH_3 and CF_3CH_2Br.

II. Thermochemistry and Unimolecular Reaction Channels for

CF_3CH_2Cl

The ΔH°_{f298} values calculated from bond additivities[28] are as follows.

CF_3CH_2Cl $\qquad$ ΔH°_{f298} = -177.5 kcal/mole

$CF_2 = CHCl$ $\qquad$ ΔH°_{f298} = - 79 kcal/mole

$CF_2 = CHF$ $\qquad$ ΔH°_{f298} = -115 kcal/mole

The thermochemical data for the rest of the reaction species were taken from Benson's[28] tables :

HF $\qquad$ ΔH°_{f298} = -64.8 kcal/mole

HCl $\qquad$ ΔH°_{f298} = -22 kcal/mole

Cl $\qquad$ ΔH°_{f298} = 28.9 kcal/mole

F $\qquad$ ΔH°_{f298} = 18.9 kcal/mole

CF_3CH_2 $\qquad$ ΔH°_{f298} = -123.6 kcal/mole[28,41(b)]

An electrostatic model[29] for predicting the heat of formation 177.3 kcal/mole of CF_3CH_2Cl was published as this work was being done. This is a perfect match to our calculated value, i.e., 177.5 kcal/mole. The heat of reaction calculated from the above data for the CF_3CH_2Cl reactions are

$CF_3CH_2Cl \longrightarrow CF_2=CHCl + HF$ ΔH°_{f298} = 33.7 kcal/mole (1)

$CF_3CH_2Cl \longrightarrow HCl + CF_3CH: \longrightarrow CF_2=CHF$ (2)

$\qquad\qquad\qquad\qquad\qquad\qquad\qquad\qquad$ ΔH°_{f298} = 40.1 kcal/mole

$CF_3CH_2Cl \longrightarrow CF_3CH_2 + Cl$ ΔH°_{f298} = 82.8 kcal/mole (3)

$CF_3CH_2 \longrightarrow CF_2=CHF + F$ ΔH°_{f298} = 27 kcal/mole (4)
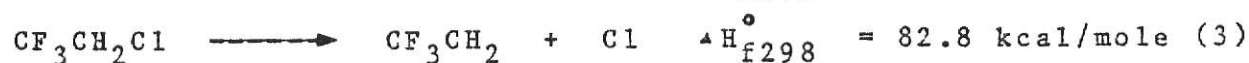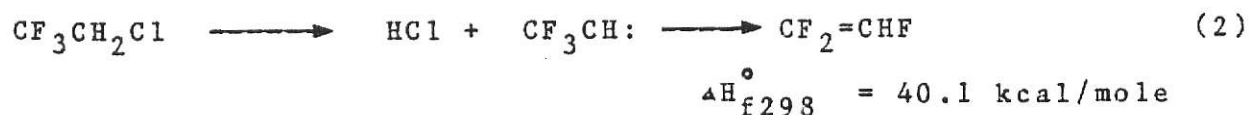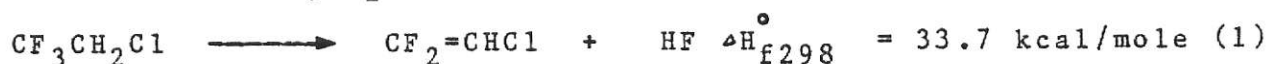
The thermal unimolecular reaction of CF_3CH_2Cl has been studied by the shock tube method by Tschuikow-Roux[10] and the

chemical activation method by Holmes[11]. In the chemical activation work of Holmes' CF_3I and CH_2ClI were photolyzed to form the chemical activated $CF_3CH_2Cl^*$.

$$CF_3I \xrightarrow[\text{Hg}]{\text{hv}} CF_3 + HgI$$

$$CH_2ClI \xrightarrow[\text{Hg}]{\text{hv}} CH_2Cl + HgI$$

$$CF_3 + CH_2Cl \longrightarrow CH_2ClCF_3^* \quad (\langle E \rangle = 100 \text{ kcal/mole})$$
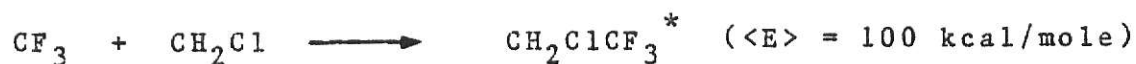
The $CF_2=CHCl$ was found as a product but no $CF_2=CHF$ was identified. In Holmes' experiment, the average energy $\langle E \rangle$, was 100 kcal/mole and the E_o for HCl elimination was set at 76 kcal/mole.

The three-centered (α,α) HX elimination and four-centered (α,β) HX elimination channels are well documented elementary processes. The α,β elimination reaction proceeds by a simultaneous breaking of the C-F and C-H bonds and formation of the C-C double bond and the H-F bond. Because of these simultaneous processes, the complex is called four-centered[30], it can be represented as :

$$CF_3CH_2Cl \longrightarrow \underset{F\text{-----}H}{\overset{F}{\underset{}{F}}\overset{H}{\underset{}{\overset{}{C}}}-\overset{}{C}\overset{Cl}{}} \longrightarrow HF + CF_2=CHCl \quad (1)$$
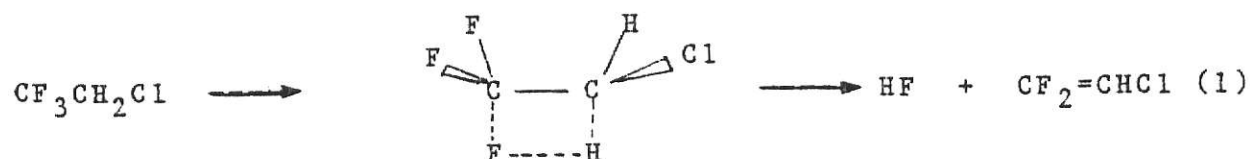
There are interesting changes in threshold energy with substitu-

tion on the 1 and 2 position for the four-centered reaction[31].
The model incorporating varying degrees of charge separation is
used for the explanation of the variation of threshold energy
with halogen substitution :

$$\delta^- C^2 \text{———} {}^1C \delta^+$$
$$\delta^+ H \text{———} x \delta^-$$
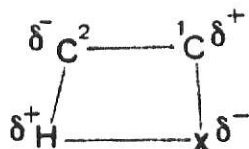
Maccoll[32] concluded that substitution of Cl or Br at the 1 and 2
positions lowered and raised E_0, respectively. Chlorine is a
strong electron accepting substituent and its expected effect
might have been to destabilize the δ^+ for substituent at the 1
position and to stabilize the δ^- or substituent at the 2 posi-
tion. The reverse is the case, which is an effect that has been
observed for conjugated systems in which partial delocalization
occurs between the cholrine non-bonded electrons and the conju-
gated system. Since the four-centered elimination transition
states have partial double bond character, the delocalization
effect causes chlorine substitution at the 1 position to stabil-
ize the δ^+. This reasoning suggests that for fluorine the
inductive effect dominates at the 1 position but delocalization
must have some importance at the 2 position, since E_o is
increased at both positions. The Arrhenius parameters for sev-
eral compounds with four-centered reaction pathway is listed in
Table 18. The log A value per reaction channel is calculated
and listed in the parenthesis, the value for C_2H_5F, CF_3CH_3 and
CH_3CH_2Cl is ~13.2.

Table 18

Molecule	rxn.	log A per reaction channel	Eo(kcal/mole)	ref
CH_3CH_2Cl	HCl eli.	13.5(13.2)	56.6	28
$1,1-C_2H_4Cl_2$	HCl eli.	13.5(12.9)	53.5	30
$1,1,2-C_2H_3Cl_3$	HCl eli.		59	
C_2H_5F	HF eli.		57.6	7(c)
		13.4(13.1)	59.9	8
$1,1-C_2H_4F_2$	HF eli.		61.7	8
CH_3CF_2Cl	HCl eli.		69	33
CF_3CH_3	HF eli.	14(13.2)	68.7	7(a)
CF_3CH_2Cl	HF eli.	12.7(12.1)	67.6	10(1120°K)
		13.8(13.2)	76	11(800°K)

Therefore, the A value obtained estimated from the shock tube[10] data for CF_3CH_2Cl was too low. The expected value is 13.2, which agrees with the one estimated by Holmes[11], will lead to an log A value for this reaction fo 13.8 for a reaction path degeneracy of 4.

The E_o for four-centered elimination is 76 kcal/mole as determined by Holmes from matching observed and calculated chemical activation rate constants. The E_o for HF elimination from CF_3CH_3 is 68.7 kcal/mole[33]. This trend is consistent with the Cl substituent at C^2 position which increases the E_o for four-centered elimination as discussed above. Therefore, the E_o value from shock tube data seems too low; as would be expected, since the A factors also were too low. Lacking any better evidence, we will utilize E_o=76 kcal/mole for HF elimination from CF_3CH_2Cl.

As mentioned before, the four-centered HF elimination from CF_3CHCl_2 was not observed[12(c)], probably because two Cls substitute on the C_2 position raise the threshold energy so much that

Cl rupture is the dominant reaction channel.

The mechanism for CF_3CH_2Cl three-centered elimination is :

$$CF_3CH_2Cl \longrightarrow \left[F-\underset{\underset{F}{|}}{\overset{\overset{F}{|}}{C}} - \underset{\underset{}{}}{\overset{\overset{H}{|}}{C}} \underset{\cdot \cdot H}{\overset{\cdot Cl}{\diagup}} \right]^+ \longrightarrow HCl + CF_3CH:$$
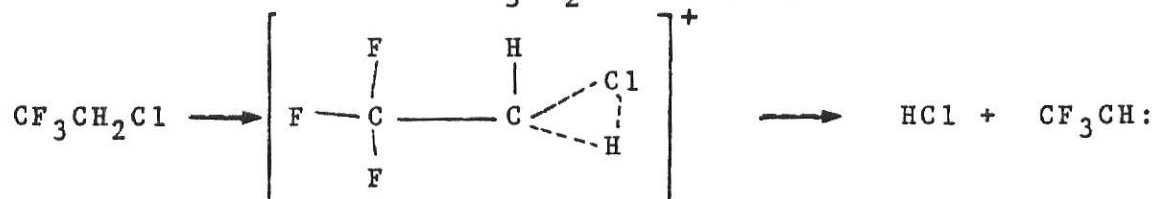
The formation of the HCl and $CF_3CH:$ is rather endothermic and $\Delta H^o \sim E_o$. The three-centered elimination of DX or HX has been observed from chemically activated CD_3CHF_2[34], $CH_2ClCDCl_2$[31], CH_2FCDF[35], and from shock heated CF_3CH_2Cl[10], and CF_3CHCl_2[37]. The three-centered elimination channel initially forms HX and a carbene, which subsequently preferentially rearranges by H migration to the olefin[31]. The energy barrier for the reverse reaction of the carbene with HX or DX is small. This energy profile is in sharp contrast to the four-centered HX elimination process which has a large reverse activation energy[36]. Rearrangement of the carbene, of course, releases a substantial amount of energy to the olefin.

The $CF_3CH:$ rearrangement by F migration has been observed by Haszeldine[38,39]; $CH_3CH:$ was generated by photolysis of the corresponding diazo-compound. From Haszeldine's work, $CF_3CH:$ did react with $CF_2=CHF$, but only at the level of 1% starting with 2.5 atm CF_3CHN_2. In my reaction system, $CF_3CH:$ could rearrange to produce trifluoroethylene or react with olefins, or presumably with toluene, too. Another possibility is $2CF_3CH: \longrightarrow CF_3CH=CHCF_3$, which is commonly observed with $2CF_2: \longrightarrow C_2F_4$, but no $CF_3CH=CHCF_3$ was observed. Also no products corresponding to $CF_3CH:$ reacting with $CF_2=CH_2$, $CF_2=CHF$, or

$CF_2=CHCl$ were detected. The only reaction channel for the carbene that we identified was fluorine migration. This is consistent with Haszeldine's result. Presumably the CF_3CH: is formed with enough energy so that the small migration threshold energy for rearrangement does not inhibit the F atom migration.

The Arrhenius parameters for some related compounds which have α,α elimination pathways are listed in Table 19. The log A per reaction channel is given in the parenthesis.

Table 19

Molecule	reaction	log A	Ea (kcal/mole)	reference
CF_3CHCl_2	HCl eli.	13.4 (13.4)	63.1	36
CF_2HCl	HCl eli.	13.84(13.84)	55.8	41(a)
CD_3CF_2H	HF eli.	13.58(13.28)	64	34(a,c)
CF_3CH_2Cl	HCl eli.	13.30(13.00)	65.5	10
CF_3CH_2Cl	HCl eli.	13.77(13.47)	80	11

The three-centered elimination generally has a 2-3 kcal/mole higher threshold energy than four-centered elimination[35]. From the experimental result for CF_3CH_2Cl discussed in the next section, the trend is the same so that the E_o may be around 78-80 kcal/mole. The value from shock tube[10] experiments seems too low. A pre-exponential factor of 13.5 per reaction channel for HCl elimination looks reasonable for three-centered elimination from the above table.

The bond energies in CF_3CH_2Cl are as follows[28]:

C-F($\sim$108) > C-C ($\sim$100) > C-H ($\sim$98) > C-Cl ($\sim$81.5)

Rupture of the weakest bond, C-Cl, was suggested as a reaction pathway at temperatures above $1270^{\circ}K$ in shock tube experiments[10]. The reason is that two additional products,

identified as $CF_2=CFCl$ and CF_3CHCl_2 were observed. A similar bond rupture was seen in CF_3CHCl_2 in shock tube[36] experiments and in C-H or C-I simple fission of CH_3I, CH_4, and many other simple molecules. The Arrhenius parameters for these bond dissociations are listed below.

Table 20

molecule	reaction	log A	Eo	T($^\circ$K)	ref.
CF_3CHCl_2	C-Cl rup.	16	78	1200	36
CH_3I	C-I rup.	15.55		1000	28
CH_4	C-H rup.	14.7	100	1200-1800	41(a)

According to table 20, the bond rupture processes must have a loose transition state and the A factor must be large. A reasonable estimate will be $10^{15.0-15.5}$. The threshold energy will be equal to the bond dissociation energy.

What is the fate of the CF_3CH_2 radicals formed from the C-Cl rupture? The ethyl radical is known to decompose by H rupture, $CH_3CH_2 \longrightarrow C_2H_4 + H$ with $\Delta H = 38.1$ kcal/mole, and has the rate constant expression[41]: $\log k_1 = 13.5 - 40.7/2.3$ RT and the reverse reaction[28] $\log k_{-1} = 10.97 - 2.8/2.3$ RT. Our compound, CF_3CH_2, can be expected to have a similar decomposition reaction. With a threshold energy ~2 kcal/mole higher than the reaction endothermicity of 27 kcal/mole. Since the threshold energy is estimated as only 29 kcal/mole, the reaction should be even more faster than the ethyl radical decomposition.

In sensitization reactions the temperature is very high, which drives the CF_3CH_2 molecules to react in a manner similar to the shock tube technique, and $CF_2CH_2 + F$ will be found. In the laser induced reaction, The $CF_2=CH_2$ formed from C-Cl rupture

may continue to absorb the laser energy and an F atom rupture from CF_3CH_2 will follow even if CF_3CF_2 lacks enough energy to react.

An important consideration is the rate of the F and Cl atoms produced by the C-Cl rupture channel. The F and Cl atoms can react with the starting material CF_3CH_2Cl or the olefins. At high reaction probability, the F-atom concentration will be of the same order as the starting material, and there is a possible chain reaction.

$$F(Cl) + CF_3CH_2Cl \longrightarrow HF(HCl) + CF_3CHCl \quad (5)$$

$$CF_3CHCl \longrightarrow F + CF_2 = CHCl \quad (6)$$

If the rate constant for (5) is 10^{-11} cm^3/molecule,sec; the time to remove 1/2 of F is 10 μs for second order kinetics. This is longer than the cooling time (2~5μs). Therefore, the F atom reaction may be quenched by the cooling wave and ultimately react with the glass walls before it reacts with cold CF_3CH_2Cl. In any event CF_2=CHCl was not observed to increase significantly and the chain reaction can be discovered.

The rate of addition of F and Cl to olefins[42] (k > 10^{10} sec^{-1}) is faster than reaction with parent molecules, we therefore consider that the addition of radicals to the olefins : CF_2=CH_2, CF_2=CHF, and CF_2=CHCl are possible. Preferential addition at the carbon atom with the fewer F substituents is expected for CF_2=CH_2 and CF_2=CHF[42]. The attack of radicals on CF_2=CHCl[42] at the two possible sites are predicted on the basis of the stability of the adduct radical. We assume the main radial reaction are : [remember D(C-F) > D(C-H) > D(C-Cl)].

$$F + CF_2=CH_2 \longrightarrow CF_2CH_2F^* \longrightarrow CF_2=CHF + H \qquad (7)$$

$$F + CF_2=CHF \longrightarrow CF_2CHF_2^* \longrightarrow CF_2=CF_2 + H \qquad (8)$$

$$F + CF_2=CHCl \longrightarrow CF_3CHCl^* \longrightarrow CF_2CHCl + H \qquad (9)$$
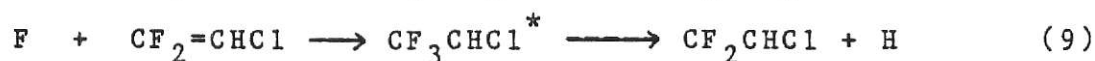
The second reaction forms C_2F_4, which is consistent with the experimental result because a trace amounts of C_2F_4 were detected. The third reaction does not change the amount of $CF_2=CHCl$, so the overall difference is the increase of $CF_2=CHF$ at the expense of $CF_2=CH_2$. The addition of F at the carbon atom with Cl of $CF_2=CHCl$ will increase the $CF_2=CHF$ at the expense of $CF_2=CHCl$, i.e.,

$$CF_2=CHCl + F \longrightarrow CF_2CHFCl^* \longrightarrow CF_2=CHF + Cl \quad (10)$$

Since reaction (9) does not do anything to the product distribution, the result observed was mainly from reaction (10). The addition of a Cl atom to the olefins will give no change of the products since the C-Cl bond is weaker than a C-F or C-H bond. Therefore the reverse reactions are dominant, providing that collisional deactivation is negligible. In conclusion, the $CF_2=CH_2$ must be derived either from "hot" CF_3CH_2 radical produced in the initial C-Cl dissociation or, more likely, from secondary infrared photolysis of CF_3CH_2 radical produced during the laser pulse. The lack of products from the F and Cl atoms is not fully understood but reaction with the walls may be the most likely end product for the low pressure laser work. For sensitization reaction, of course, the secondary reactions are important and indeed $CF_2=CHF$ is a much more important product (and does not correspond just to HCl elimination as the toluene experiments proved).

There are many examples of secondary MPA reactions. Secondary reaction from CF_3OOCF_3 of Steinfeld's work[43,44] is a recent example of this. When CF_3OOCF_3 is subjected to infrared radiation in the 9-19 μm region, at fluences above a few mJ/cm^2, symmetric cleavage occurs at the O-O bond.

$$CF_3OOCF_3 \xrightarrow{\text{nhv}} 2\ CF_3O$$
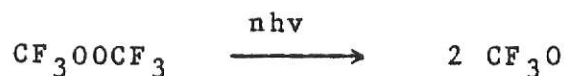
The CF_3O produced may continue to absorb infrared photons and further dissociate :

$$CF_3O \xrightarrow{\text{mhv}} CF_2O + F$$

The SF_4[24] and $CClF$[1] observed in the multiphoton dissociatin of SF_6, $CFCl_3$, respectively, which provided the basis for false speculation of mode-controlled chemistry, was found to be due principally to secondary multiphoton dissociation or chemical reactions involving the primary products SF_5 and $CFCl_2$.

The A factors for four and three-centered eliminations for typical cases are in the range of 13.2-13.4 per reaction channel (Table 18,19). In C-Cl rupture reaction, the loss of a heavy atom such as Cl is accompanied by a significant increase in the moment of inertia in the activated complex, and a significant reduction in the bending modes associated with the departing Cl atom. The changes described above lead to a relatively high A-factor[28] for the C-Cl rupture process, we estimate log A = 14.8. The simple bond dissociation has no back reaction energy barrier, so $E_0 \approx \Delta H^o$, and we set this value as 83 kcal/mole. We summerize the A and E_0 values which are the best fit to our experiment data and also the other results in the literature in Table 21. Further information about the transition state models are given in Appendix I.

Table 21

channel	prod.	ΔH^o kcal/mole	logA	Eo (kcal/mole)
HF eli.	$CF_2=CHCl$	33.7	13.77	76
HCl eli.	$CF_2=CHF$	40.1	13.80	80
C-Cl rup.	CF_3CH_2Cl	82.8	14.80	83

Calculated at $800^o K$.

III. Sensitized Reactions of CF_3CH_2Cl

Sensitized excitation produces a significantly different initial population of excited molecules compared to direct laser pumping. Low pressure direct-pumping excitation produces molecules with a high level of vibrational energy but which are rotationally and translationally cold. Excitation by multiple energy transfer steps resulting from collisions between excited absorber molecule and the reactant molecule will generate a thermalized system at the temperature defined by the amount of energy absorbed and the heat capacity of the system. In my work, a purely thermal excitation of CF_3CH_2Cl was produced by CO_2 laser MPA of a non-reactive sensitizer molecule, SiF_4.

In order to remove secondary reactions, sensitization with toluene was also carried out at nearly the highest laser energy ($\emptyset$ = 0.6) used in sensitization reactions. Similar experiments were done with CF_2=CHCl and CF_2=CHF as the reactants; but, no products were observed. The product distribution for sensitization with and without the toluene is similar at low fluence, i.e., with $\emptyset$ < 0.3 J/cm^2, CF_2=CHCl was the main product (Figure 22,24). At low fluence the third channel, C-Cl rupture, was not significant and the trace amounts of F and Cl atom did not cause the secondary radical reactions to be important. When the fluence is raised, the main change in products is the growth of CF_2=CHF at the expense of CF_2=CHCl. At $\emptyset$ = 0.35 J/cm^2, without toluene (Figure 22), the distribution is CF_2CHF = 60%, CF_2CH_2= 20%, and CF_2CHCl= 20%, but with the toluene (Figure 24), CF_2CHF= 15%, CF_2CH_2= 40%, and CF_2CHCl= 45%. This shows that

radical reactions play an important role in sensitization reaction. In the absence of radical scavenger, the secondary mechanism was described in the previous section. The radical scavenger has little or no effect on the sensitized reaction probability (Figure 21) even though the product distribution is affected.

Three main products, $CF_2=CH_2$, $CF_2=CHF$, and $CF_2=CHCl$, were found in laser sensitized reaction with toluene. The $CF_2=CHCl$ and $CF_2=CHF$ are from the HF four-centered elimination, and from the HCl three-centered elimination, respectively. The amount of $CF_2=CHCl$ is always more than $CF_2=CHF$ (Figure 25), but the relative yield of $CF_2=CHF$ increases with 0. The pre-exponential factors for these two channels are close; so, the threshold energy for HF elimination must be lower than HCl elimination. The $CF_2=CH_2$ product from C-Cl rupture is very fluence dependent, this channel has a high E_0 and A factor. The rather strong dependence of the product ratio upon fluence is expected, because these three channels have different pre-exponential factors and Eo values.

Now we shall try to assign the temperature for sensitization reactions in order to make a more quantitative comparison of the product ratios to the Arrhenius rate constant ratios. The absorbed energy is related to temperature[45], i.e. $\langle E \rangle = \int_{298}^{T} CpdT$. The absorption measurement for 5 torr of SiF_4 at P(40), the 1027 cm^{-1} laser line, were done. The detail experimental result and temperature assignment are in Appendix II. The assigned temperatures are indicated in Figure 25.

We now compare the sensitization product ratio with the predicted results from the temperatures and transition state models. (The activated complex models are listed in appendix I). The temperature and the product ratios for the experimental results along with the theoretical values deduced from the k_a value for each channel at certain temperatures(Appendix II) are listed in Table 22. Table 23 shows the results from Moore's temperature assignment[13] which involves a more elaborate transport property model for 5 torr of SiF_4. Figure 38A shows the product ratio of HF elimination vs. HCl elimination and Figure 38B shows the product ratio from HF elimination vs. C-Cl rupture. If the calculated curves and experiment values are parallel, the assignment of the difference of the threshold energies between two reaction channels must be good. The assignment for log A values are no better than ±0.5 and hence the agreement in Figure 38B is acceptable. From Figure 38A, if E_{oHF}=76 kcal/mole, and E_{oHCl} = 79 kcal, a cross-over between experimental data and calculated value indicate that the difference in threshold energies is not good enough. A larger difference is needed and E_{oHCl}=80 kcal/mole was found to be a better assignment. A small deviation for the calculated and experimental data for E_{oC-Cl}=83 kcal than E_{oC-Cl} = 83.5 kcal/mole is shown in Figure 38B. So 83 kcal/mole for C-Cl rupture threshold energy was accepted. The temperature assignment of this work is similar to the temperature of Moore's work up to $1350^{o}K$ (Figure 42). Above this temperature our method gives higher values of T. This difference can be examined in a
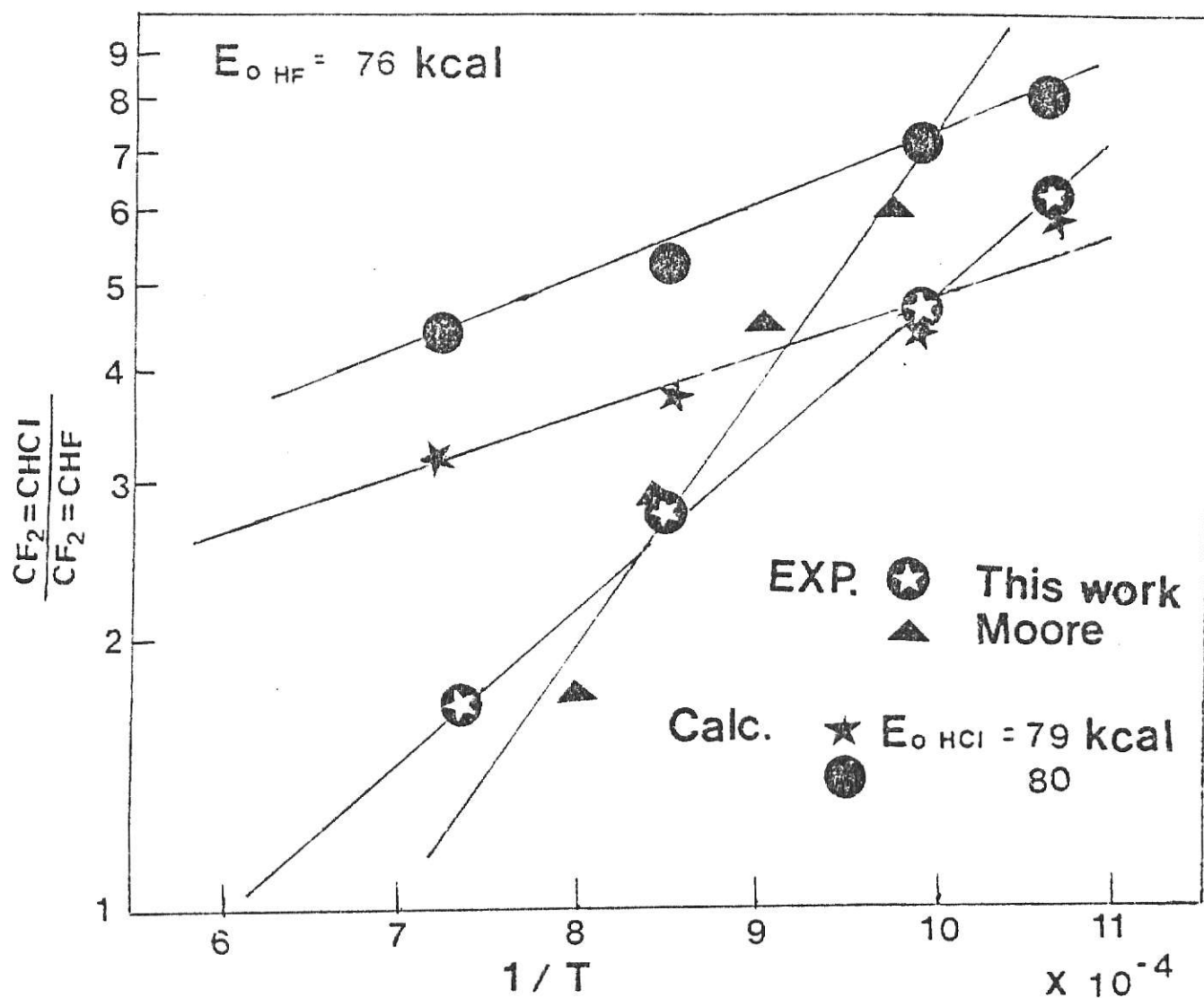
Figure 38A   Product ratio, $CF_2=CHCl/CF_2=CHF$, vs $1/T$ for
experimental and calculated sensitization results
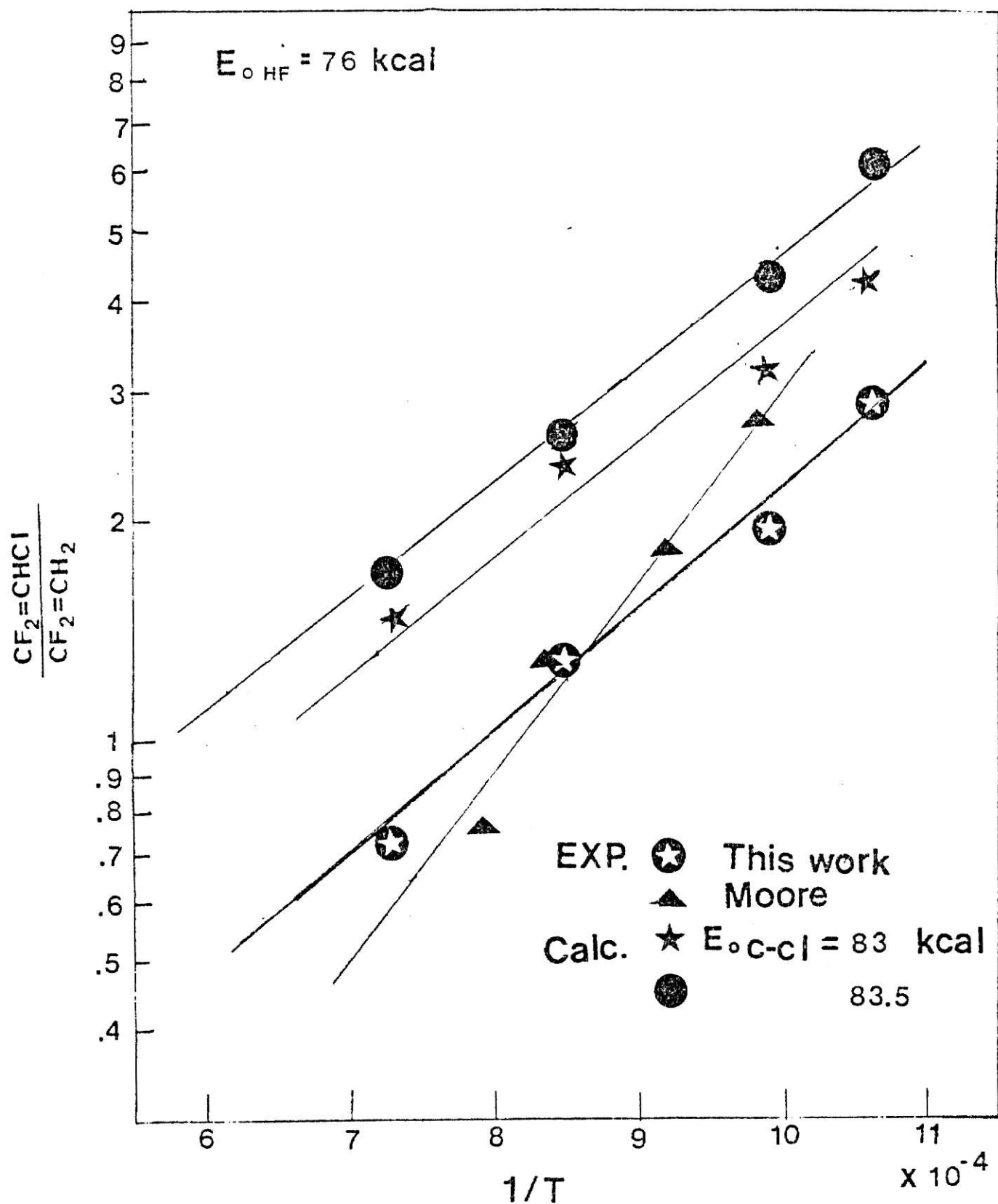
Figure 38B Product ratio, $CF_2=CHCl/CF_2=CH_2$, vs 1/T for experimental and calculated sensitization results

different way by looking at the fractional reaction per pulse.

Table 22   X = CF_2CHCl/CF_2CHF,   Y = CF_2CHCl/CF_2CH_2

$\emptyset$	T	$\frac{1}{T}$ x10^{-4}	exp		HCl eli.		C-Cl rup.	
	^{o}K		X	Y	Eo=80 X	Eo=79 Y	Eo=83 X	Eo=83.5 Y
0.19	946	10.6	6.2	2.9	8.2	5.5	4.2	6.5
0.22	1010	9.9	4.8	1.9	7.3	4.7	3.0	4.4
0.36	1175	8.5	2.8	1.3	5.3	3.7	2.4	2.7
0.43	1380	7.2	1.7	0.7	4.2	3.3	1.5	1.8

Table 23   X = CF_2CHCl/CF_2CHF,   Y = CF_2CHCl/CF_2CH_2

laser energy Joule	Temp.(^{o}K)	1/T(x10^{-4})	X	Y
0.092	1025	9.76	6.2	2.9
0.125	1100	9.09	4.8	1.9
0.145	1200	8.33	2.8	1.3
0.170	1300	7.69	1.7	0.7

For a first order reaction, $1 - P(\emptyset) = [C]/[C]o = e^{-k\Delta t}$, where $P(\emptyset)$ is the reaction probability from our sensitized experiments. The rate constant, k, can be deduced from the estimated temperature and the transition state model, Δt is the reaction time, the latter is associated with the time for the cooling wave, which is $\sim 10 \mu s^{13}$, so Δt was set at 10 μs and 16 μs for comparison. The value of $[C]/[C]o$ can then be calculated as shown in Table 24A,B. The data from the temperature assignment in this work is shown in Table 24A. Table 24B shows the results from Moore's temperature assignment. If we compare the $1-P(\emptyset)$ and $[C]/[C]o$ columns of the Tables, the agreement looks similar for both temperature assignment. The 10 μs, 16 μs reaction times do not effect $[C]/[C]_o$ too much, since the reac-

tion rate was small. Both temperatures assignments seem a little low but this strongly depends on the rate constant assignments which are uncertain by factor of 2-5. We conclude the temperature assignment is satisfactory for our purpose.

Table 24A

$\emptyset$ (J/cm^2)	P($\emptyset$)	1-P($\emptyset$)	Temp $^\circ$K	1/T x10^{-4}	k sec^{-1}	[C]/[C]o t=10μs	t=16μs
0.19	0.005	0.995	946	10.6	0.00023	1.00	1.00
0.22	0.013	0.987	1010	9.9	0.0040	1.00	1.00
0.36	0.041	0.957	1175	8.5	1.12	1.00	0.99
0.43	0.045	0.955	1380	7.2	161.4	0.99	0.99

Table 24B

Temp $^\circ$K	1/T x10^{-4}	k sec^{-1}	[C]/[C]o t=10μs	t=16μs
1025	9.76	0.0063	1.00	1.00
1100	9.09	0.0976	1.00	1.00
1200	8.33	2.01	0.99	0.99
1300	7.69	27.54	0.99	0.99

IV. Laser Induced Unimolecular Reactions

(1) P($\emptyset$) vs. reactant pressure

It was demonstrated that experiments at 0.05 torr of neat parent   reactant   were   free   of   thermally   assisted   induced reaction[2] for CF_3CH_3 and several acetates. Figure 15 illustrated the effect on P($\emptyset$) of varying the pressure of neat CF_3CH_2Cl at the same laser frequency. The enhancement of P($\emptyset$) with the increase of reactant pressure results from two general tendencies which reinforce each other: (i) the higher pressure promotes intermolecular collisional transfer of energy and (ii) the higher pressure lengthens the time before the onset of the cooling wave[14]. Thus, the thermal time regime begins more quickly after the pulse and lasts for a longer time as the reagent pressure is increased.

We found no effects of pressure on P($\emptyset$) for $\emptyset$ = 1.5 - 2.5 J/cm^2 at moderate pressure (0.05-0.80 torr). In fact pressure had no discernible trend at $\emptyset$ = 2.17 and 1.55 up to 3.2 torr. It might be possible that at lower fluence molecules remain in the low energy levels and not all (depending on fluence) molecules reach the quasi-continuum. A small fraction of the molecules could behave as a cold bath gas. Thus post pulse quenching could compensate for enhancement from (i) and (ii). Thus, there may be compensating effects and that is why there was no obvious enhancement of reaction probability with pressure at lower fluence. The absorption at low fluence did suggest bottlenecking. The increase of $\sigma_L(\emptyset)$ with CF_3CH_2Cl pressure may be explained by rotational relaxation during the laser

pulse. Collisions bring more molecules into the rotational states which are resonant with the laser. For low energy fluence, the collisional deactivation at high vibrational energy is dominant and rotational relaxation is not easily observed from $P(\emptyset)$ data, but it is suggested from $\sigma_L(\emptyset)$ data.

(2) P($\emptyset$) and product distribution with added inert or scavenger gases

The degree of quenching depends upon the nature and pressure of the bath gas and on laser fluence. The inert gases N_2 and He were used as the buffer gas to check on rotational bottlenecking. The quenching was very mild because the pressures were low. There was little quenching and no enhancement for He up to 10 torr and the product distribution does not change (table 7). The He is very inefficient and if we increase the pressure to 50 - 100 torr, there should be an obvious quenching. There was some quenching with N_2. The efficiency of N_2 (table 7) molecule is between that of toluene and He, this is expected. The Po($\emptyset$)/P($\emptyset$) was around 1.7 at 3.5 torr of N_2. There was no enhancement of reaction with addition of He or N_2, as is observed for laser irradiation of small molecules, such as CF_3CH_3[7(a)], which usually is attributed to collisional rotational hole filling. Measurement of the reaction yield vs bath gas pressure, however, is not the most sensitive way to search for rotational bottlenecks. The long mean life time of the low-energy molecules allows for more deactivating collisions with the bath gas. There might be a little rotational hole filling which enhanced the reaction probability, but the enhancement was not so obvious as in CF_3CH_3 molecule with He buffer gas. Instead, it was compensated by the quenching effect. The small difference in product distribution with added He is attributed to experimental deviation.

We now compare the collisional deactivation studies of

CF_3CH_2Cl and ethyl 3-cyclohexene-1-carboxylare[26].

Table 25

⬡–COOC$_2$H$_5$	quencher	∅	torr	Po(∅)/P(∅)
	He	2.2	2	50
CF_3CH_2Cl	He	2.4	10	1

Both molecules at the ∅ chosen have similar reaction probability (0.01). It is very obvious that CF_3CH_2Cl is much more difficult to be quenched. For large molecules, the reaction rate constants near the threshold energy are small, and lead to significant postpulse effects. Much of the reaction occurs after the laser pulse has terminated, especially for the lower fluence. The long mean life time of the low-energy molecules allows for more deactivating collisions with the bath gas. In contrast, a large fraction of the CF_3CH_2Cl molecule reacts during the laser pulse. Thus, higher pressure are needed for quenching of CF_3CH_2Cl.

The product distribution is similar both for neat CF_3CH_2Cl and with added toluene at the same fluence for the direct laser initiated reaction. This means the main three products are not affected by radical reactions in the low pressure laser induced reaction.

The toluene collisional deactivation of CF_3CH_2Cl is very significant compared to N_2 and He, and only 1.2 torr is required for half quenching required at ∅ = 3.42 J/cm^2, and 0.06 torr at ∅ = 1.61 J/cm^2. The reason is that toluene is a much bigger molecule than He and N_2, so the quenching effect is more prevalent. Under these conditions, toluene was mainly used as a

bath gas rather than a radical scavenger. From Figure 19 and 20, the trend of increasing $Po(\emptyset)/P(\emptyset)$ values with higher pressure of toluene shows that toluene is more effective in deactivation at low energy fluence than at high energy fluence. The explanation is the same as above. At lower fluence the molecules have less energy and postpulse effects are more important; the molecules are at low energy with low reaction rate constants and are deactivation more easily at the same pressure than at higher fluence, for which the energy of the molecules is higher.

(3) Absorption measurement

Multiphoton energy absorption measurements are as fundamental as reaction probability to describe laser induced reaction. Beer's law applied to the multiphoton processes of CF_3CH_2Cl except at $\emptyset=0.30\pm0.05$ J/cm^2 at 1085 cm^{-1}. If $\emptyset=0.30\pm0.05$ J/cm^2, collisional effects apparently contributed to the absorption process. The σ_L were calculated assuming that all the molecules within the irradiated volume are responsible for the absorption of photons. At sufficiently high fluence the σ_L values will always decline because of depletion of molecules by chemical reaction during the laser pulse, which depletes the number of absorbing molecules. The absorption measurement of CF_3CH_2Cl at low fluence was difficult due to the very low cross-section as well as the non-Beer's law pressure dependence.

If the density of rotational lines is quite high, the σ_L value at low fluence should be the same as the broad band cross-section measured at 1 cm^{-1} resolution. This phenomenon was observed in most big molecules, ethylacetete[6], ethyl fluoroacetate, but in Figure 34 only the CF_3CH_2Br data extrapolate to the broad-band spectroscopic cross-section, i.e., 6.2 x 10^{-19} cm^2/molecule. The σ_L values at low fluence for CF_3CH_3 and CF_3CH_2Cl are 2 to 3 times smaller than the broad band cross-section. Although the $\sigma_L(\emptyset)$ for CF_3CH_3 did increase at the lowest $\emptyset$, the values were never equal to the broad band cross-section. This was not found for CF_3CH_2Cl, the increase in σ_L at very low fluence was not found for either the R(30) or R(44) irradiation experiments. The sharp declines in σ_L with

fluence for in CF_3CH_3 and CF_3CH_2Br are probably due to anharmonicity, which may take the second, third steps etc. out of resonance. The low, but constant σ_L for CF_3CH_2Cl probably is a consequence of fluence dependent rotational fractionation with more molecules absorbing as $\emptyset$ is increased.

After all the work was completed, some checks were made on the absorption measurements to verify the previous data. These results are given in Table 16A,B and are shown in Figure 34 by special symbols. The recheck absorption measurements at high laser fluence for CF_3CH_2Cl matched with the old data. No significant difference were observed. experiments also were done with added He. The data are in Table 16A. Collisional deactivation by He decrease the CF_3CH_2Cl cross section; no rotational hole filling was observed in the $\emptyset = 3$ J/cm^2 range.

(4) Reaction Probability Measurements of Laser Induced

Unimolecular Reaction

Several experiments were done with CF_3CH_2Br to check the earlier studies and in particular to see if $P(\emptyset) \sim 1$ at high laser fluence. The data are shown below and fitted the old data quite well (Figure 35,36). The $P(\emptyset) \sim 50\%$ from $\emptyset = 2.5-3.5$ J/cm^2. The reaction probability appears to saturate at $P(\emptyset)=0.5$ as was claimed in earlier work.

Table 26 CF_3CH_2Br, 0.05 torr, A = 2.74 cm^2
            1082 cm^{-1} laser line with telescope

i	$\emptyset$	$P(\emptyset)$
10	1.19	0.106
10	1.64	0.252
5	2.10	0.388
5	2.80	0.545
5	3.50	0.452

The $P(\emptyset)$ results for CF_3CH_2Cl are thought to be free of any significant thermal contribution to the yield. The experimental limitations to product measurements constrained the measurements to $P(\emptyset) > 10^{-4}$. At low to intermediate fluences, $P(\phi)$ has a high order dependence on fluence and $P(\emptyset)$ approaches 0.8 for $\emptyset > 5$ J/cm^2. The slope of the line from a plot of $\ln P(\emptyset)$ vs. $\ln\emptyset$ indicate that reaction yield scales as the third power of fluence, which is similar to the finding for the organic acetates. At higher $\emptyset$, the dependence is less on $\emptyset$ and the reaction yield approaches 0.8 ± 0.2 at high fluence.

We now compare the reaction probability of CF_3CH_2Br, CF_3CH_2Cl, and CF_3CH_3. At the same fluence (Figure 35), the CF_3CH_2Br reaction showed the highest extent of reaction and

Figure **35**   Reaction probability vs. energy fluence for

R(30), 001-020, excitation of CF_3CH_2Cl

R(26), 001-020, excitation of CF_3CH_2Br

R(16), 001-100, excitation of CF_3CH_3
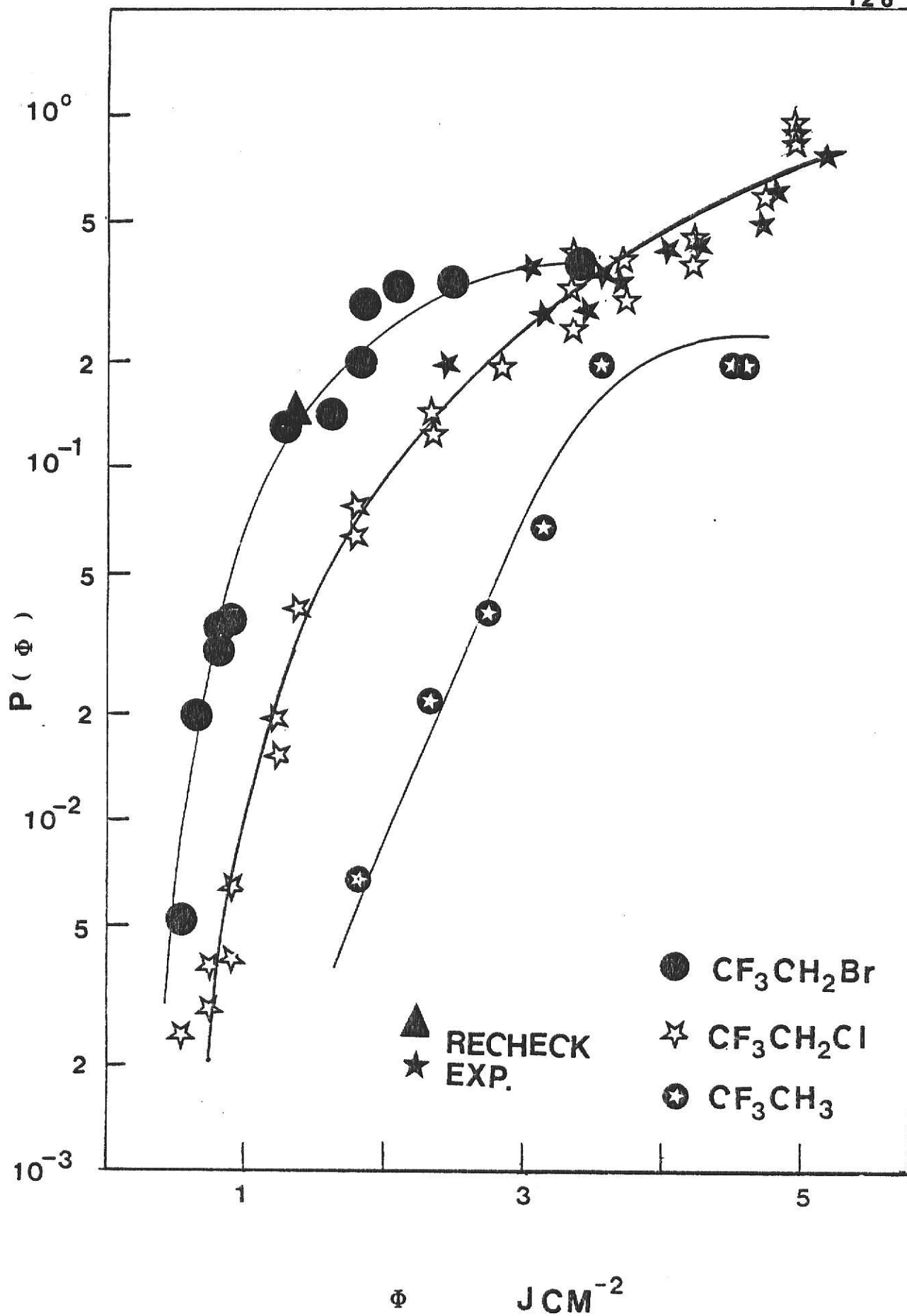
CF_3CH_3 the lowest. But if we compare the reaction probability vs. absorbed laser energy per mole, Figure 36, these three reactions appear in a different way, assuming the absorption data are correct. One explanation is that only a fraction of the molecules in the irradiated volume actually abosrb the laser energy. If so, a two-component distribution of molecules is produced after laser excitation and the fraction absorbing energy will have a much high mean energy than predicted by the $<E>$ calculated assuming all molecules absorb the energy. The highly activated molecules have high k_E values and react more readily. The fraction that absorbs the energy probably is fluence dependent, i.e., becomes larger at higher fluence. However for CF_3CH_3 and CF_3CH_2Br this fraction never reaches unity since $P(\emptyset) < 0.5$.

The CF_3CH_3 is considered as a small molecule (just a general term that fits certain observations). The CF_3CH_3, CF_3CH_2Cl showed similar reaction extent at lower average absorbed laser energy, but for $<E> > 12$ kcal/mole, CF_3CH_3 has a somewhat higher $P(\emptyset)$ than CF_3CH_2Cl at the same $<E>$. The threshold energy for HF elimination from CF_3CH_3 is 68 kcal/mole, from Figure 36, 20% reaction happens at $<E> = 23$ kcal/mole. This energy is much lower than the threshold energy, and there must necessarily a fractionation if only 1/4 of the molecules absorb the energy one can explain the 20% reaction, i.e., all the molecules that, in fact, absorb the energy do react, and $<E>$ reach 100 kcal/mole.

The threshold energies for three channels of CF_3CH_2Br are

Figure 36   Reaction probability, $P(<E>)$, vs average
energy absorbed per mole, $<E>$, for
R(30), 001-020, excitation of CF_3CH_2Cl
R(26), 001-020, excitation of CF_3CH_2Br
R(16), 001-100, excitation of CF_3CH_3
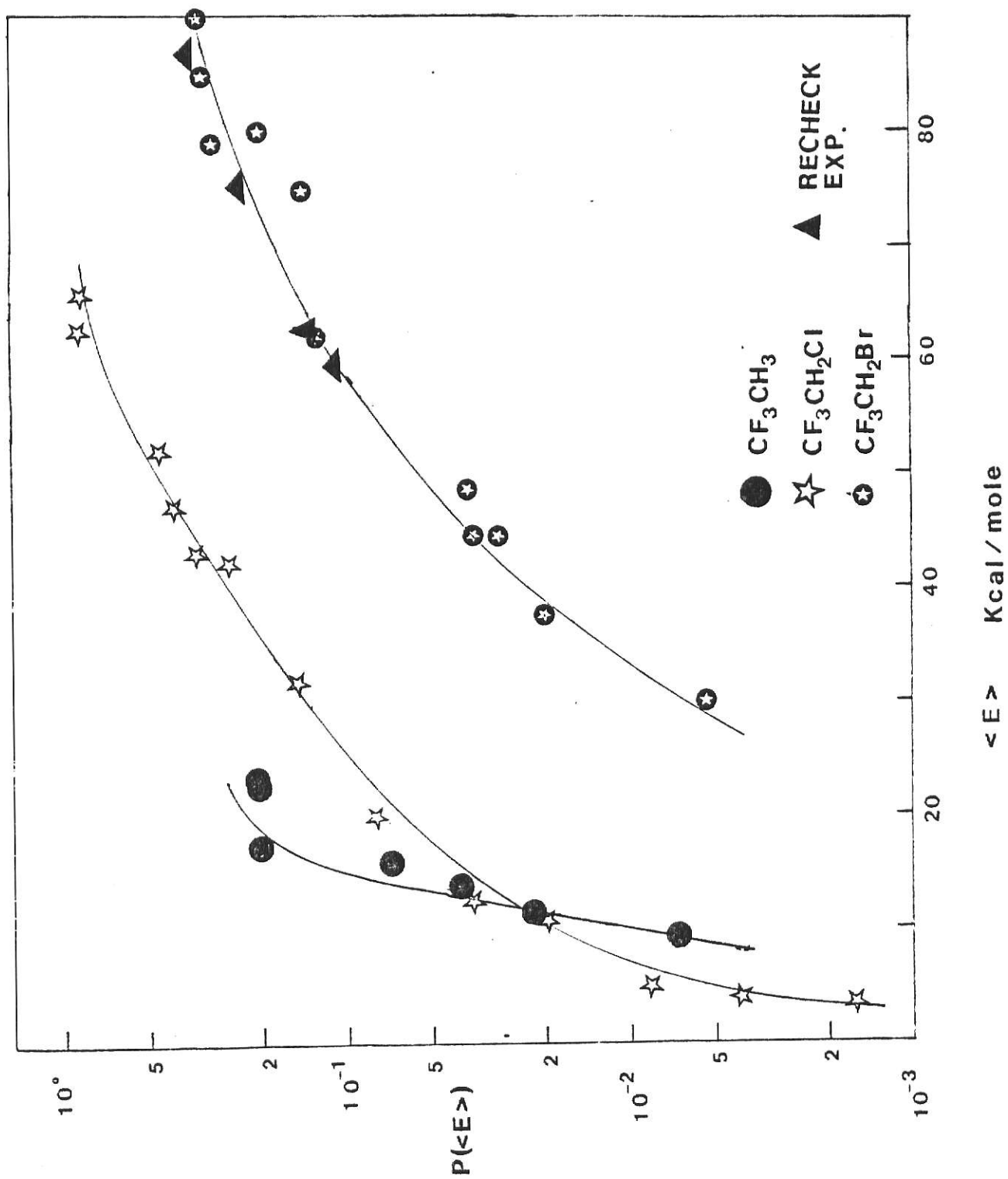
~66, ~62, and ~67 kcal/mole for HF elimination, HBr elimination and C-Br rupture respectively. From table 15B, 37% reaction happened at $<E>$ = 105 kcal/mole, so almost no fractionation is required for this molecule, all the molecules in the irradiated region absorbed the laser energy and the average energy is close to the predicted ones. In Figure 36, CF_3CH_2Br showed the lowest reaction probability when compared to CF_3CH_3 and CF_3CH_2Cl at the same $<E>$, even the $P(\emptyset)$ is the highest one at the same $\emptyset$. In the next section, we examine the ratio of reaction products and reaction probability for CF_3CH_2Cl vs E to get limits for the average energies of reacting molecules.

(5) Comparison of Product Distribution and RRKM Rate Constants.

The threshold energies and pre-exponential factors for the three reaction channels of CF_3CH_2Cl were given in Table 21. The RRKM rate constants were calculated and the dependency of k_E upon E and upon Eo for C-Cl rupture is shown in Figure 39. According to the RRKM results, the higher Eo channel (C-Cl rupture) increasingly competes with the low Eo channel (HF eli.) and becomes dominant at higher energy; the crossover in reaction channels occurs when the energy in the parent molecule is ~105 kcal/mole. This gain in the high Eo channel is a consequence of its much looser transition state (larger pre-exponential factor).

In Bert Holmes' experiments, E_{min} was 100 kcal/mole; The HCl and C-Cl rupture channels were not observed in chemical activation. At <E>=100 kcal/mole, the k_E for HF elimination and C-Cl rupture are both approximately 3×10^6 sec^{-1} for Eo(C-Cl) = 83 kcal/mole. So this threshold energy must be the lower limit for C-Cl rupture. For Eo(C-Cl) > 83, the k_E(C-Cl) will be smaller than k_E(H-F) at <E> = 100 kcal/mole. This is consistent with the fact that CF_2=CHCl was the only channel that observed in Holmes' experiments. We choose Eo(C-Cl) = 83 kcal/mole and Eo(H-Cl) = 80 kcal/mole as the threshold energies for comparison with the MPD experiments . These values also are consistent with the sensitized experiments.

A comparison between the product ratio of HF elimination from the laser induced reaction and $k_{HF}/k_{HF}+k_{HCl}+k_{C-Cl}$ (Table 27A) from RRKM calculation is shown in Figure 40. Since the <E>
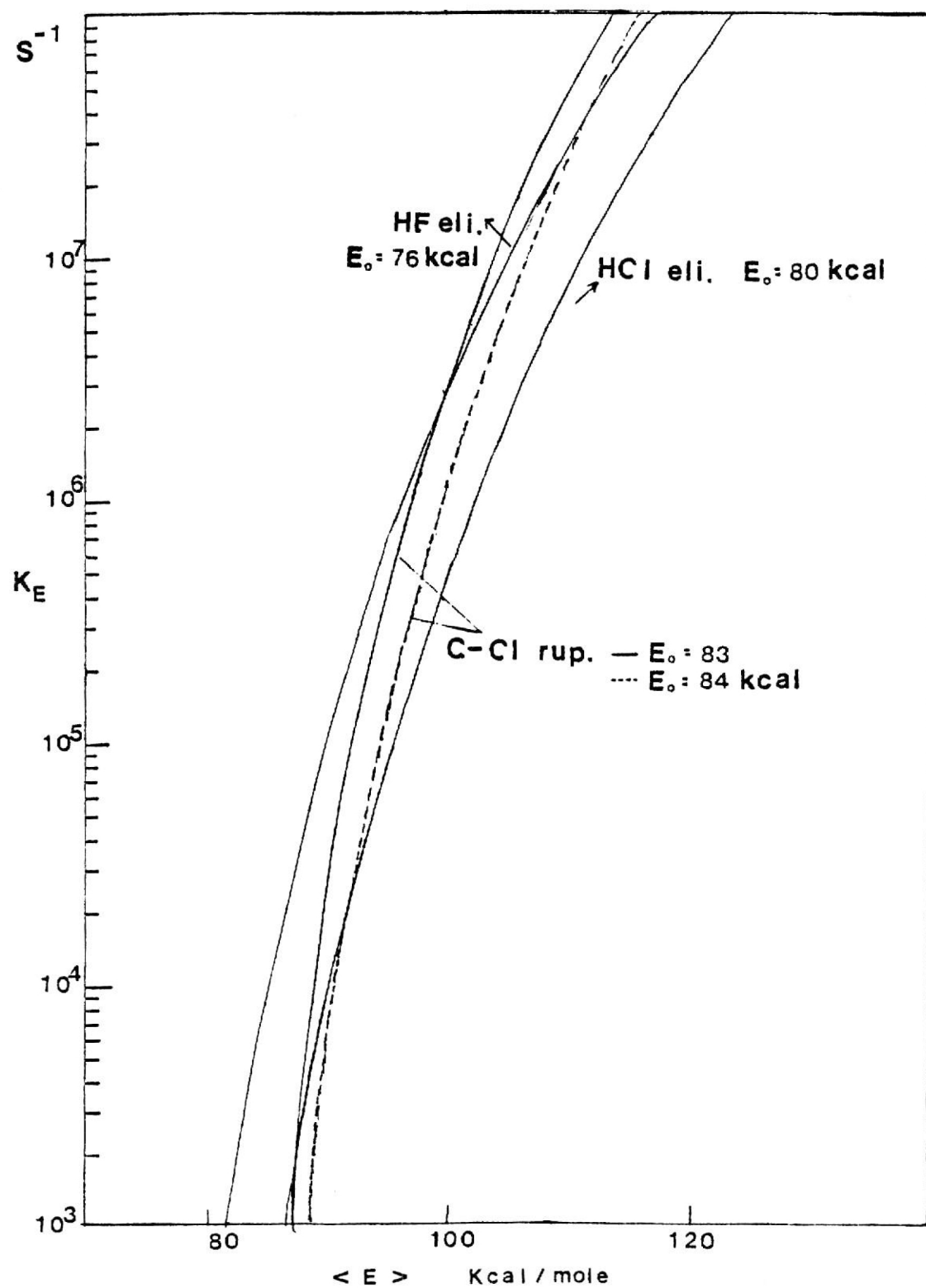
Figure **39**   The RRKM rate constant curves for CF_3CH_2Cl reactions
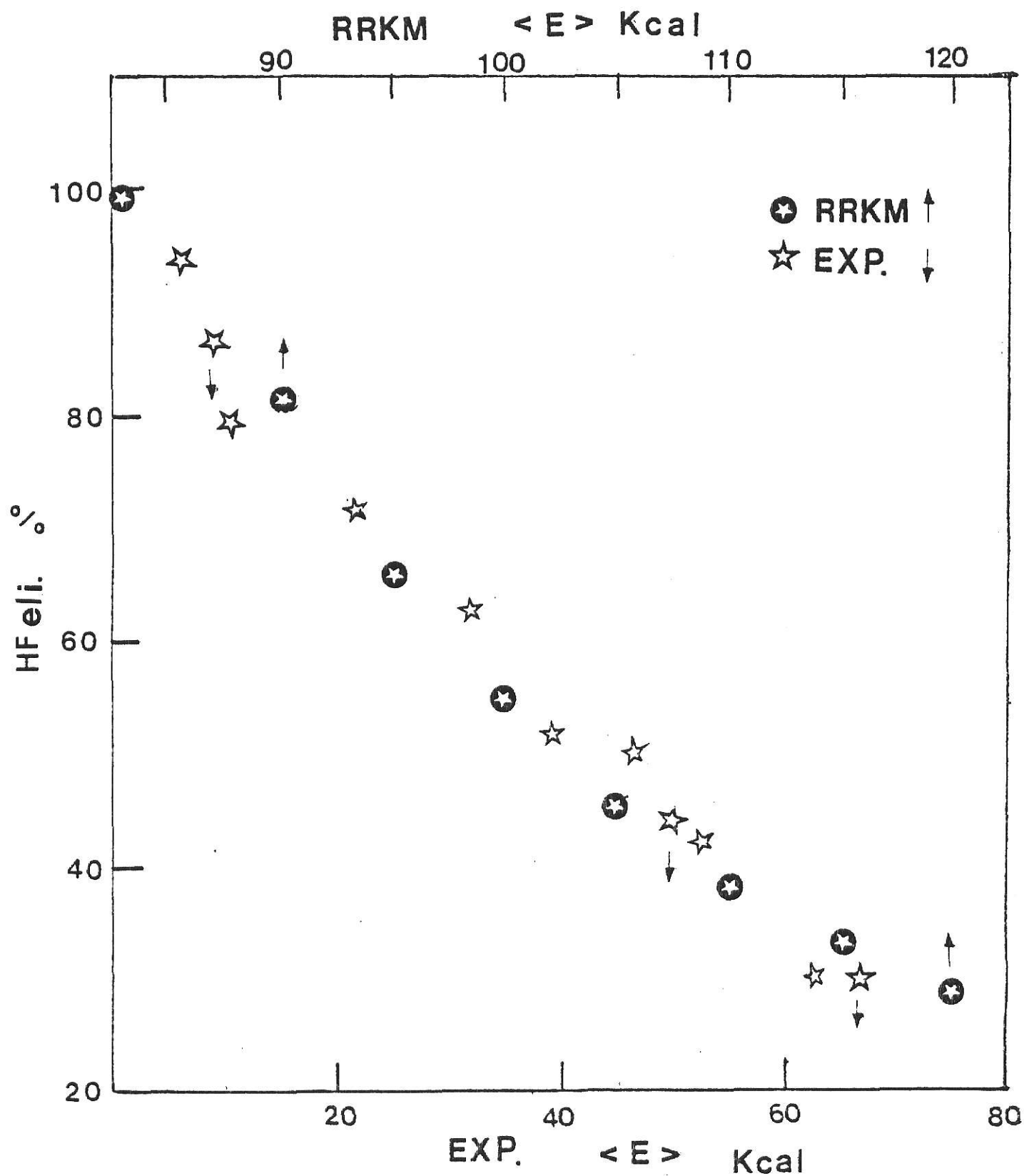
Figure 40   The comparison of HF elimination between experiment

value and RRKM calculation

assigned from the absorption experiments is lower than from the RRKM calculation, we put a scale for <E> in the same graph that matched the experimental ratios to do the comparison. It is obvious that if we slide the <E> calculated from the $\sigma_L(\emptyset)$ up 55 kcal/mole, the experimental product ratio then match the RRKM calculated results.

Table 27A $R = k_{HF}/k_{HF}+k_{HCl}+k_{C-Cl}$

<E> kcal/mole	k_{HF} sec^{-1}	k_{HCl} sec^{-1}	k_{C-Cl} sec^{-1}	R
83	3.5×10^3	6.8×10^1	3.6×10^6	0.98
90	1.2×10^5	1.0×10^4	1.7×10^4	0.82
95	7.4×10^5	9.9×10^4	2.8×10^5	0.66
100	3.2×10^6	5.9×10^5	2.2×10^6	0.54
105	1.1×10^7	2.5×10^6	1.1×10^7	0.41
110	3.1×10^7	8.6×10^6	4.2×10^7	0.38
115	7.6×10^7	2.4×10^7	1.3×10^8	0.33
120	1.7×10^8	6.0×10^7	3.4×10^8	0.30

On the strong-collision assumption the first order rate constant for de-energization is equal to the collision frequency[37], i.e., $k_E=$ =zP, where z is the collision number, P is the total pressure and $z = \pi\sigma_d^2(8kT/\pi\mu)^{1/2}$. For comparing the collision frequency for $P_{1/2}$(toluene) with the magnitude of k_E, this also is a way to set the <E>. From the result in Tables 9 and 10, $P_{1/2}$(toluene) = 0.06 torr for 0=1.61 and $P_{1/2}$(toluene) = 1.2 torr for $\emptyset$=3.42 J/cm^2. The calculates result is shown below:

Table 27B

	$T = 1000^{\circ}K$	sec^{-1} $T = 500^{\circ}K$	$T = 300^{\circ}K$
$P_{1/2} = 0.06$ torr	1.9×10^6	2.6×10^6	3.4×10^6
$P_{1/2} = 1.2$ torr	3.7×10^7	5.3×10^7	6.7×10^7

The temperature will not make too much difference to the k_E value here. The $\langle E \rangle \approx 95$ kcal/mole for the total $k_E \approx 3 \times 10^6$ sec^{-1} and $\langle E \rangle \approx 105$ for $k_E \approx 5 \times 10^7$ sec^{-1}. The experiment value for $\emptyset = 1.61$ J/cm^2 is $\langle E \rangle \approx 15$ kcal/mole and $\langle E \rangle \approx 45$ kcal/mole for $\emptyset = 3.42$ J/cm^2. From Figure 40, the k= value matched well with RRKM calculation for the product ratios and $\langle E \rangle$ 95 kcal/mole in RRKM calculation is related to $\langle E \rangle = 20$ from the experiment, $\langle E \rangle = 105$ kcal/mole in RRKM calculation is related to $\langle E \rangle = 45$ kcal/mole from the experiment. This, then, is further support that $\langle E \rangle$ must be larger than the absorption results as shown.

The experiments from Figure 40 show $P(\emptyset) = 15\%$ for $\langle E \rangle = 10$ kcal/mole, a 1/9 fractionation is necessary for $\langle E \rangle = 85$ kcal/mole in RRKM value. for $\langle E \rangle = 40$ kcal/mole, $P(\emptyset) = 25\%$, a 1/3 fractionation can still explains the $\langle E \rangle = 105$ kcal/mole in RRKM value. For the highest reaction probability $P(\emptyset) = 80\%$ and $\langle E \rangle = 67$. If 8/10 fractionation happened, it will only lead $\langle E \rangle = 84$ kcal/mole, which is much lower than the 120 kcal/mole predicted from matching the product ratios from the RRKM calculations. As mentioned in the result section, the absorption measurements at high laser fluence were extropolated from the values in the 2-3 J/cm^2 regime. It seems unlikely that the $\sigma_L(\emptyset)$ should be larger than the extrapolated values. The main question is the reaction probability measurement, at $\emptyset > 4$ J/cm^2, the uncertainty in $\emptyset$ is ± 1 J/cm$_2$, because of the big uncertainty in the irradiated area. If the fluence at 4-5 J/cm^2 was really 3-4 J/cm$_2$ because the area was larger, the $P(\emptyset)$ would decrease from 80% to 50-60%, i.e., all the $P(\emptyset)$ data points in $\emptyset = 4-5$ J/cm^2 region move back

to $\phi = 3-4$ J/cm^2 region and $P(\phi)$ declines to 0.5-0.6. Because $\phi = $ Joule/A and $P(\phi) = V/A[1-(C_i/C_o)^{1/i}]$, as ϕ is decreased from area measurement, $P(\phi)$ will decrease, then all the $P(\phi) < 50\%$. If the $P(\phi)$ was really 50%, then < 50% by fractional absorption would be adequate to explain the <E>.

This is a hypothesis and is not totally satisfactory because the data points were collected from three different series of reactions.

CONCLUSION

The infrared multiphoton laser-induced reaction of CF_3CH_2Cl, a molecule with three reaction channels, provides insight into the laser driven unimolecular reactions of halogenated ethanes. The following points were established.

(1) The absorption cross-section, was measured from $\emptyset = 0.1$ to $\emptyset = 3$ J/cm^2 at 1085 cm^{-1}.

(2) The absolute reaction yields and the product channel ratio were very dependent on laser fluence, the maximum yield was $P(\emptyset) \sim 0.8$. The C-Cl rupture was the main reaction channel at high fluence.

(3) The reaction probability was independent of parent pressure in the range of 0.05 - 0.80 torr, but increased significantly at higher pressure.

(4) The addition of toluene reduced the absolute yield indicating that collisional quenching of excited molecules was competitive with reaction for P > 0.05 torr at $\emptyset = 1.61$ J/cm^2 and P > 0.8 torr at $\emptyset = 3.42$ J/cm^2. No significant effect of He, N_2 as buffer gas was observed for pressure up to 2 torr for N_2 and pressure up to 10 torr for He. The product ratio was virtually independent of bath gas, including toluene.

(5) The experimental yields and product ratios were measured for sensitization experiments to determine the reaction mechanism; the yields and product ratios were compared to the expected values from the assigned temperatures and the elementary rate constants.

(6) RRKM calculations of rate constants for the three channels

were done vs energy. The calculated results, assuming a frac-
tional energy distribution, were compared to the experimental
data.

(7) A conflict between the experimentally measured energy and
the energy of the reacting molecules assigned from RRKM rate
constants can only be resolved by assuming significant rotation-
al fractionation with the fraction being highly dependent on
fluence.

References

1. Y.T.Lee, Ann. Rev.of Phy. Chem.,$\underline{30}$,379, 1979

2. W.C.Danen, J.C.Jang. in "Laser Induced Chemical Processes", J.I.Steinfield, ed., Plenum press, New York, 1981

3. (a) D. M. Brenner, Chem. Phys. Lett. $\underline{57}$, 357, 1978

   (b) D. B. Brenner, J. Phys. Chem. $\underline{86}$,41,1982

4. V.S. Letokhov ,Chemical and Biochemical Application of Lasers. Vol.III, C.B. Moore, ed., Academic press, N.Y. 1977
   M. A. West "Lasers in Chemistry", 1977
   E. Grunwald, "Megawatt IR Laser Chemistry" , John Wiley and Sons, N.Y. 1977

5. Clara Jang's Ph.D. thesis, Kansas State University, 1982

6. (a) Wayne C. Danen,V.C.Rio, and D.W. Setser, J.Am.Chem.Soc.104,5431, 1982

   (b) J.C.Jang,D.W. Setser, and W.C.Danen, J.Am.Chem.Soc. 104,5440, 1982

7. (a) J.C.Jang and D.W. Setser, J. Phys. Chem . $\underline{83}$,2809 1979

   (b) T.H.Richardson and D.W. Setser, J. Phys. Chem. $\underline{81}$,2301 1977

   (c) H.W.Chang, N.L.Craig, and D.W. Setser, J. Phys. Chem. $\underline{76}$,954,1972

8. J. F. Caballero and C. Wittig, Chem. Phys. Lett. $\underline{82}$,63,1981

9. J.Carlos, J.C.Jang and D.W. Setser, to be submitted in J. Phys. Chem. 1983

10. G.E.Millward and E.Tschuikow-roux, Int. J. Chem. Kin. $\underline{IV}$, 559, 1972

11. B. E. Holmes, private communication, 1983

12. (a) J. S. Francisco, W. D. Lawrence and J.I. Steinfield

    J. Phys. Chem. 86, 724, 1982

    (b) H. L. Dai, H. H. Kung and C. B. Moore, J. Chem. Phys.

    73, 6124, 198

    (c) J. B. Marling and I. P. Herman, J. Chem. Phys.

    72, 5603, 1980

13. H.L.Dai, E.Specht, M.R. Berman and C.B. Moore,

    J. Chem. Phys. 77,4494,1982

14. (a) F. M. Lussier, and J. I. Steinfeld, Chem. Phys. Lett.

    277,58,1978

    (b) P.A. Hackett, J. Malatesta, W. S. Nip, C. Willis and

    P. B. Corkum, J. Phys. Chem. 85,1152,1981

15. G.A.Crowder, J. of Fluorine Chem. 3,125,1973/74

    D.F.Harnish and R.P.Hirschmann, App. Spect. 24,28,1970

16. Aa. S. Sudbok P.A. Schulz, Y.R. Shen and Y.T. Lee,

    J. Chem. Phys. 69,2316,1978

17. C.R.Jr.Quick, C.Wittig, J. Chem. Phys. 69,4201,1978

18. N.R. Isenor, M.C. Richardson, Appl. Phys. Lett. 18,224,1971

19. J.L.Lyman, R.J. Jonsen, J.Rink, C.P. Robinson, and S.D.

    Rockwood, Appl. Phys. Lett. 27,89,1975

20. M.J. Coggiola, P.A.Schulz, Y.T. Lee and Y.R. Shen.

    Phys.Rev.Lett,38,17,1977

21. E. Wurzberg, L.J. Kovalenko, and P.L.Houston, Chem.Phys.

    35,275,1978

22. D.S.King and J.D. Stephenson, Chem. Phys. Lett. 51,48,1977

23. J.W.Hudgens, J. Chem. Phys.68,777,1978

24. Aa.S.Sudbo, P.A.Schulz, E.R.Grant. Y.R.Shen and Y.T.Lee
    J.Chem.Phys. $\underline{70}$,912,1979

25. D.F.Dever,E.J.Grunwald, J. Am. Chem. Soc. $\underline{98}$,5055,1976

26. D.W. Setser, Hanh H. Nguyen and W.C. Danen, J. Phys. Chem
    $\underline{87}$,408,1983

27. P.J.Marcoux and D.W. Setser J. Phys. Chem. $\underline{82}$,97,1978

28. S.W.Benson, "Thermochemical Kinetics", 2nd ed. 1976

29. G. S. Buckley and A. S. Rodgers, J. Phys. Chem, $\underline{87}$,126,1983

30. J.C. Hassler and D.W. Setser, J. Chem. Phys. $\underline{45}$,3246,1966

31. K. C. Kim and D. W. Setser, J. Phys. Chem. $\underline{78}$,2166,1974

32. (a) A. Maccoll, Chem Rev. $\underline{69}$,33,1969

    (b) K. R. Maltman, E. Tschuikow-Toux, and K. H. Jung.,
        J. Phys. Chem. $\underline{78}$,1035,1974

33. Aa.S.Sudbo, P.A.Schulz, E.R.Grant. Y.R.Shen and Y.T.Lee
    J.Chem. Phys. $\underline{68}$,1306,1978

34. (a) M. J. Perona, J. T. Bryant, and G. O. Pritchard,
        J. Amer. Chem. Soc. $\underline{90}$,4782,1968

    (b) K. C. Kim, D. W. Setser and B. E. Holmers,
        J. Phys. Chem. $\underline{77}$,725,1973

    (c) B.E. Holmes, D. W. Setser and G. O. Prichard, Int. J.
        Chem. Kin. $\underline{8}$,215,1976

35. D. W. Follmer and G. O. Pritchard, Int. J. Chem. Kinet.,
    $\underline{6}$,573,1974

36. G.E.Millward and E.Tschuikow-roux, Int. J. Chem. Kin.
    $\underline{V}$, 363, 1973

37. J. Robinson and K. A. Holbrook, " Unimolecular Reactions "
    Wiley, N.Y. 1972

38. Part I, R. Fields and R. N. Haszeldine, J. Chem. Soc. 1881,1964

39. Part I, J. H. Atherton, R. Fields and R. N. Haszeldine, J. Chem, Soc. (C), 366, 1971

40. K. C. Kim and D. W. Setser., J. Phys. Chem. $\underline{76}$,283,1972

41. (a) S. W. Benson and H. E. O'Neal "Kinetic Data on Gas Phase Unimolecular Reactions", NSRDS-NBS21, 1970

   (B) J. A. Kerr and M. J. Parsonage, "Evaluated kinetic data on gas phase addition reaction", Butterworths, London, 1972

42. J. M. Tedder and J. C. Walton. Acc. Chem. Res. $\underline{9}$,183,1976

43. J.S.Francisco, M.A.Findeis, and J.I.Steinfeld. Int.J. Chem. Kinetics, $\underline{13}$,627,1981

44. Fumin Zhang, J.S. Francisco, and J.I Steinfeld, J. Phys. Chem. $\underline{86}$,2402,1982

45. JANAF thermochemical tables, 2nd ed. U.S. Bureau of Standards, publication NSRDS-NBS 37

46. (a) H.W. Chang, Master thesis, Kansas State University 1969

   (b) H.W. Chang, Ph.D. thesis, Kansas State University 1971

Appendix I RRKM Model for the Three Reaction Channels

of CF_3CH_2Cl

1. The four-centered HF elimination activated complex

Any model must fit the estimated thermal Arrhenius A factor ($\sim10^{13.5}$) and use the known vibrational frequencies of CF_3CH_2Cl. The procedure for selecting the model consisted of three distinct parts:

(i) The out-of-ring vibrational frequencies.

These frequencies were chosen by analogy with CF_3CH_2Cl and $CF_2=CHCl$. These frequencies are grouped and are 2999(1), 1200(3), 1134(1), 700(2), 550(2), 500(1), 145(2). The out-of-ring frequencies, once chosen, were not varied and they are not parameters[30].

(ii) The in-plane-ring vibrational frequencies.

The frequencies were chosen to be the same as CF_3CH_3[7(c)] HF four-centered elimination and which were calculated by assigning bond orders of 1.1, 0.8, 0.1, and 0.1[7(c)] to the C-C, C-F, F-H and C-H bonds, respectively. The internal coordinates were the four bond stretches and the bending of the H-C-C valence angle, The frequencies for in-plane-ring vibrations are 1200,1134,700 , 550 and 30 cm^{-1}. as the bending force constant appreciately affects only the normal mode used as the reaction coordinate, which does not enter into the calculation, i.e., 30 cm^{-1} is dropped for the calculation.

(iii) Ring Puckering

The torsion frequency of the molecule becomes the ring puckering frequency in the transition state; this frequency was taken to be an adjustable parameter whose value was determined by matching calculations with experimental results. It was set[45(a)] at 500 cm^{-1} for CF_3CH_2Cl.

The grouped frequencies for four-centered elimination are:
2999(1), 1200(4), 1134(2), 700(3), 550(3), 500(2), 145(2)

2. The three-centered HCl elimination activated complex.

The frequencies were obtained from Holmes, who developed the transition state frequencies by dividing them into three categories.

(1) out-of-ring frequencies: The out-of-ring frequencies should be the same as the carbene CF_3CH:

(2) Ring frequencies: The ring frequencies were chosen to be the same as $CHFCl_2$ three-centered HCl elimination[45(b)] with the bond order of 0.2(C-H), 0.2(H-Cl) and 0.8(C-Cl), the deduced frequencies are 1034, 503, 236 cm^{-1}. The frequency corresponding to the reaction coordinate is 236 cm^{-1}, which is dropped for the calculation of k_E.

(3) Interaction frequencies: The interaction frequencies of the ring and molecule(three frequencies) were adjusted until the preexponential factor was close to the estimated value. The frequencies were chosen to be similar with $CHFCl_2$ three-centered HCl elimination[49(b)], they are 500(1) and 600(2).

The grouped frequencies for HCl elimination are:

3044(1), 1400(2), 1201(4), 864(4), 541(2), 310(2), 100(2)

3. The C-Cl rupture channel

We chose C-Cl stretching as the reaction coordinate so the frequency at 801 cm^{-1} was dropped. The other changes relative to the molecule are

C - C - Cl deformation	180 cm^{-1}	$\longrightarrow$	45 cm^{-1}
C - C stretching	330 cm^{-1}	$\longrightarrow$	80 cm^{-1}
C - C torsion	109 cm^{-1}	$\longrightarrow$	70 cm^{-1}

The ratio of the moment of inertia of complex versus molecule was set at 2.00 because of the loose transition state. The grouped frequencies are 3019(2), 1266(6), 880(2), 574(3), 355(1), 75(2), 45(1).

In summary, the frequencies, reaction path degeneracy and ratios of moment of inertia are listed in Table 28.

Table 28

	transition states		
CF_3CH_2Cl	HF eli.	HCl eli.	C-Cl rup.
3019(2)	2999(1)	3044(1)	3019(2)
1261(6)	1200(3)	1400(2)	1266(6)
853(3)	1134(1)	1201(4)	880(2)
572(3)	700(2)	864(4)	574(3)
342(2)	550(2)	541(2)	355(1)
180(1)	500(1)	310(2)	75(2)
109(1)	145(2)	100(2)	45(1)
path degeneracy	4	2	1
$(I^+/I)^{1/2}$	1.00	1.04	2.00
log A_0(sec^{-1})$^+$	13.3	13.6	14.9

+ per reaction channel, 1025°K

Appendix II   Laser Absorption Measurement and Temperature

Assignment for SiF_4

The absorption measurements of SiF_4 at 1027 cm^{-1}, the P(40)

laser line, were done. Because of the high absorbance of SiF_4,

we chose a cell with only 3 cm in length, so the absorption will

not be too large, this will raise the accuracy of the experimen-

tal result. The cross-sections depended on SiF_4 pressure, i.e.,

the multiphoton absorption of SiF_4 does not follow Beer's law.

Figure 41 shows the cross-section for 5 torr of SiF_4 under the

irradiation of P(40) laser line, which was compared to Nguyen's

work for 3 torr of SiF_4 under the irradiation of P(34) laser

line. The absorbed energy for 5 torr of SiF_4 was calculated

from the $\sigma_L(\emptyset)$ from Figure 41. From the JANAF table[45] for

SiF_4, the temperature was assigned directly from $<E> = H^\circ - \Delta H^\circ_{298}$

column. The transmittance, cross-section, absorbed energy and

temperature assignment vs laser fluence are shown in Table 29.

Table 29

$\emptyset$ J/cm^2	Joule	$\sigma_L(\emptyset)$ $\times 10^{-19}$ $cm^2/molecule$	Absorbed Energy kcal/mole	T $^\circ K$
0.19	0.08	5.5	14.3	946
0.22	0.10	5.1	16.0	1010
0.36	0.13	4.9	19.8	1175
0.43	0.16	4.8	25.0	1380
0.47	0.22	4.5	29.5	1558
0.59	0.26	4.3	34.2	1744

In Moore's work[13], an internal iris was set at 8.0 mm diameter,

to give a multimode beam with a near-Gaussian profile. In our

work, a constant fluence beam was used. Thus the T will not be

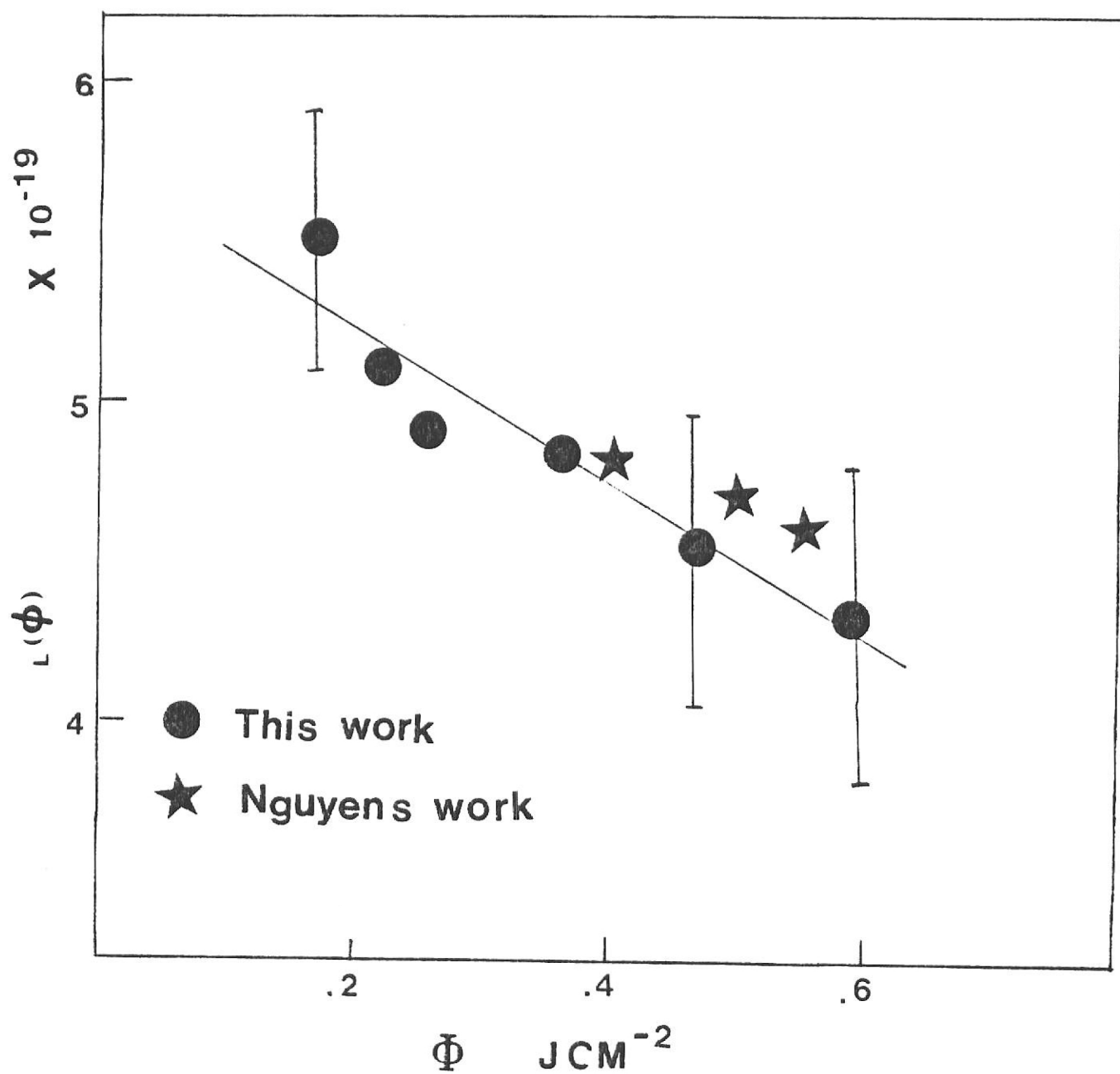exactly the same for the same absorbed energy. For the ease of

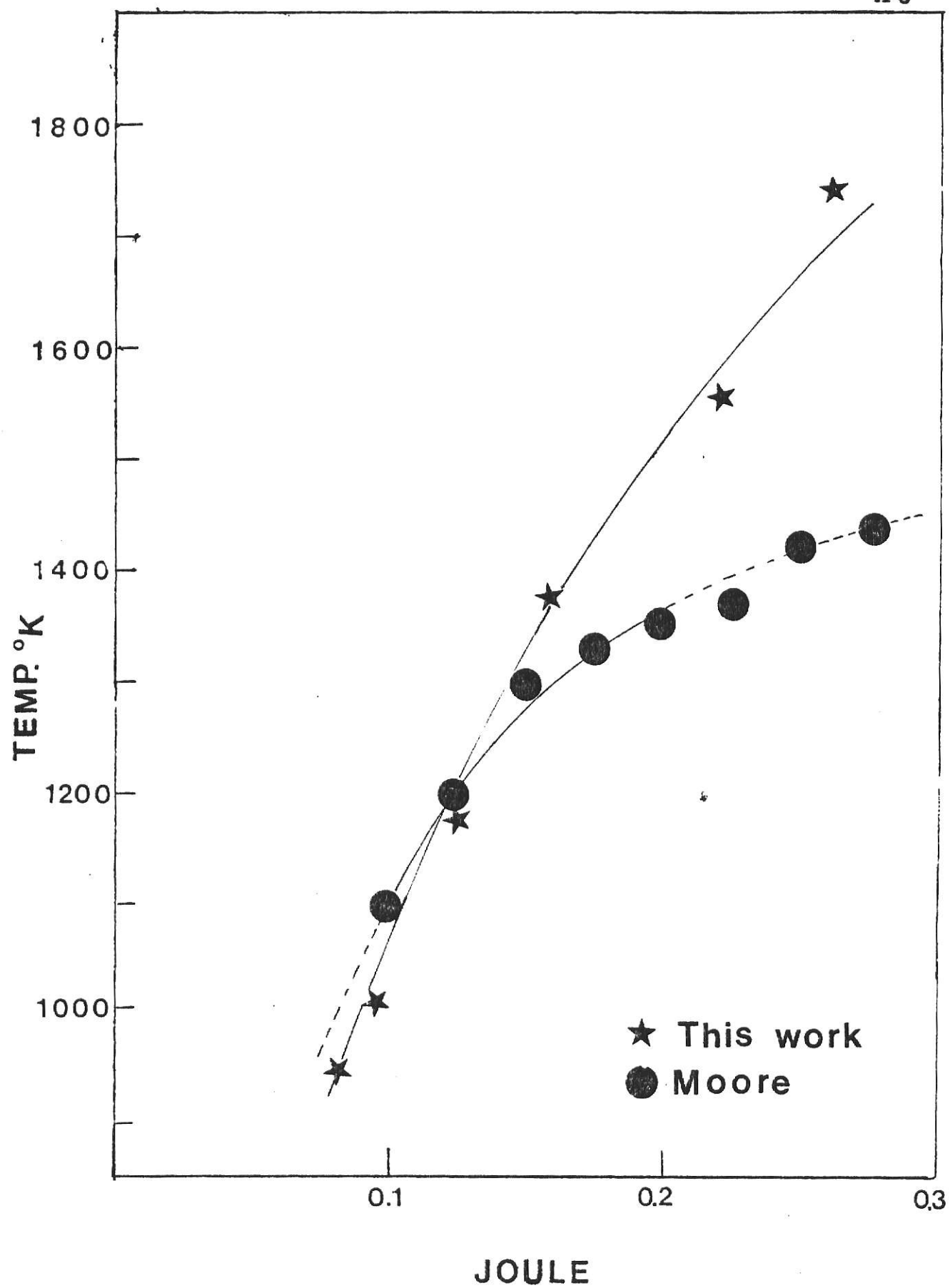Figure **41** Cross-section of 5 torr SiF_4 vs laser energy fluence

Figure **42**   Temperature assignment vs laser energy

comparison between this work and Moore's[13] results(From Figures 10 and 23 in Moore's paper, we can get the temperature at certain laser pulse energy corresponding to 1100-1500°K), we convert the laser fluence of this work to laser energy as shown in Table 30.

Table 30

laser energy Joule	temperature °K this work	Moore	reaction probability
0.08	946	1025	5.4×10^{-3}
0.10	1010	1100	1.3×10^{-2}
0.13	1175	1200	4.1×10^{-2}
0.16	1380	1300	4.5×10^{-2}
0.22	1558	1375	2.7×10^{-1}
0.26	1744	1400	2.8×10^{-1}

From Figure 42, at low temperature region, the temperature assignment was close, but larger difference occurred at laser energy > 0.2 Joule.

Hanh did some more absorption experiments at P=10 torr SiF_4 at 1033 laser line with 3 cm^{-1} cell. The cross-sections derived and temperature calculations is listed below.

Table 31

ϕ_2 J/cm²	x 10^{-19} cm²/molecule	ϕ J/cm²	Temp. °K
0.22	4.1	0.300	830
	4.0	0.375	844
	3.9	0.420	855
0.30	3.3		870
	3.0	0.460	872
	2.7		880
0.45	2.8	0.475	918
	2.5		928
	2.3	0.500	932
0.63	2.4		954
	2.1		
0.76	2.1		
	1.9		
	1.7		
0.86	1.8		
	1.5		

Hanh used $E = \int_{298}^{T} C_v dT$, but in this work, $E = \int_{298}^{T} C_p dT$ was used, this may be why the assigned temperature was lower.

INFRARED LASER-INDUCED REACTIONS

OF

HALOGENATED ETHANES

by

Tsae Shyan Lee

B. S., National Taiwan University,1979

AN ABSTRACT OF MASTER'S THESIS

submitted in partial fulfillment of the

requirements for the degree

Master of Science

Department of Chemistry

KANSAS STATE UNIVERSITY
Manhattan, Kansas

ABSTRACT

The multiphoton absorption and multiphoton dissociation of CF_3CH_2Cl were studied. The dependence of the reaction probability and product distribution on the laser fluence, reactant pressure, and bath gas pressure were determined. The absorption measurement were done at two different laser frequencies to determine the laser reaction cross-sections. Sensitization reaction with SiF_4 were done and compared to the laser reactions.

The three main reaction channels for CF_3CH_2Cl laser reaction are four-centered HF elimination, three-centered HCl elimination and C-Cl rupture. The product ratio was very dependent on the incident laser energy. Addition of toluene as a bath gas significantly lowered the reaction probability, especially at lower laser fluence, but had only a minor influence on the product distribution. As the bath gases, He and N_2, had no significant effect to the reaction probability. The absorption measurement follow the Beer's law except at very low laser fluence. The direct and sensitized excitation of CF_3CH_2Cl gave similar result, demonstrating that the absorbed laser energy was randomized before chemical reaction.

The Eo and A factors were determined from sensitization reaction and further approved from RRKM calculation. This work provides a better understanding and comparison of the CO_2 laser induced multiphoton process in CF_3CH_2Cl, CF_3CH_2Br and CF_3CH_3. This provide the evidence of only a certain, fluence-dependent, fraction of molecules absorb the laser energy.